MAREES TERRESTRES

BULLETIN D'INFORMATIONS

131

1 MAI 1999

Association Internationale de Géodésie

Commission des Marées Terrestres

Editeur Dr. Bernard DUCARME
Observatoire Royal de Belgique
Avenue Circulaire 3

BIM 131

1 mai 1999

Working Group
On
Analysis of Environmental Data
For the Interpretation of Gravity Measurements.

Working Group
on
Calibration of Gravimeters

Preface

During the Earth Tide Symposium in Brussels, 1997, the working group on

Analysis of Environmental Data for the Interpretation of Gravity Measurements

was founded, and I was asked to chair this group. Being a chairman of several working groups since 1981 I asked my co-worker, Corinna Kroner, to join the organization of this group and to be prepared to take over later. Another change was necessary due to the fact that I moved with my group to the Institute for Geosciences of the University of Jena: The decision was made to move the famous 'Bonn - Meeting' to Jena as well, and we organized the workshop from September 1 - 4, 1998.

Again we hosted another working group of the Earth Tides Commission: Michel van Ruymbeke spent one afternoon for a meeting of his group on

Calibration of Gravimeters

In the following, (most) of the papers prepared for this meeting are presented. This time no conclusions are added, because we decided to continue the discussion by email to prepare a report to be submitted to the next Earth Tide Symposium in Mizusawa, Japan, in the year 2000. Since there are only three years between these symposia a second workshop does not seem to be feasible.

Until then we hope to collect more experiences to fulfil the task to study the effect of environmental signals to gravity. We still need to work for the following topics:

- The individual corrections need to be addressed and the magnitudes of the effects must be estimated.
- Since all environmental parameters are intercorrelated and station dependent we have to define the aim of the correction needed for the individual tasks.
- The accuracy of the data and of the corrections has to be estimated.

Since these points are also of most importance to the GGP stations we have to exchange the experiences gained from this network, too.

This was the first meeting of a working group of the Earth Tide Commission in Jena (not to mention former meetings of the East-European tidal working group). I had the feeling that the environment provided by the institute and the short trip to our Geodynamic Observatory Moxa was in continuation of the 'Bonn - Meeting', although there was no replacement for our former host, Manfred Bonatz.

This time 25 scientists from 9 countries participated. I wish to thank all participants for their contributions and for their support of the successful work of these working groups. This meeting was not only supported by the 'Deutsche Forschungsgemeinschaft' but also by the provicial government of Thuringia, which is gratefully acknowledged. I thank the International Center and especially B. Ducarme for publishing all the material in the Bulletin of the International Center of Earth Tides.

Gerhard Jentzsch

Working Group
on
Analysis of Environmental Data
for the Interpretation of Gravity Measurements

Workshop Program

1. Kroner, C.: Environmental effects and gravity – an overview
2. Boy, J.P. & Hinderer, J.: Global atmospheric loading and gravity corrections
3. Schwahn, W.: The separation of solid earth tides M3 and atmospheric tide S3 by appropriate wave group formation with regard to modern potential developments
4. Zürn, W. & Neumann, U.: Gravity signals from atmospheric gravity waves and their modeling
5. Hsu, H.T. et al.: Influence of the atmospheric pressure on gravity observations based on the superconducting gravimeter at the new Dynamics Geodesy Station in Wuhan/China
6. Neumeyer, J., Barthelmes, F., Dittfeld, H.J. and Wolf, D.: Estimates of Environmental effects in superconducting gravimeter data
7. Harnisch, M. & G.: Hydrological influences in the registrations of superconducting gravimeters and ways to their elimination
8. Meurers, B.: Air pressure signatures in the SG data of Vienna
9. Braitenberg, C.: The hydrological induced strain/tilt signal – a review
10. Zürn, W. & Widmer, R.: Efficiency of air pressure corrections in the records of the Balleny Islands earthquake, March 25, 1998
11. Venedikov, A. & Ducarme, B.: Various effects on the SG tidal data and the determination of the polar motion
12. Jahr, Th. & Jentzsch, G.: An introduction to the Geodynamic Observatory Moxa
13. Kroner, C.: Monitoring of environmental influences at the Geodynamic Observatory Moxa
14. Kääriäinen, J. & Virtanen H.: On the non–tidal phenomena observed by the superconducting gravimeter 020 at station Metsähovi, Finland

15. Venedikov, A., Vieira, R., Tor, C., Arnoso, J., Gil, E., and Velez, E.: Study of various effects and pertubations in gravity tide long series obtained in the Lanzarote Geodynamic Laboratory

16. Dittfeld, H.J.: First tests of a data aquisition system at Potsdam

17. Eperné, I.P. & Mentes, G.: Results of Extensometric Tidal Measurements at the Sopron Station

18. Mentes, G.: Results of Extensometric Deformation Measurements at the Sopron Station

19 Mentes, G., Varga, P., and Kümpel, H.–J.: Recording of recent crustal movements by borehole tiltmeters in the vicinity of a tectonic fault

20. Varga, P., Grafarend, E., and Engels, J.: Earth tide generated variations of the second degree geopotential

21. Xi, Q.; Some remarks on the recent tidal potentials

Environmental Effects on the Gravity Vector - a short Overview

by

Gerhard Jentzsch and Corinna Kroner *)

1. Introduction

This article is based on the introduction prepared by co-author C. Kroner at the beginning of the meeting of the working group on 'Analysis of Environmental data for the Interpretation of Gravity Measurements' at the University of Jena, September 1998. The aim was to report about the recent developments and to recall some of the most recent papers in this field. Here, we do not only repeat this talk, but we also want to sum up the results of the discussion at the end of the meeting. The state of knowledge regarding environmental effects in geodynamic signals like gravity, tilt, strain, aquifer and earthquakes as it emerged from our discussion is summarized in Tab. 1.

2. Environmental effects on gravity

For studies of periodic or long-term variations of the gravity field the consideration of environmental influences is of fundamental importance. Variations in environmental conditions can cover relevant signals or even simulate them. In order to get reliable results from the observations regarding the earth's dynamic properties not only nature and magnitude of environmental effects have to be known, but also a way of correction must be provided. In the following a brief summary is given about the state of experience and knowledge about environmental effects in gravity and their reduction.

Presently, significant influences are proved due to variations in barometric pressure, soil moisture, and ground-water table. But we cannot exclude that other changes in the environment also produce non-neglectable effects. Gravity effects might be produced by snow covering, variations in air humidity, and by wind. But this is only guessing as no thorough studies connected to this have been undertaken yet.

Among the effects known barometric pressure is the one best investigated. The influence of barometric pressure can be distinguished by its physical nature into attraction and deformation effects. This is the reason for the frequency-dependent regression observed between gravity and barometric pressure.

3. Correction of air-pressure effects

Regarding the removal of pressure effects we can distinguish between regression/statistical methods and corrections basing on a physical approach. One method of pressure reduction still widely used is to fit a regression coefficient between the local barometric pressure series and gravity.

---

*) Institut für Geowissenschaften, Friedrich-Schiller-Universität Jena, Burgweg 11, D-07749 Jena

Nowadays, we know the deficiencies this simple statistical approach has, it allows the removal of up to 70 to 90% of the barometric pressure effects contained in gravity. The major improvement regarding this statistical method was to take the frequency-dependence of the regression into consideration (comp. Warburton & Goodkind, 1977; Crossley et al., 1995). In addition, one had to cope with a different regression behaviour at solar harmonics caused by their global character (Spratt, 1982). This altogether resulted in a frequency-dependent admittance function with special corrections at solar harmonics. In general the statistical principle only works for barometric pressure effects originating from correlated barometric pressure variations. This means that all uncorrelated variations remain uncorrected. Another problem arises when gravity data also contain other periodic effects or disturbances correlating with barometric pressure. Applying a statistical method these components are corrected, too. This can lead to the removal or distortion of gravity signals of interest.

An alternative to the statistical correction principle is given by a physical approach developed by Merriam (1992) and Sun (1995). Within this approach the attraction and deformation effect of the air masses is calculated either using three-dimensional global barometric-pressure distributions or by assuming a model atmosphere and using global, lateral distributed pressure data. This method has two distinct advantages: firstly, it allows the correction of pressure variations uncorrelated with each other, and secondly the calculation of the correction is carried out independently of the gravity data. Thus, it can be ascertained that only barometric pressure effects are reduced in gravity. Disadvantages are that the correction calculation becomes more laborous. It is more time-consuming and the necessary pressure data often cannot be easily obtained. Global data usually have a low sampling rate of 2 to 4 values per day, and the grids available are calculated from lateral pressure models. Another disadvantage lies in the fact that the reaction of the oceans with regard to pressure variations has to be taken into account separately. Depending on the frequency range the reaction of the oceans corresponds to an inverted barometer, non-inverted barometer response or a combination of both. Recent studies were undertaken by Pascal Gegout and Jacques Hinderer.

A third form of correction is sort of a hybrid correction: a combination of the statistical and physical approach. The regional and global pressure influence is removed by applying a correction based on Merriam's and Sun's physical approach. The local correction is carried out by fitting a regression coefficient between gravity and local barometric pressure (Kroner, 1997).

Each of the methods mentioned has its own merits and deficiencies. The correction procedure choosen usually depends on the pressure data available and the goal of the studies.

4. Discussion and future needs for the corrections

What is our present state of experience regarding barometric pressure? We find, reductions with a frequency-dependent admittance as well as with atmospheric Green's functions can lead to improved corrections compared to the application of a single regression coefficient. But, after the correction usually the gravity data still contain barometric pressure effects. Actually, we should get better results with atmospheric Green's functions than obtained so far as this procedure allows the inclusion of uncorrelated pressure variations.

How might we achieve improvements? Improvements might be possible if hourly pressure data of regional barometric stations are used for the corrections in addition to global pressure charts. 'Regional' corresponds to an area with distances between some ten and several 100 km from the gravimeter location. Other means of improvement could be the consideration of lateral differences in local pressure variations. But this requires the existence of a local pressure network. Additionally, an improvement might also be achieved by an improved modeling of the barometric pressure influence on ocean and coast.

We know now that in order to perform the pressure corrections we need air-pressure information not only from the local station but also from the region; in some cases even global information is necessary. Today, this pressure information is very expensive, therefore, we have to try to convince the national agencies to make these data available for free for scientific use. And the International Center for Earth Tides (ICET) should collect the monthly data from ECMWF*) / Reading to provide it for the use of the tidal community.

Our basic problem is related to the fact that all environmental parameters are intercorrelated, and this correlation is not only station dependent but also related to the aim of research. This means that we have to raise the questions why we need the correction and what is the specific purpose. To do so we need to address the individual problem and the magnitude of the effect. Further, we have to name the accuracy of the data and of the respective corrections.

With regard to these questions we find that we encounter the problem of the lack of information regarding the influence of other environmental variations on gravity. Besides barometric pressure variations experiences with effects due to groundwater-table and soil moisture changes exist. We know that changes in both can produce significant gravity effects (comp. i.e. Klopping et al., 1995; Delcourt-Honorez; Neumeyer & Dittfeld, 1997). There are first tentative attempts for corrections by assuming an infinite Bouguer plate. In general, hydrological effects are not well investigated as often vital data are missing, i.e. regarding underground properties or the accuracy and temporal resolution of the observed environmental parameters. In addition, hydrological effects are strongly depending on local conditions. Therefore, results from one station are only transferable to another station under constraints. This means a lot of studies relying to hydrological effects need still to be done.

Finally, we also need to deal with the question, how barometric pressure variations affect soil moisture and groundwater table changes. If there is an influence, is it always instantaneous or do we also have to deal with retarded effects? Although we know a lot about the relation of the environment and the gravity vector we still need to know more, especially in connection with the potential resolution and stabilities of state-of-the-art instruments.

5. References and a selection of publications related to environmental effects

Crossley, D.J., Jensen, O.G. and Hinderer, J., 1995: Effective barometric admittance and gravity residuals. Phys. Earth planet. Inter., 90, 355 - 358

Delcourt-Honorez, M., 1995: Hydrogeological effects on the local gravity. Cahiers du Centre Europeen de Geodynamique et de Seismologie, 11, Proc. Sec.

*) ECMWF: European Center for Middle Range Weather Forecast, Reading, England

Workshop on `Non tidal gravity changes, intercomparison between absolute and superconducting gravimeters', Walferdange, 6.-8. Sept. 1994, 161 - 167

Dittfeld, H.J., 1995: Nontidal features in the SG-record at Potsdam. Cahiers du Centre Europeen de Geodynamique et de Seismologie, 11, Proc. Sec. Workshop on `Non tidal gravity changes, intercomparison between absolute and superconducting gravimeters', Walferdange, 6.-8. Sept. 1994, 79 - 99

Ducarme, B., Van Ruymbeke, M. and Poitevin, C., 1986: Three years of registration with a superconducting gravimeter at the Royal Observatory of Belgium. Proc. 10th Int. Symp. Earth Tides, Madrid, Sept. 1985, Ed. R. Vieira, Consejo Superior de Investiciones Cientificas, 113 - 129

Gegout, P., 1995: De la variabilite de la rotation de la terre et du champ de gravite, consequente aux dynamique de l'atmosphere et des oceans. Ph.D.-thesis, Uni Strasbourg, France

Gegout, P. & Cazenave, A., 1993: Temporal variations of the earth's gravity field for 1985-1989 derived from Lageos. Geophys. J. Int., 114, 347 - 359

Hinderer, J., Crossley, D. and Xu, H., 1993: Gravity noise levels from a 2 year comparison of two superconducting gravimeter data. Bulletin d' Informations des Marees Terrestres, 116, 8612 - 8626

Hinderer, J., Crossley, D. and Xu, H., 1994: A two year comparison between the French and Canadian superconducting gravimeter data. Geopys. J. Int., 116, 252 - 266

Klopping, F.J., Peter, G., Berstis, K.A., Carter, W.E., Goodkind, J.M. and Richter, B., 1995: Analysis of two 525 day long data sets obtained with two side-by-side, simultaneously recording superconducting gravimeters at Richmond, Florida, U.S.A. Cahiers du Centre Europeen de Geodynamique et de Seismologie, 11, Proc. 2nd Workshop `Non tidal gravity changes, intercomparison between absolute and superconducting gravimeters', Walferdange, 6.-8. Sept. 1994, 57 - 69

Kroner, C., 1997: Reduktion von Luftdruckeffekten in zeitabhängigen Schwerebeobachtungen. Ph.D.-thesis, TU Clausthal, Germany

Kroner, C., Hsu, H.T., Jahr, T., Jentzsch, G., Tao, G.X. and Weise, A., 1995: Long-term stability and tidal parameters of the SG-record at Wuhan, China. Proc. 12th Int. Symp. Earth Tides, Beijing, Aug. 1993, Science Press, Beijing, 265 - 276

Merriam, J.B., 1992: Atmospheric pressure and gravity. Geophys. J. Int., 109, 488 - 500

Merriam, J.B., 1995: The atmospheric pressure correction in gravity at Cantley Quebec. Proc. 12th Int. Symp. Earth Tides, Beijing, Aug., 1993, Science Press, Beijing, 161 - 168

Müller,T. & Zürn, W., 1983: Observation of gravity changes during the passage of cold fronts. J. Geophys., 53, 155 - 162

Neumeyer, J., 1994: Acquisition, processing and evaluation of GFZ Potsdam SCG data. Bulletin d'Informations des Marees Terrestres, 120, 8938 - 8945

Neumeyer, J., 1995: Frequency dependent atmospheric pressure correction on gravity variations by means of cross spectral analysis. Bulletin d' Informations des Marees Terrestres, 122, 9212 - 9220

Neumeyer, J. & Dittfeld, H.J., 1993: First results of the registration with the superconducting gravimeter installed at the gravimetric observatory Potsdam. Bulletin d'Informations des Marees Terrestres, 117, 8649 - 8652

Neumeyer, J. & Dittfeld, H.J., 1997: Results of three year observation with a superconducting gravimeter at the GeoForschungsZentrum Potsdam. J. Geod., 71, 97 - 102

Rabbel, W. & Zschau, J., 1985: Static deformation and gravity at the earth's surface due to atmospheric loading. J. Geophys., 56, 81 - 99

Smylie, D.E., Hinderer, J., Richter, B. and Ducarme, B., 1993: The product spectra of gravity and barometric pressure in Europe. Phys. Earth Planet. Int., 80, 135 - 157

Spratt, R.S., 1982: Modelling of atmospheric pressure variations on gravity. Geophys. J. R. astr. Soc., 71, 173 - 186

Sun, H.-P., Ducarme, B. and Dehant, V., 1995: Correction of the atmospheric pressure on gravity measurements recorded by a superconducting gravimeter at Brussels. Proc. 12th Int. Symp. Earth Tides, Beijing, Aug. 1993, Science Press, Beijing, 317 - 330

Sun, H.-P., 1995: Static deformation and gravity changes at the earth's surface due to the atmospheric pressure. Ph.D. thesis, Cath. Uni. Louvain, Belgium

Van Dam, T. & Wahr, J.M., 1987: Displacements of the earth's surface due to atmospheric loading: effects on gravity and baseline measurements. J. Geophys. Res., 92, 1281 - 1286

Virtanen, H. & Kääriäinen, J., 1995: The installation of and first results from the superconducting gravimeter GWR 20 at the Metsähovi station, Finland. Reports of the Finnish Geodetic Institute, Helsinki

Warburton, R.J. & Goodkind, J.M., 1977: The influence of barometric pressure variations on gravity. Geophys. J. R. astr. Soc., 48, 281 - 292

Tab. 1: Environmental effects in geodynamic signals - state of knowledge

	air pressure	groundwater	precipitation	soil moisture	wind	temperature	solar radiation
gravity	• global: free access ICET should collect • regional: ø 2000 km, oceans/atm./earth • local: ø 100 km, correction of air press. and groundwater, dynamics	• topography ⇒ pumping results • investigate effects and model • river and lake loads	• different instrum. rate < 1 h ⇒ spatial distr. (local!) snow/rain	• different measurem. • fluid perculation ⇒ Mäkinen ⇒ how to monitor? ⇒ modeling?	• short-period noise • long-period modulation • secondary effects (C_w) ⇒ should be monitored	+ humidity • are instrum. effects ⇒ should be monitored	/ ? (eclipse)
tilt strain	• local effect (≈ 0.7 nrad/hPa) ⇒ cavity, topography	• pore pressure ⟺ • rain fall function • geology • tiltmeter below water table • pressure gradient	• test statistical models		↕	• should be investigated ⇒ stress • thermo stress • thermoelastic stress	
aquifer	• transfer function between precipitation, air pressure and ground water				• investigate special events • compare disturbing signals and correlate to different inputs • think about experiments		
earthquakes	• correction using theoret. seismograms						

Atmospheric pressure effects on gravity: local versus global corrections

Jean-Paul BOY and Jacques HINDERER

EOST (ULP-CNRS UMR 7516)
5, RUE DESCARTES
67084 STRASBOURG FRANCE

Abstract

This paper is a review of the different methods of pressure corrections on surface gravity measurements. The classical way is to use the local pressure estimation with the empirical barometric admittance function. This simple method does not allow to correct atmospheric effects of large scale. We need then the use of a global network of barometers to model the atmospheric loading. In this present paper, we show two models of global pressure loading using different assumptions: in a first step, we suppose the atmosphere to be a surficial thin layer and in a second step, we consider a stratified model of the atmosphere where the physical parameters evolve with the altitude. We compute the atmospheric Green's functions for both models and show the improvement of a global pressure loading corrections in a tidal analysis of a 9 year long record of Superconducting Gravimeter (SG) data near Strasbourg, France.

1. Introduction

Atmospheric pressure is one of the major sources of surface gravity perturbations. Local pressure correction using the classical local admittance (Crossley *et al.*, 1995) cannot take into account global and/or regional meteorological structures such as thermal waves (S_1 and its harmonics) and long period phenomena (anticyclona and depression). As an introduction, we show that the surface pressure field is characterised with large scale variations using ECMWF (European Center for Medium Range Weather Forecast) data (ECMWF, 1994).

In section 2, we present the modelisation of global atmospheric loading using different hypotheses of vertical profiles. In section 3, we show the improvement of modelling global pressure loading in a 9 year tidal analysis of SG data (GWR T005) located near Strasbourg, France.

We study the spatial coherency of the surface pressure field using the spectral energy function given by:

$$R(n,t) = \sum_{m=0}^{n} \left[\left(p_n^m(t) \right)^2 + \left(\tilde{p}_n^m(t) \right)^2 \right] \qquad (1)$$

where $p_n^m(t)$ and $\tilde{p}_n^m(t)$ are respectively the cosine and sine terms of degree n and order m of the harmonic expansion of the pressure field. At each degree n, we can associate a wavelength $\lambda(n)$, which is a function of n and Earth's radius a:

$$\lambda(n) = 2\pi \frac{a}{n}$$

Figure 1 shows the spectral energy of the surface pressure field for the year 1994. The atmosphere is characterised by low harmonic degree variations. Lowest degrees (1 and 3) correspond to the daily thermal waves S_1 (Haurwitz and Cowley, 1973) and associated wavelengths are larger than 10000 kilometers. Degrees 6 and 7 (wavelengths around 6500 kilometers) correspond to major harmonic degrees of typical meteorological structures (anticyclona and depression), as shown by Spratt (1982). Such properties easily show that local pressure measurements are unable alone to fully allow the correction of atmospheric loading of large scale on gravity.

2. Local pressure correction

Pressure corrections are usually done with the help of barometric admittance (Crossley *et al.*, 1995), which is a simple transfer function between pressure and gravity both measured locally. This correction allows a reduction of at least 90% of atmospheric noise for periods lower than one day, because of the high correlation between pressure and gravity residues (i.e. corrected for Earth tides) as shown by Figure 2.

A better local correction is to use the frequency dependent admittance function (Crossley *et al.*, 1995). Figure 3 shows this admittance function computed from a 9 year long record of local barometric pressure and gravity data from SG T005 installed near Strasbourg, France; each admittance value is computed using two different frequency windows (500 and 1000 points).

However, for periods exceeding 10 days, correlations between pressure and gravity residues become very low, because of the spatial extent of the pressure field. We need then to model pressure loading on a more global scale to correct atmospheric contributions on surface gravity for long period phenomena.

3. Atmospheric Green's functions

In this section, we present the atmospheric Green's functions with different hypotheses of atmospheric profiles. For the theoretical calculations, we refer the reader to previous papers (Merriam, 1992; Boy *et al.*, 1998).

3.1. Surface loading

The elastic $GE(\psi)$ and Newtonian $GN(\psi)$ Green's functions are respectively equal to (Boy *et al.*, 1998):

$$\begin{cases} GE(\psi) = -\dfrac{G}{g_0 a^2}\displaystyle\sum_{n=0}^{\infty}\left(2h_n' - (n+1)k_n'\right)P_n(\cos\psi) \\ GN(\psi) = +\dfrac{G}{g_0 a^2}\left(\dfrac{1}{4\sin(\psi/2)} - 2\pi a^2\delta(\psi)\right) \end{cases} \tag{2}$$

where g_0, G and ψ are the mean surface gravity; gravitational constant and solid angle. $h_n^{'}$ et $k_n^{'}$ are surface Love numbers of degree n (Hinderer et Legros, 1989).

Induced gravity changes at point of coordinates (θ, λ) are equal to:

$$\Delta g(t,\theta,\lambda) = \iint \left(GN(\psi) + GE(\psi)\right) p(t,\theta^{'},\lambda^{'}) ds^{'} \qquad (3)$$

with $p(t,\theta^{'},\lambda^{'})$ the pressure field at coordinates $(\theta^{'},\lambda^{'})$.

3.2. Stratified loading

For a stratified loading, the elastic Green's function is the same as in the surface loading hypothesis, but Merriam (1992) shows that the Newtonian Green's function is equal to:

$$GNS(\psi,z) = G\frac{a-(a+z)\cos\psi}{\left(a^2+(a+z)^2-2a(a+z)\cos\psi\right)^{3/2}} \qquad (4)$$

where z is the altitude of atmospheric masses.

Induced gravity changes in (θ, λ) are equal to:

$$\Delta g(t,\theta,\lambda) = \iint GE(\psi) p(t,\theta^{'},\lambda^{'}) ds^{'} + \iiint GNS(\psi,z)\rho(t,\theta^{'},\lambda^{'},z) dz ds^{'} \qquad (5)$$

with $\rho\left(t,\theta^{'},\lambda^{'},z\right)$ the atmospheric density.

Figure 4 shows gravity induced effects of spherical caps as a function of the radius. For solid angles larger than 20 degrees, the Newtonian attraction is no longer a function of the density stratification. The Bouguer approximation is reached for a solid angle of 3 degrees. For the surface Newtonian approximation, the limit of – 0.42 μgal/mbar is due to the Dirac function (Equation 2). The elastic deformation is smaller and has a sign opposite to the Newtonian attraction for solid angles smaller than 50 degrees.

3.3. Atmospheric density profiles

We need to compute density profile variations in order to compute the loading of a stratified atmosphere. We can use global atmospheric data from ECMWF to rebuild density from pressure p, temperature T and specific humidity q. Another way is to suppose a simple hydrostatic model of the atmosphere.

3.3.1. Hydrostatic density profiles

For altitudes smaller than 12 kilometers, the temperature can be modelled as a linear trend:

$$T(z) = T_0 + \alpha z$$

with T_0 the surface Temperature. The density is also a function of the surface pressure P_0 and surface temperature T_0.

$$\rho(z) = \frac{P_0}{RT_0}\left(1+\alpha\frac{z}{T_0}\right)^{g/R\alpha} \qquad (6)$$

Figure 5 shows pressure, temperature and density variations for the hydrostatic approximation and the US Standard Atmosphere (1976).

3.3.2. ECMWF data

The density ρ is a function of pressure P, temperature T and specific humidity q (Gill, 1982):

$$\rho(z) = \frac{P(z)}{RT(z)\left(1-q(z)\frac{1-\varepsilon}{\varepsilon}\right)} \qquad (7)$$

where R and ε are the gas constant for dry air and the ratio of gas constants between water vapour and dry air.

3.4. Oceanic response to atmospheric loading

The oceanic response to atmospheric loading is classically modelled using two different hypotheses:

- the non-inverted barometer ocean (NIBO) where the atmospheric loading is fully transmitted to the solid Earth,
- the inverted barometer ocean (IBO) where the atmospheric loading is compensated by sea depth variations, and there are hence no net pressure variations on the sea floor.

However both approximations do not fully take into account all interactions between oceans, atmosphere and solid Earth. For this study, we use the non-global ocean static

response (Gegout and Legros, 1998) model. For the consequences in the computation of Green's functions, we refer the reader to Boy *et al.* (1998).

4. Tidal analysis of a 9 year series of SG T005

We use a 9 year series of SG T005 measurements between 1987 and 1996. This gravimeter was installed near Strasbourg, France and no change in the equilibrium levitation force (compensating the mean gravity) occured during the entire recording period. The instrumental drift is best modelled with a exponential function having a time constant of 840 days. The polar motion contribution is subtracted by taking into account a static oceanic response to the rotational potential generated by the Earth's polar motion. For more details, we also refer the reader to Hinderer *et al.* (1998) as well as to Loyer et al. (1999).

Figure 6 shows the long period amplitude gravimetric tidal factors obtained from the ETERNA software (Wenzel, 1996) which is known to rely on very accurate lunisolar tidal potential developments.

Three different pressure corrections are considered in the frame of the tidal analysis:

- first, no pressure correction at all,
- then, a local pressure correction with a constant barometric admittance,
- finally, a global surface loading using a static oceanic response.

It is noticeable that the global pressure correction allows a better estimation of the semi-annual amplitude factor, since a local pressure correction cannot model the seasonal circulation of the atmosphere of large spatial extent. For other long period tides, the oceanic tidal influence is larger than atmospheric perturbations and it is quite hard to see potential improvements due to a specific pressure correction. The difference between the Schwiderski (1980) model and the Lyard *et al.* (1998) recent model are small except for the fortnightly M_f tide.

5. Conclusion

A global pressure correction allows a better estimation of long period tidal factors than does a local pressure correction. Even if theoretical arguments point out easily the need for a global correction because of the relationship existing between frequency and length scale in the atmospheric phenomena, establishing the proof of the advantage of global versus local corrections is difficult because of other gravity contributions in the long period range. For instance, the oceanic tides, which seem to be well modelled by the Lyard *et al.* (1998) hydrodynamic solutions, are larger than pressure forcing for monthly and fortnightly tides.

Other gravity perturbations due to rainfall or watertable level changes are also present in the long period band and are a further obstacle to check the efficiency of pressure corrections and to allow the study of the (an)elastic response of the Earth to body tides. The Green's function show the strong importance of pressure loading in the vicinity of the station. For more accurate local and/or regional pressure loading, we need to have a high precision barometer network to densify ECMWF global circulation models which are presently limited to a grid of 100 km equidistant points. We also need to compute more carefully the Newtonian and elastic contributions: indeed, for small solid angles, a Love number decomposition (as a function of the degree in a spherical harmonic expansion) is not appropriate and a local rheological model (e.g. semi-infinite plane with different layers) may become crucial.

References

Boy, J. P., Hinderer, J. and Gegout, P.; 1998, Global atmospheric loading and gravity, *Phys. Earth Planet. Inter.*, **109**, 161-177.

Crossley, D., Jensen, O. and Hinderer, J., 1995, Effective barometric admittance and gravity residuals, *Phys. Earth Planet. Inter.*, **90**, 221-241.

ECMWF, 1994, The description of ECMWF/WCRP Level III-A global atmospheric data archive.

Gegout, P. and Legros, H., 1998, The response of non-global oceans to continental atmospheric loading, I-A model of non global static oceans, *Geophys. J. Int.*, in press.

Gill, A. E., 1982, Atmosphere-Ocean Dynamics, *Academic Press,* New-York, 666 pp.

Haurwitz, B. and Cowley, A. D., 1973, The diurnal and semi-diurnal barometric oscillations, global distribution and annual variation, *Pageoph.*, **102**, 193-222.

Hinderer, J. and Legros, H., 1989, Elasto-gravitational deformation, relative gravity changes and Earth dynamics, *Geophys. J. Int.*, **103**, 219-231.

Hinderer, J., Boy, J.P., and Legros, H., 1998. A 3000 day registration of the Superconducting gravimeter GWR T005 in Strasbourg (France), *Proc. 13th Int. Symp. Earth Tides*, Brussels, eds P. Paquet and B. Ducarme, 617-624.

Loyer, S., Hinderer, J., and Boy, J.P., 1999. Determination of the gravimetric factor at Chandler period from the Earth's orientation data and superconducting gravimetry observations, Geophys. J. Int., **136**, 1-7.

Lyard, F., Biancale, R. and Schwintzer, P, 1998, A new long period ocean tide model. Application to the satellite orbit determination and global gravity field model, *Proc. 13th Int. Symp. Earth Tides*, Brussels, eds P. Paquet and B. Ducarme, 519-519.

Merriam, J. B., 1992, Atmospheric pressure and gravity, *Geophys. J. Int.*, 109, 488-500.

Schwiderski, E. W., 1980, On charting global ocean tides, *Rew. Geophys. Space Physics*, **18**, 243-268.

Spratt, R. S., 1982, Modelling the effect of atmospheric pressure variations on gravity, *Geophys. J. R. astr. Soc.*, **71**, 173-186.

U.S. Standard Atmosphere, 1976, National Oceanic and Atmospheric Administration, Naval Aeronautic and Space Administration, United States Air Force, Washington D.C., October, 1976.

Wenzel, H. G., 1996, The nanogal software: Earth tide data processing package ETERNA 3.30, *Bull. Inf. Marees Terr.*, **124**, 9425-9439.

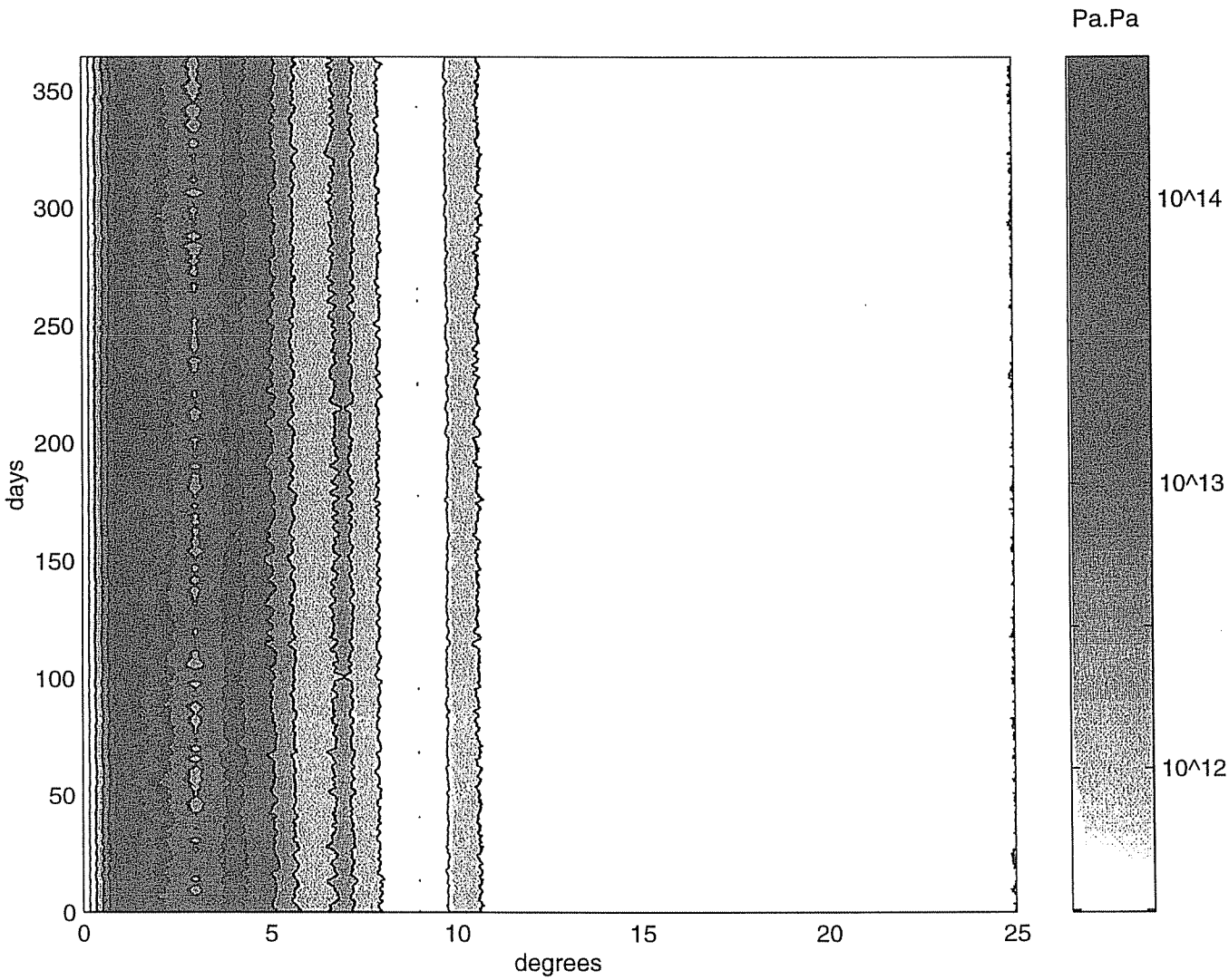

Figure 1: Time-dependent energy spectrum (as a function of the harmonic degree) of the atmospheric pressure field for the year 1994; the units are in Pa^2.

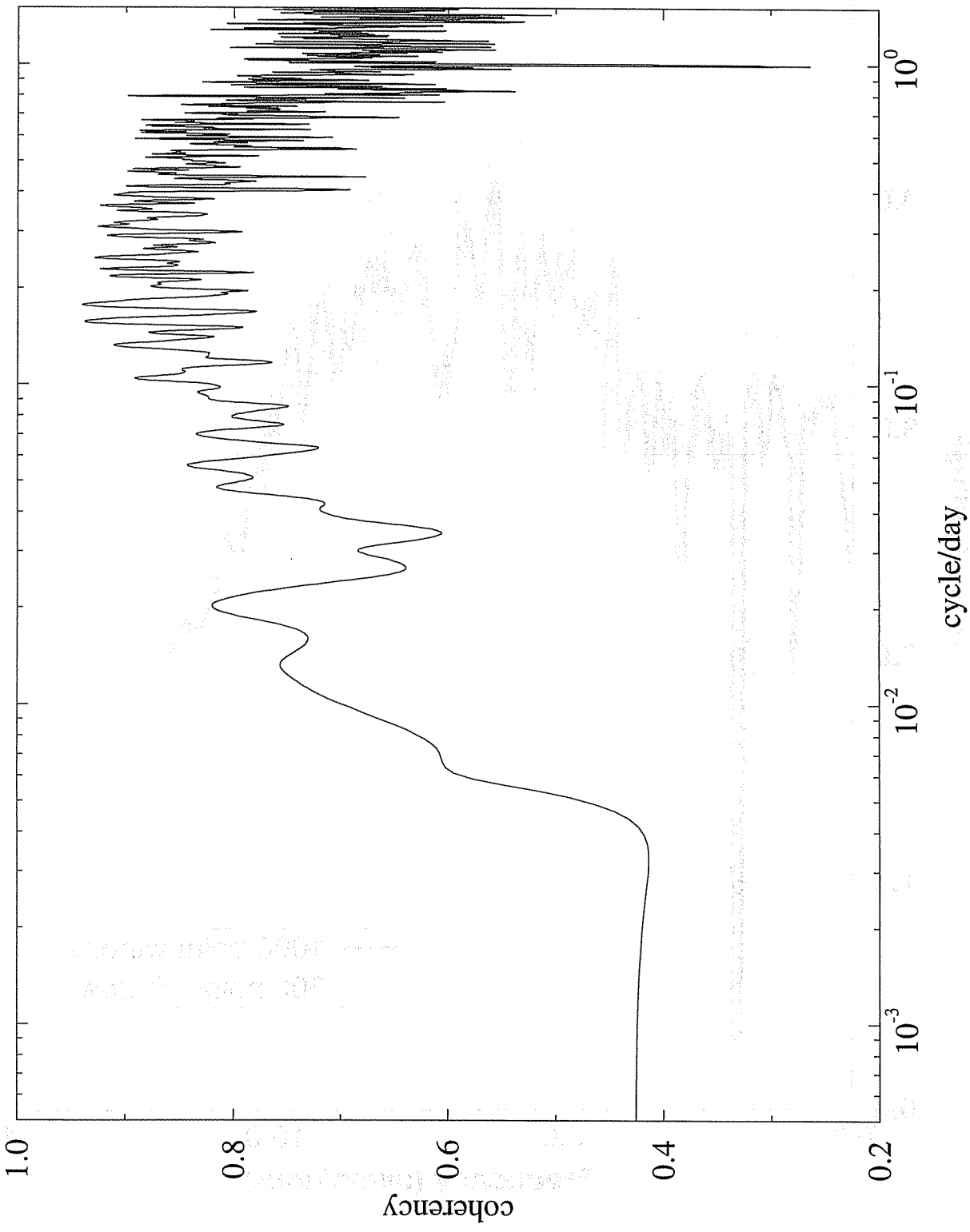

Figure 2: Spectral coherency between atmospheric pressure and gravity residual signals.

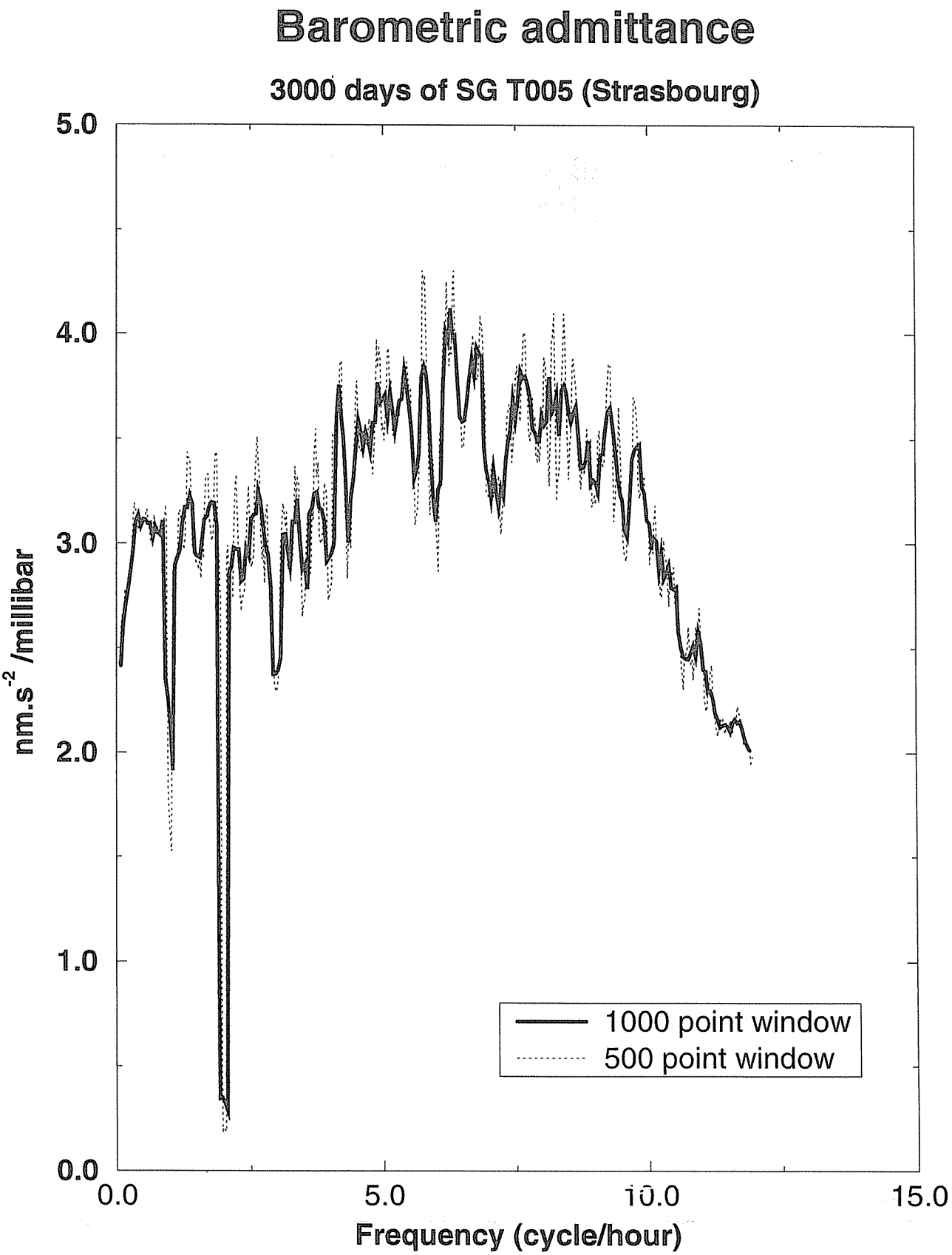

Figure 3: Local barometric admittance as a function of frequency as computed from pressure and gravity residues in Strasbourg for a 9 year long record (1987-1996).

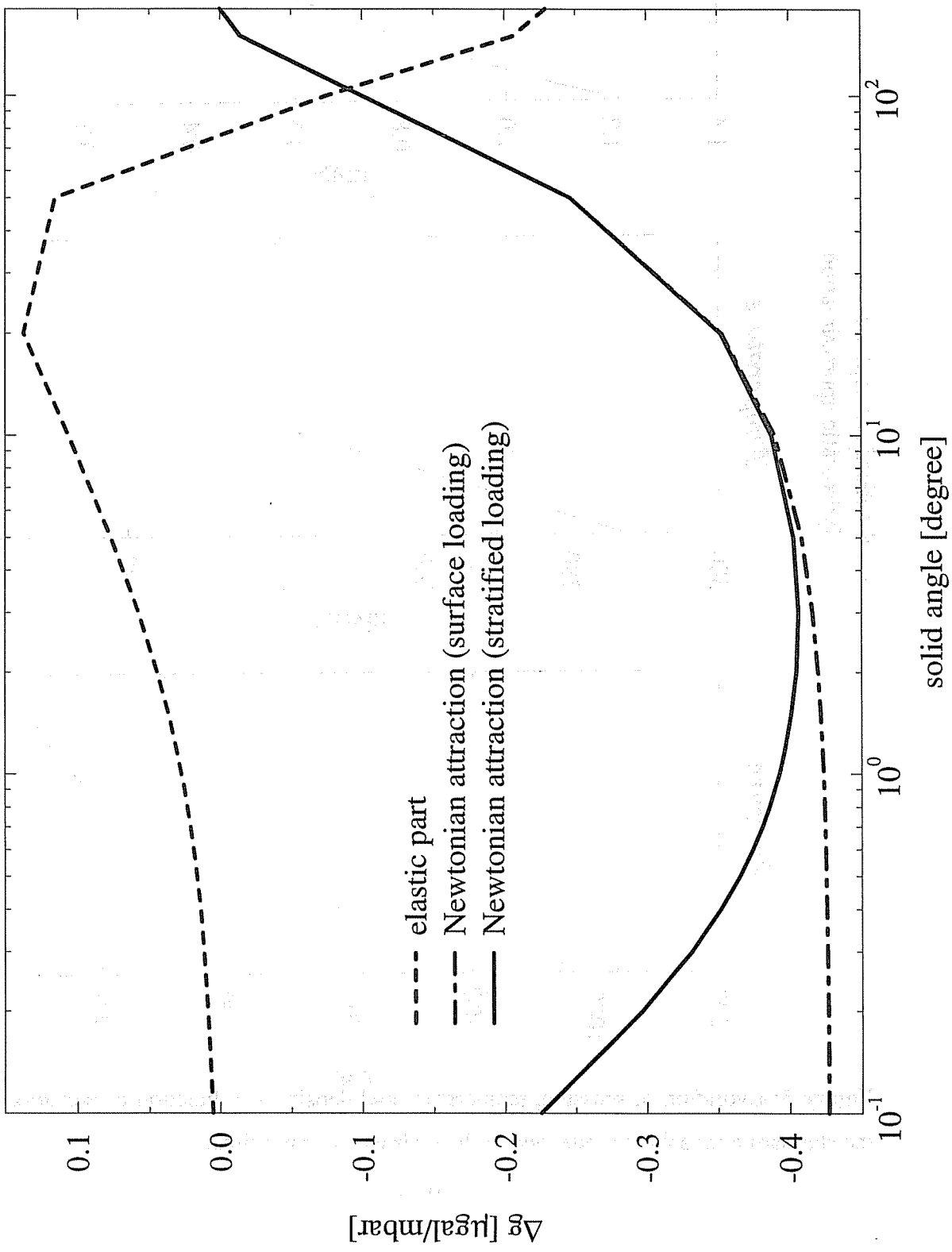

Figure 4: Gravity-induced effects from atmospheric pressure changes on spherical caps of increasing solid angles.

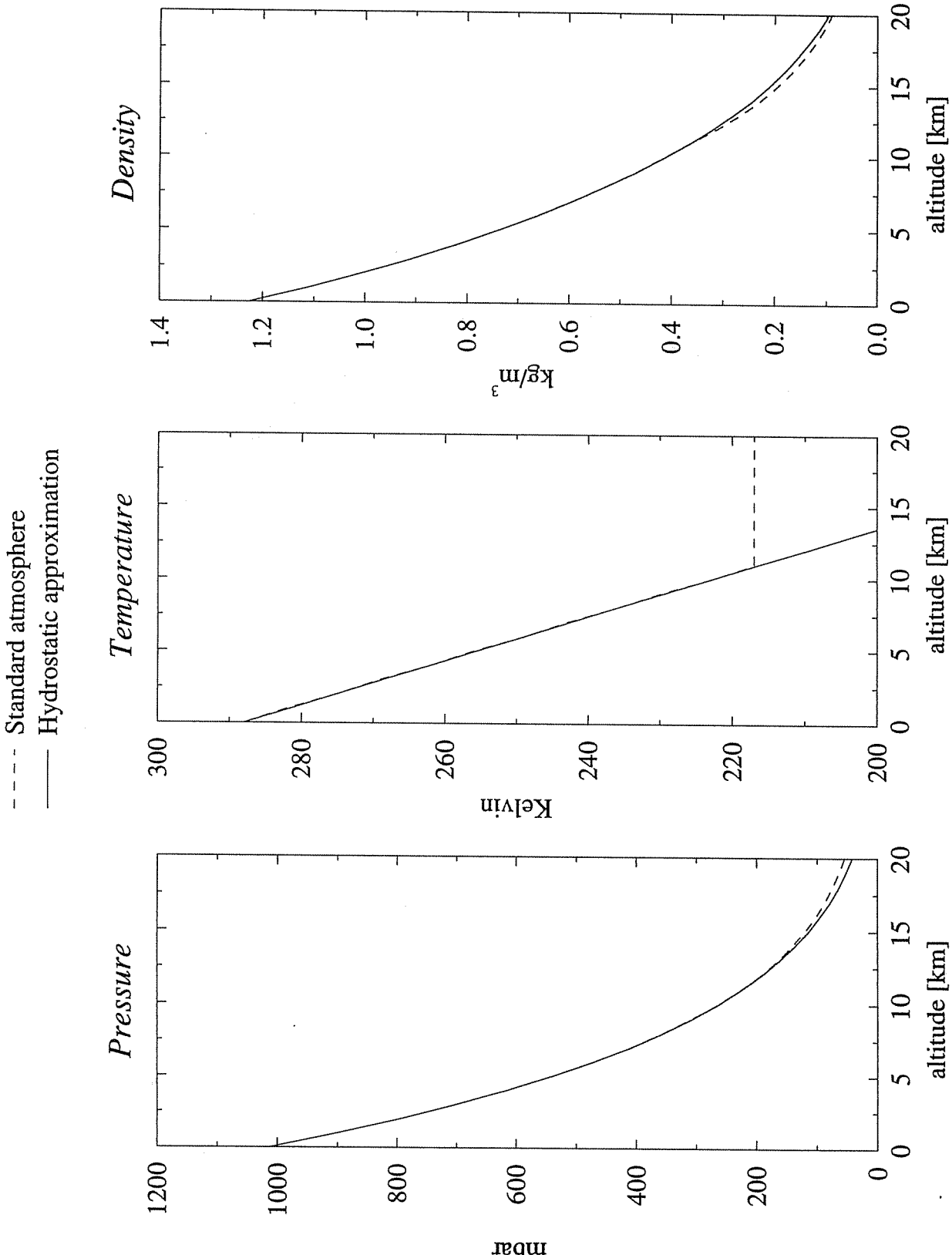

Figure 5: Evolution of pressure, temperature and density as a function of elevation for the standard atmosphere model and in the hydrostatic approximation.

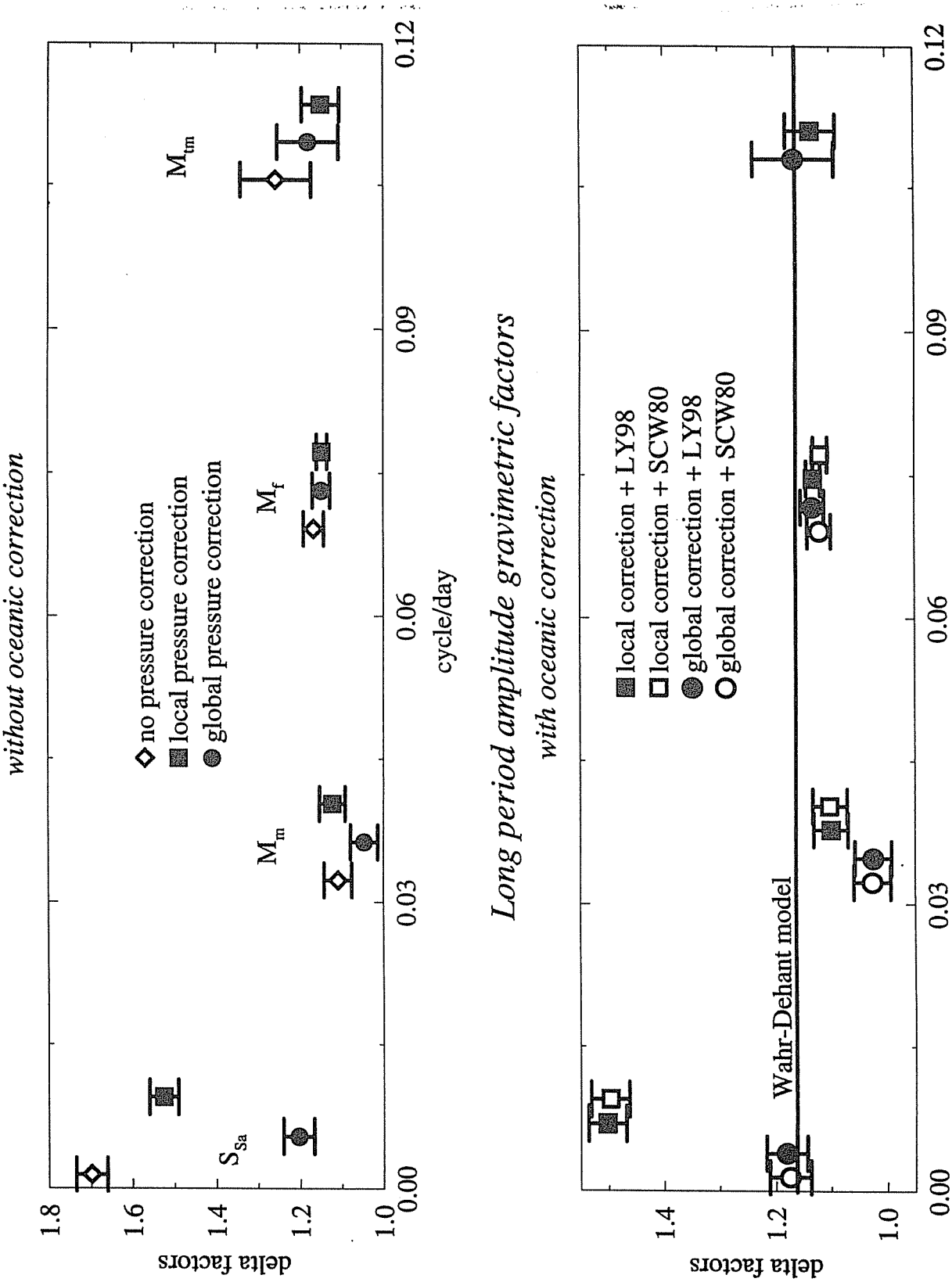

Figure 6: Long period amplitude gravimetric factors acccording to different hypotheses of atmospheric pressure and ocean loadings.

The separation of the tides M_3 and S_3 by appropriate wave group formation with regard to modern potential developments
- Arguments for establishing a wave group S_3 -

Wolfgang Schwahn

Bundesamt für Kartographie und Geodäsie
D-60598 Frankfurt a.M., Richard - Strauss - Allee 11
E-mail: lebed@no5.ifag.de

Abstract

In the present pilot study the impact of modern tidal potential developments on the optimal parametrization of the gravity variation by wavegroups is investigated in the terdiurnal range, especially in narrow range around 3 [cpd] (45 [°/h]). As an example, the wavegroup M_3 has been chosen. The new potential developments D exceed 3.0 cpd. Compared with the prominent M_{3D} wave at 2.89841 cpd (43.4761564 °/h) the maximum S_{3D}-tide at 3 cpd (45.00000 °/h) is in the order of 10^{-3}, in relation to near moon-related contributions at 3.007904 (45.118564) of 1/5 or $2* 10^{-1}$.

In the same spectral range there is a ***non-tidal-potential*** tidal-like gravimetric contribution S_{3PG}: Depending on the site, a strong air pressure tide S_{3P} with two side lobes due to an annual modulation produces S_{3PG}. Basing on D two variants of a new wavegroup have been studied:
(a) narrow range S_{3DA}-group, borders following the annual modulation of air pressure: 2.996667 ... 3.003333 cpd (44.95 ... 45.05°/h), like (b) and two moon waves at the left border,
(b) central S_{3DC}-group only: 2.99800 ... 3.00200 cpd (44.97 ... 45.03 °/h), only one sun wave.

For the gravimetric time series of the sites Potsdam, BFO, and Medicina (near Bologna) the numerical estimates for the gravimeter factor of these S_{3D}-groups will be given. For the station Potsdam (6 years of observations) the effect is maximum:

$$\delta(S_{3DA}) = 16.52 \text{ +- } 0.89, \kappa(S_{3DA}) = 57.47 \text{ +- } 3.07°,$$
$$\delta(S_{3DC}) = 21.73 \text{ +- } 0.91, \kappa(S_{3DC}) = 46.80 \text{ +- } 2.41°.$$

This confirms the prevailing air pressure influence. The parametrization was successful: the spectral peak in the residuals **disappears now completely** in contrast to the residuals obtained for a common M_3 - wavegroup. The parameters are different because of in S_{3DA} waves due to sun and moon have been integrated. The results for BFO and Medicina are discussed in short.

The influence of S_{3PG} on the gravimeter factor $\delta(M_3)$ obtained for a common M_3 - wavegroup (including the S_3-tidal region) is in the order of 10^{-3} due to the predominant contributions by the moon. Nevertheless to obtain from the point of view of geophysics pure **solid** earth tidal parameters, the region 2.99667 ... 3.00333 cpd, 44.95 ... 45.05 °/h with strong **air pressure** S_{3P} tide should
- be **omitted** in forming the wave group M_3,
- be established as a wavegroup of its own: S_{3DC}. The parameters are related to S_{3PG} .

Introduction

Modern potential developments (BÜLLESFELD (1985), TAMURA (1987), HARTMANN and WENZEL (1995), ROOSBEEK (1996)) include smaller tidal amplitudes and therefore a broader as well as denser spectral range than the previous one. In connection with this spectral

broadening and densifying it should be taken care that no other relevant gravimetric phenomenon than the solid Earth tide „occupy" just this modified extended / densified spectral region. Concerning the analysis of solid earth tides, the wave grouping based on modern potential developments must be arranged in accordance with this conception.

(1) Seen from a **geophysical** aspect there have been at least two criteria for arranging wave groups up to now:
(i) Due to the different and manifold influences of the sun (tidal forces, thermal tides, and atmospheric tides, esp. pressure ones) with respect to the moon (tidal forces only, very small air pressure tide M_{2P}, neglectable in gravimetry) on gravity time series, a decomposition into pure "moon wave groups" and "sun wave groups" is desirable. From this point of view the "moon wave groups" are more reliable for the purpose of Earth model validation than these mainly due to the sun. The wavegroup S_1 is the best example.
(ii) Due to the different degree in the tidal development and the different response of the earth on these forces a grouping into the groups with uniform degree is desirable. If this is not possible, then a beat period of the gravimeter factor according to the difference of the prominent constituents due to the different degree follows, for instance for the N_2 and L_2 wavegroups (SCHWAHN, ELSTNER, DITTDELD (1989)).

(2) In the light of **practical mathematics** wavegrouping depends on the length of the time series: The construction (shaping) of a separate wavegroup is possible if the product (difference in frequency $\Delta\omega$ in [°/h] , [cpd] resp. between the two large constituents) times (length of the time series L_{TS} in [hours] or [days] resp.) exceeds 360° or 1 cycle.

Considering (1) and (2) and the above noted aspect the paper will discuss and propose
- spectral distribution of the waves in the terdiurnal range,
- the possibility to discriminate and split up waves originated by sun or moon
- the results of tidal analyses of three gravity time series at Potsdam, BFO and Medicina.

The special discussion will be carried out due to the presence of strong (with respect to the tidal contribution) gravity contributions by air pressure spectral lines in the region of 2.9966667 up to 3.0033333 cpd (44.95 ... 45.05 °/h).

1. The amplitude spectrum of gravity waves in the terdiurnal range due to modern potential developments. Arrangement due to sun or moon

To compute the amplitude spectrum of the gravimetric tidal forces at Medicina near Bologna, Italy (co-latitude $\theta_{MEDICINA}$ = 45.478°, eastern longitude $\lambda_{MEDICINA}$ = 11.646°) the tidal potential development by HARTMANN and WENZEL (1995) and their formulas 17a, 17c, 18c with fully normalized LEGENDRE functions and their derivatives for the order m = 3, degree l = 3,4,5 were used. Fig. 1 presents in a logarithmic scale the amplitudes, which exceed $1*10^{-1}$ pms^{-2}, on the left hand the prominent M_3-wave (**5337** pms^{-2}, 0.5337 μgal), the fourth cluster from the left being the most interesting one for investigating the S_3-region (3 cpd, 45.00000°/h). The result of zooming this range is represented in fig. 2 (see also fig3, centre and lower part). At a glance, on 45.00000°/h an amplitude of **6**.44 pms^{-2} can be seen as well as at 45.04571°/h an amplitude of 7.05 pms^{-2}. The first is created by the sun, the latter by the moon. A complete sketch of the contribution by these two celestial bodies is given for the sun in the centre, for the moon in the lower part of fig. 3. Keep in mind (see fig.2) the contribution by the moon at 45.045710°/h in the order of **37**.85 pms^{-2}. (Note: for the site Potsdam the relations are nearly the same, only the absolute values are changed due to, e.g. for m=3, l=3 $\sin^3(\theta_{POTSDAM}) / \sin^3(\theta_{MEDICINA}) = 0.660042$).

2. The air pressure spectrum in the terdiurnal range at Potsdam

In fig. 3 the uppermost part is the representation of the spectrum in the terdiurnal range for the air pressure at Potsdam (ELSTNER and SCHWAHN, 1998). This is the spectral picture of a pure terdiurnal wave (ω_{S3} =45.00000 °/h) and its annual modulation ($\Delta\omega$ = 0.04106776 °/h) producing side lobes at ω_{S3} +-$\Delta\omega$, i.e. at 44.958932 °/h (2.997262 cpd) and 45.04106776 °/h (3.002738 cpd). These three air pressure waves produce at the same spectral places gravity waves S_{3PG} of non-tidal-potential origin (see e.g. ZÜRN and RYDELEK (1994), fig. 7). Comparing in fig. 2 vertically from left to right the non-tidal S_{3P} with the tidal waves S_{3D} it can be established that the left maximum in the pressure has a weak correspondence in the gravity forces by the sun, the central peak coincides with those due to the sun and the left hand peak with a small frequency shift (45.045710 - 45.041068 = 0.004642 °/h), with those due to the moon.
This statement relative to the moon is of importance: all the spectral lines in the air pressure spectrum are related to the sun's radiation **only**, especially the relation between the two side lobes (ELSTNER and SCHWAHN (1998)). In the spectrum of tidal forces there is at the place of right side lobe in pressure the Moon's contribution. This means that the annual modulation of S_{3D} is represented by a different origin – by the sun ***and*** the moon.

3. Formation of a S_3-wavegroup

In the „classical" development the spectrum ends below 3 cpd, the wavegroup M_3 is with in the limits 2.794392 (41.915886°/h) ... 2.97191 cpd (44.578605 °/h) (CHOJNICKI (1973)). Now, on the base of modern potential developments new wavegroups can be arranged. A common used proposal for the M_3-region is the range 2.75324 (41.298658°/h) up to 3.08125 cpd (46.21880°/h), TAMURA-wave numbers 1109 - 1190, BÜLLESFELD-wave numbers 1122 – 1204. Therefore within such a group the tidal-potential-waves 1177 – 1179 (TAMURA) or 1191 – 1193 (BÜLLESFELD) or the set of waves represented in fig. 3 in the range of S_3 +- 0,05 °/h (HARTMANN and WENZEL) extract from the observations the gravimetric contribution S_{3PG} of the pressure S_{3P} in so far as an optimum coincidence in amplitude and phase shift κ between both time series is aimed at by the least squares method. (Further influences S_{3I} in the observations may modify this relation).

Due to the facts that (i) there are (see fig. 3) only three waves larger than 1 pms^{-2} can be attributed to the logical intersection between the spectra S_{3PG} and S_{3D} and (ii) their relation to the predominant M_3 –wave is in the order of 10^{-3} the expectation follows that an influence on the results for the ***wavegroup*** M_3 as having been used up to now can be neglected. Practical results confirm this.

This situation is not satisfactory from the point of view of
- a clear discrimination of tidal-potential and non-tidal-potential contributions. At least, this region should be excluded,
- the parametrization of the gravity spectrum. Using as usually the broad M_3 –wavegroup then in the residuals a sharp spectral peak remains. This fact requires a parametrization!

As a first step the ***wavegroup*** M_{31} was confined to the "classical" upper border. Then, two wave groups S_{3D} for two ranges were designed:
(a) narrow range S_{3DA}-group, whose borders follow the annual modulation of air pressure: 2.996667 ... 3.003333 cpd (44.95 ... 45.05°/h), like (b) and two moon waves at the left border,
(b) central S_{3DC}-group only: 2.99800 ... 3.00200 cdp (44.97 ... 45.03 °/h), only one sun wave.

At last but not least a second ***wavegroup*** M_{32} (3.006667 ... 3.06666 cpd, 45.10 ... 46.000) was constructed to get an insight into tidal contributions of the order of a few ten pms^{-2}, or, in other words, of the order of a hundredth of the predominant M_3 –wave.

For practical aspects: when using short time series do not forget (see fig. 2) the strong contribution of the moon at 45.118564 °/h (37.85 pms^{-2}), i.e. five up to six times larger than central S_{3D} or the moon's contribution at 45.045710! The difference in frequency is approx. 0.073 °/h, i.e. for a time series of a half year it is impossible to shield the S_{3DA}-group from this influence.

4. Results

Here, only numerical results can be given. The success of parametrization will be discussed on the base of the residual spectrum provided by ETERNA 3.30 package (WENZEL (1998)). All considerations concerning air pressure corrections, the fine high-resolution structure of the residual spectrum and of other influences in the S_3 –region etc. must be delayed.
In the figures 4, 5 and 6 the residual spectra for the stations Potsdam, Black Forest Observatory (BFO) and Medicina have been plotted. In all figures from top to bottom

- (a) the residuals due to a M_3 wavegroup 2.541944 ... 4.347615 including the S_3- and the M_4-wavegroups.
- (b) the residuals due to wavegroups the M_{31}, S_{3DA}, M_{32}, and M_4.
- (c) the residuals due to M_{31}, S_{3DC}, M_{32} and M_4.

4.1 Potsdam (see fig. 4)
The gravity time series of the site Potsdam, SCG TT70 (see, e.g. DITTFELD (1998)) in the time interval 06/1992 – 10/1998 (6.4 years) has been analyzed. The gravimeter factors are

$$\mathbf{\delta(S_{3DA}) = 16.52 +- 0.89,\ \kappa(S_{3DA}) = 57.47 +- 3.07°,}$$
$$\mathbf{\delta(S_{3DC}) = 21.73 +- 0.91,\ \kappa(S_{3DC}) = 46.80 +- 2.41°.}$$

$\delta(M_{32})$ as well as $\delta(M_4)$ are not significant. The residual spectrum is shown in fig. 4. Here no spectral peak is left in the residuals for (b) and (c). The parametrization was successful, in (c) a small deviation points on the right side lobe. $\mathbf{\delta(S_{3DC})}$ **is relevant only.** The difference between the gravimeter factors consists in the incorporation of moon terms in $\mathbf{S_{3DA}}$ **in contrast to** $\mathbf{S_{3DC}}$ and reduces the value because no such good approximation could be found as for (one) sun wave. Further analyses must follow esp. on the character of the modulation.

4.2 Black Forest Observatory (see fig. 5)
For a quick study of a short time interval the Bfet1907.dat (02/1991 – 11/1991, 9 months) in the ETERNA 3.30 software package was used. The gravimeter factors S_{3DA} and S_{3DC} are in the order of 5, but the spectral peak does not vanish for (b) and diminishes by ¼ from 120 to 90 pms^{-2} on the half for (c), i.e. the least squares approximation takes away the persistent term in S_{3PG} for (c). The parametrization for (b) is unsuccessful also due to the fact of an insufficient spectral distance to the neighbouring spectral peak in D. The time interval is too short.

4.3 Medicina near Bologna (see fig. 6)
Two years of gravity observations 11/96 – 10/98 by the superconducting gravimeter SG023 in Medicina in the framework of SELF II have been analyzed, sampled in 10-sec-sampling rate, compressed by least squares to 1-min-samples and then decimated in the TSoft-routine to 10-min-samples. From the uppermost part in fig. 6 can be concluded that there are no accentuated spectral peak with respect to the other two stations in contrast to the predicted dependence in latitude of S_{3P}. As a consequence the parametrization fails and in case (b) an artifact appears.

5. Conclusions

The rise of modern potential developments enables the parametrization of the gravity spectrum in the terdiurnal range in terms of wavegroups due to the tidal potential. Prerequisite for such an investigation is a long-term time series which allows a high resolution.
For the M_3-wavegroup presently in use the error for the gravimeter factor due to their wide borders is in the order of 10^{-3} . This may have been sufficient up to now for the check of Earth models, but it is not optimal for obtaining a **white gravity residual spectrum** in the presence air pressure tides.

Acknowledgements: I thank the staff of the Stazione Radioastronomica di Medicina as well as the personnel of the Gravimetric Department of the Bundesamt fuer Kartographie und Geodäsie for the support given in the registration and analysis of the gravimetric time series of the SG023 at Medicina, my special thanks go to Mr. P. WOLF and Mr. G. HARNISCH. I am very also grateful to Dr. H.-J. DITTFELD, GFZ Potsdam, for placing the time series of the TT70 at my disposal, Prof. H.-G. WENZEL for the ETERNA 3.30 package, P. VAUTERIN, ROB, for providing me with the TSoft package. Dr. G. WEBER, BKG, supported me with the graphic software.

Literature

BÜLLESFELD, F.-J. (1985): Ein Beitrag zur Darstellug des gezeitenerzeugenden Potentials. DGK, Reihe C, Heft Nr. 314, München 1985

DITTFELD, H.-J. (1998): The long-periodic constituents in the SG TT70 record at Potsdam. Proceed. 13th Intern. Sympos. Earth Tides Brussels 1997, ed. B. DUCARME and P. PAQUET, 599 - 605, Brussels 1998

CHOJNICKI, T. (1973): Ein Verfahren zur Erdgezeitenanalyse in Anlehnung an das Prinzip der kleinsten Quadrate. Mitt. Inst. Theoret. Geodäsie Bonn, Nr. 15, Bonn 1973

ELSTNER, C.; SCHWAHN, W. (1998): Precise Mean Parameters for Daily and Subdaily Persistent Air Pressure Waves at Potsdam for the Period 1893 – 1992. Proceed. 13th Intern. Sympos. Earth Tides Brussels 1997, ed. B. DUCARME and P. PAQUET, 469 – 476, Brussels 1998

HARTMANN, T.; WENZEL, H.-G. (1995):Catalogue HW95 of the tide generating potential. Bull. Inf. Marees Terr., vol. 123, 9278 – 9301, Bruxelles 1995

SCHWAHN, W.; ELSTNER, C.; DITTFELD, H.-J.(1991): Third degree effects producing temporal variations of the gravimetric tidal parameters for N_2 and L_2 wave groups. Proceed. 11th Inter. Sympos. Earth tides Helsinki 1989, 645 – 653, Stuttgart 1991

TAMURA, Y. (1987): A harmonic development of the tide-generating potential. Bull. Inf. Marees Terr., vol. 99, 6813 - 6855

WENZEL, H.-G. (1998): Earth Tide Data Processing Package ETERNA 3.30: The Nanogal Software. Proceed. 13th Intern. Sympos. Earth Tides Brussels 1997, ed. B. DUCARME and P. PAQUET, 487 - 494, Brussels 1998

ZÜRN, W.; RYDELEK, P.A. (1994): Revisiting the Phasor-Walkout Method for detailed Investigation of Harmonic Signals in Time series. Surveys in Geophysics, vol. 15, 409 - 431

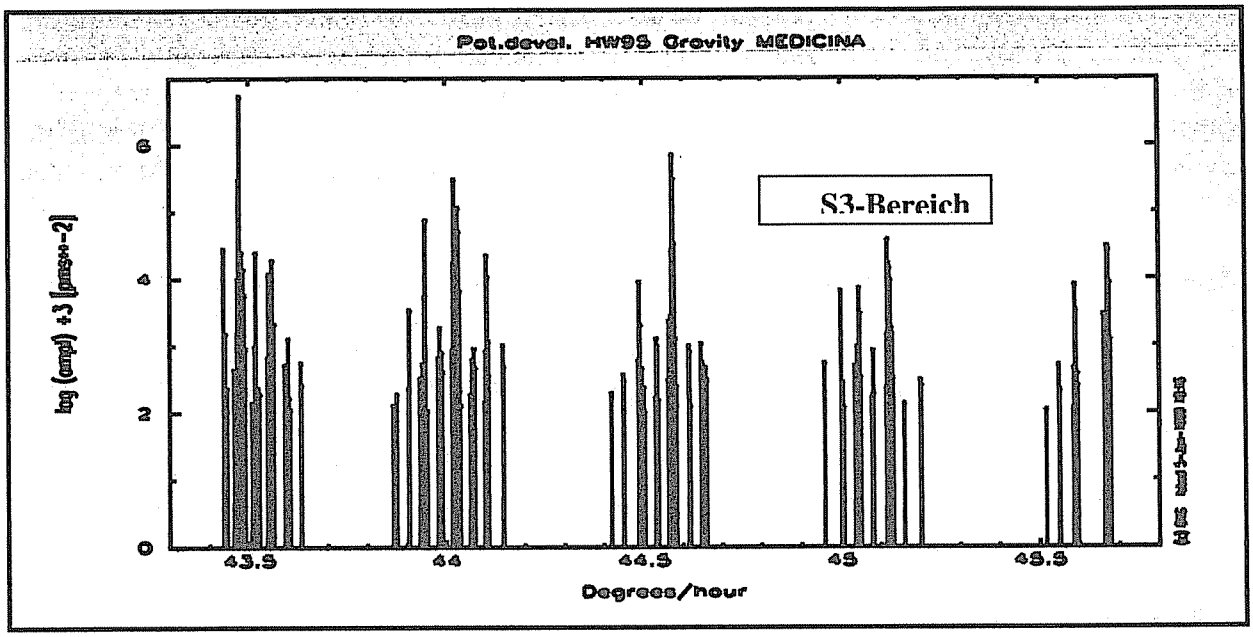

Fig. 1: Amplitude spectrum of tidal gravity at Medicina on the basis of the tidal potential by HARTMANN and WENZEL (1995) in logarithmic scale, unit pms^{-2}, 3 corresponds to 10^0, waves with amplitudes < 10-1 pms^{-2} being omitted. Note the value of M_3 (left) with respect to the cluster at 45°/h, the region of interest is considered in this paper.

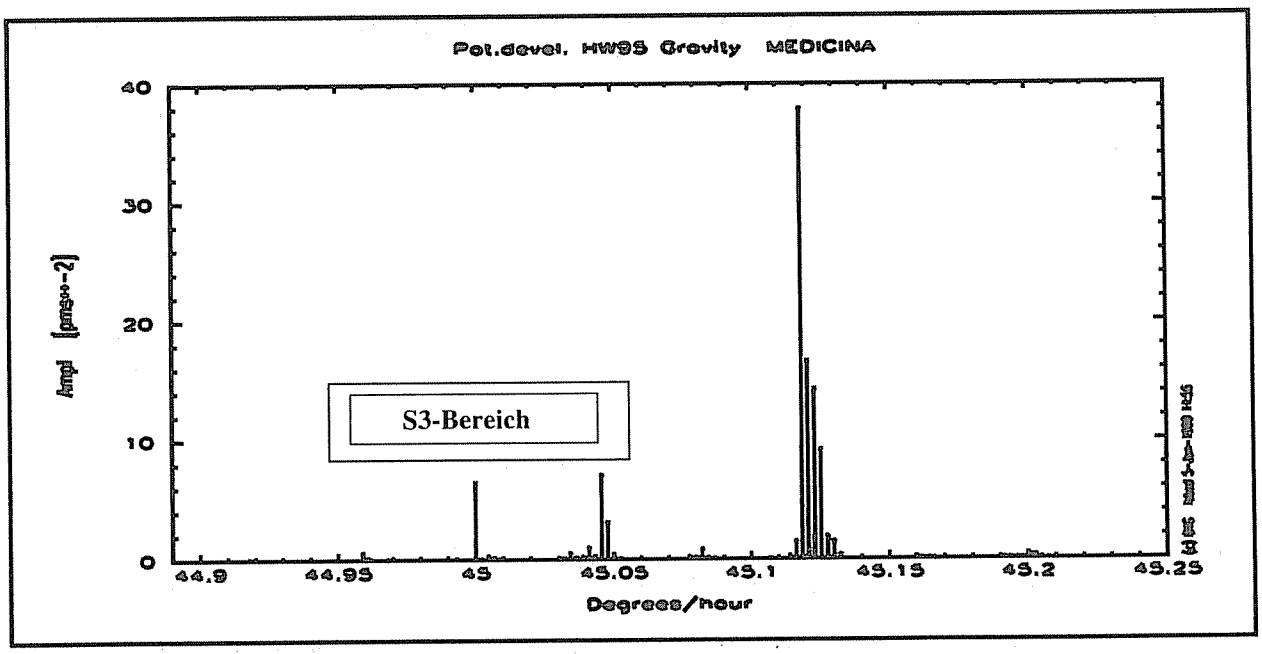

Fig. 2: High resolution spectrum in the region of 45°/h. Here, a few waves are in the neighbourhood of 45°/h in the order of 6 ..7 pms-2 and , at 45.11, a few of 37 pms^{-2}.

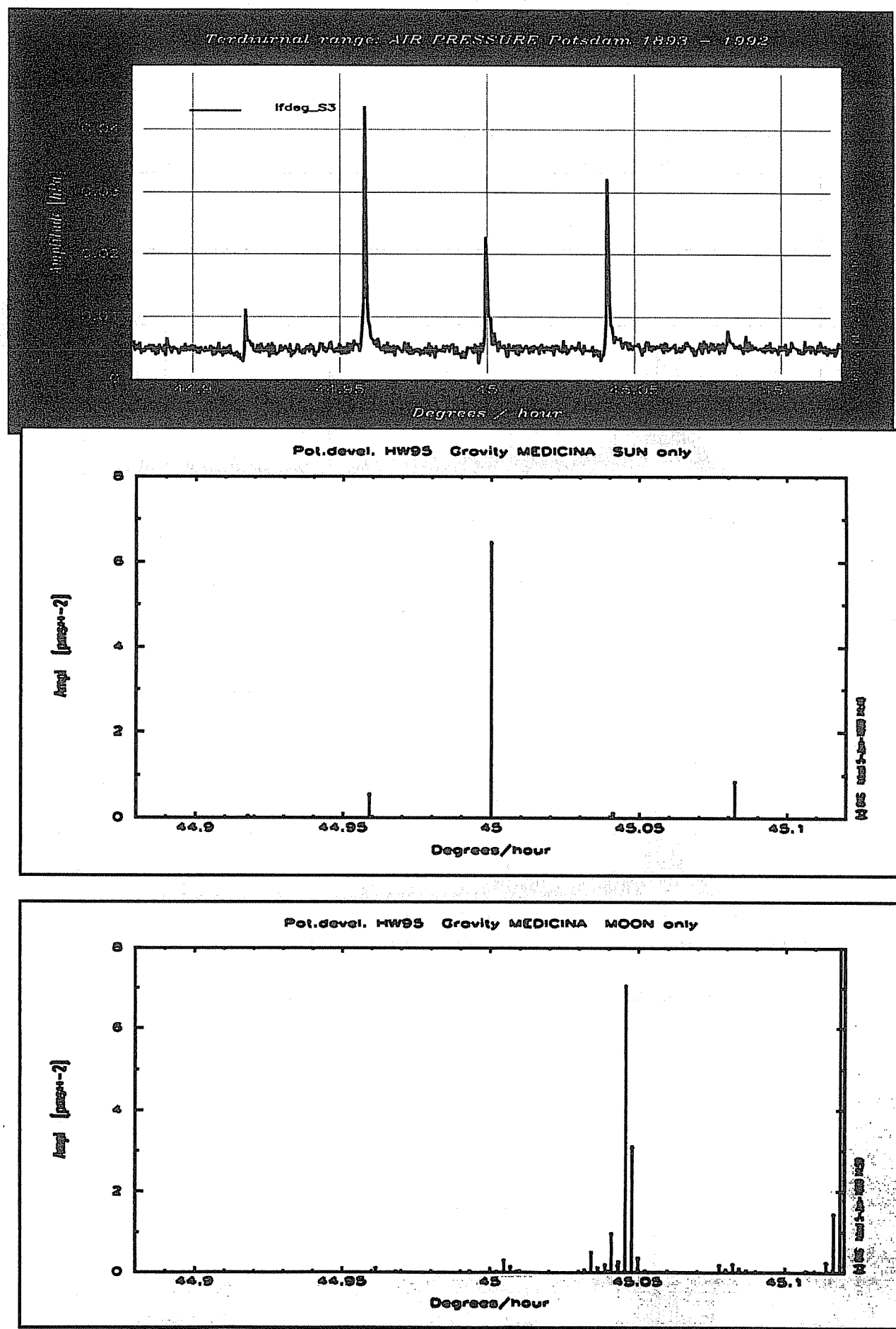

Fig.3: Amplitude spectrum in the very narrow band 44.88 ... 45.12 °/h for (from top to bottom) (for Potsdam the gravity spectrum must be multiplicated by 0.66)

- air pressure at Potsdam (ELSTNER and SCHWAHN (1998)),
- gravity at Medicina due to the sun
- gravity at Medicina due to the moon.

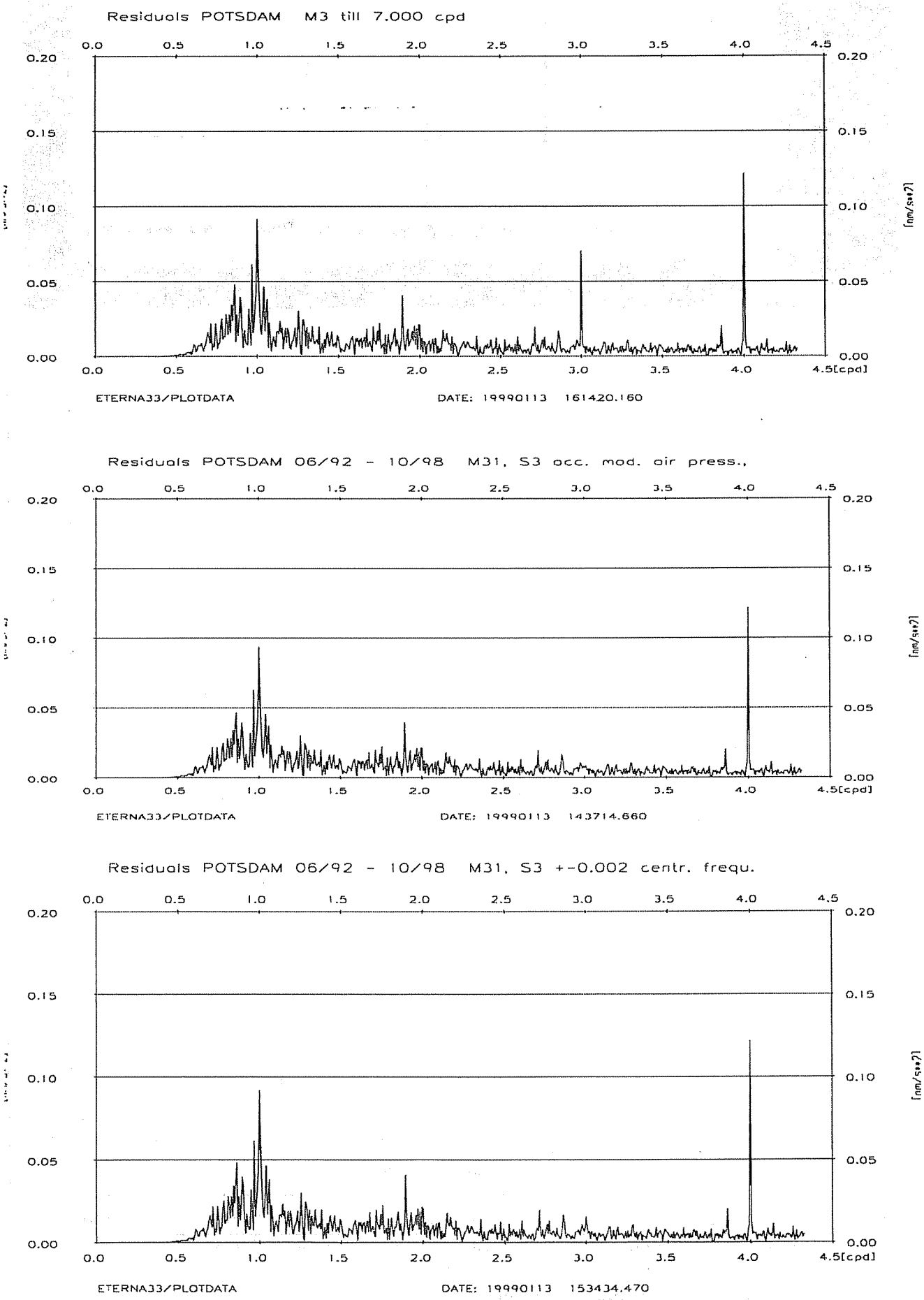

Fig.4: Gravity residual spectra for the site Potsdam, using different wave group arrangements for the parametrization of the gravity variation.

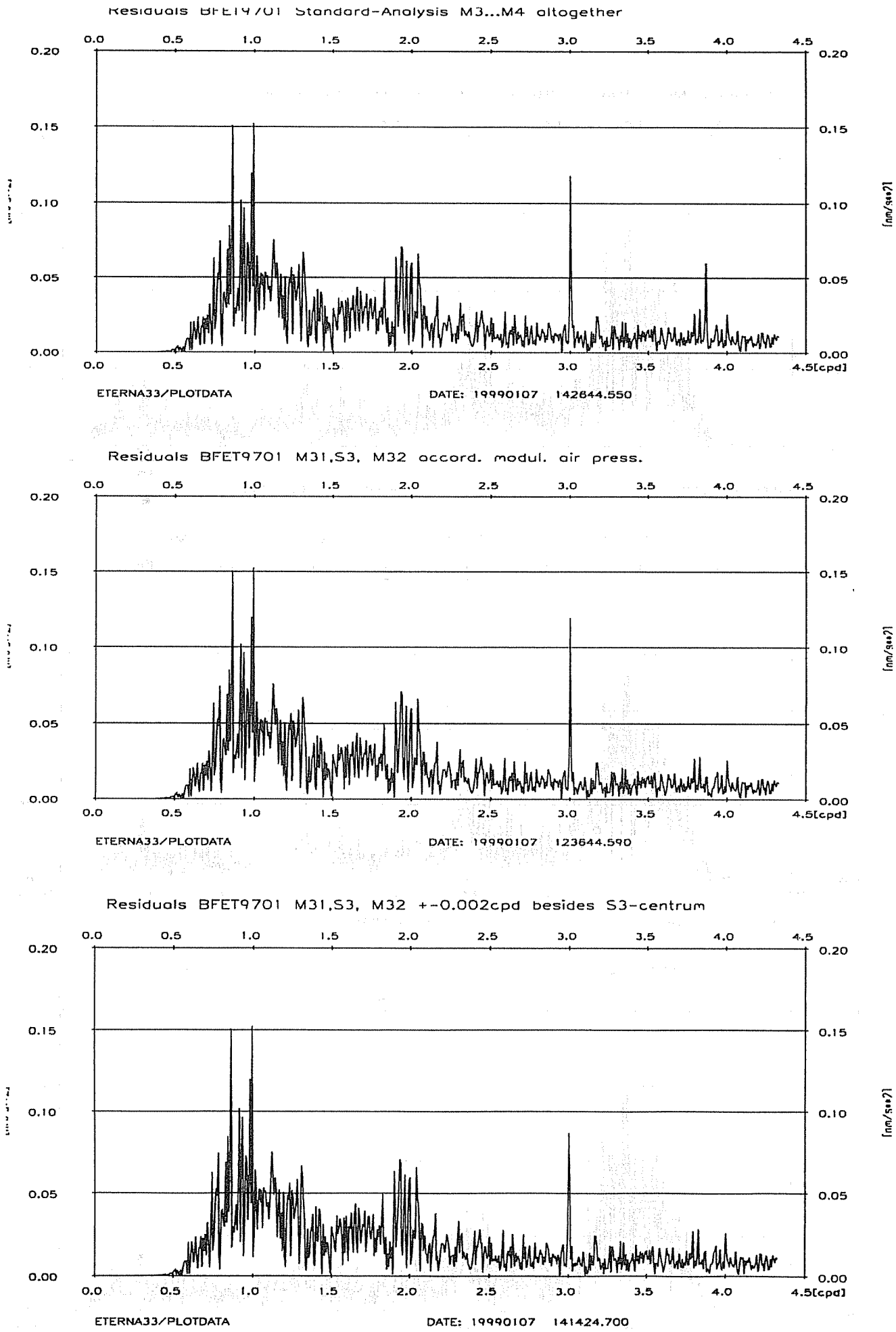

Fig.5: Gravity residual spectra for the site BFO, using different wave group arrangements for the parametrization of the gravity variation.

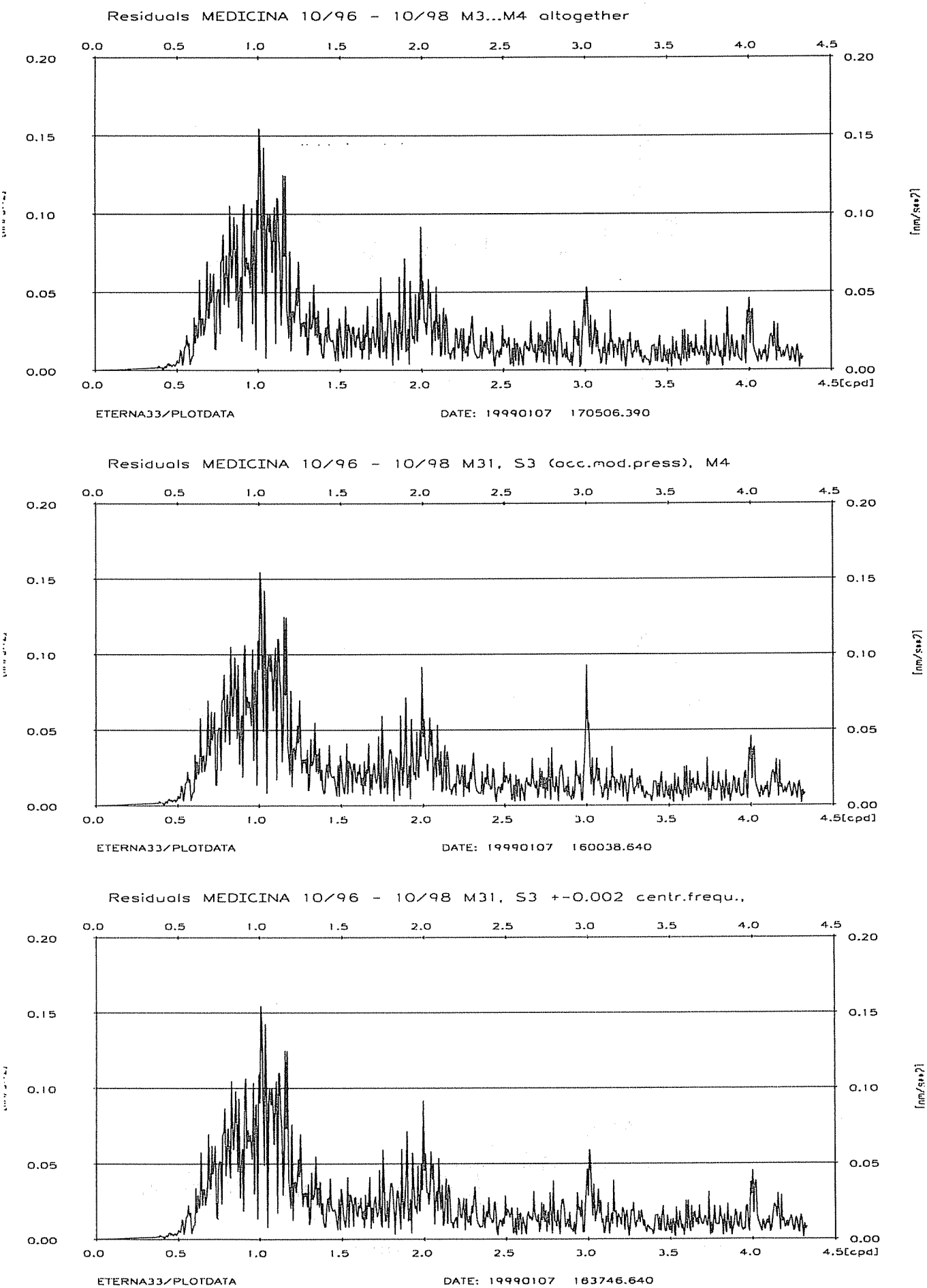

Fig.6: Gravity residual spectra for the site Medicina using different wave group arrangements for the parametrization of the gravity variation.

Gravity signals from atmospheric waves and their modeling

by

Udo Neumann and Walter Zürn

Geophysical Institute, Karlsruhe University, Hertzstr. 16
D-76187 Karlsruhe, Germany
and
Black Forest Observatory Schiltach, Heubach 206
D-77709 Wolfach, Germany,

Abstract

The influence of local air pressure on seismic and deformation records is well established observationally and theoretically. However, most work has been done at periods of several hours and longer. Gravity-acoustic waves are an abundant phenomenon in the atmosphere with a wide frequency range and they also corrupt seismic records. Here we present a simple model for the effects of such waves and apply it to two examples in the period range between 5 minutes and one hour: the Lamb wave generated by the explosion of Mount St. Helens in 1980 and a local wave-like pressure disturbance at BFO ($48.33^{o}N$, $8.33^{o}E$, 589 m amsl).

1 Introduction

Gravity observations are influenced by local barometric pressure at periods longer than one hour (e. g. Warburton and Goodkind, 1977). Corrections for these effects can be applied with success with a simple frequency-independent or slightly frequency-dependent regression coefficient (e. g. Crossley et al. 1995). Variance reductions of up to 90 % are possible. These effects appear to be rather well understood as the Newtonian attraction of the sensor mass by the air masses overhead (mainly) and additional effects due to loading of the earth's surface by these masses: free air effect, inertial forces, tilts and so on.

At periods of about an hour and less only very few studies have been carried out. Grosse-Brauckmann (1979) studied the effects of air-pressure correlated noise in a borehole-tiltmeter and found that tilt by loading was the dominating mechanism in the free mode frequency band. Müller and Zürn (1983) modeled the effects of passing cold fronts on the output of the ET-19 gravimeter at BFO (period range between 10 minutes and one hour) with Newtonian attraction by the air and found good agreement with the observations in magnitude and phase. Zürn and Widmer (1995) were able to lower the noise level in data from the same gravimeter after the Shikotan earthquake (OCT 4, 1994) for periods between 500 and 5000 s to the extent that in one case the previously hidden fundamental spheroidal free oscillation ${}_{o}S_{2}$ clearly stood above the noise floor. A simple frequency-independent coefficient of 3.4 $nm/s^{2}/hPa$ was used in this case. This success could be repeated with several other

quakes (see Zürn et al. 1999, this volume). Virtanen (1996) and Van Camp (1998) tested this procedure successfully also using the records from different superconducting gravimeters for different earthquakes. Likewise Beauduin (1996) and Beauduin et al. (1996) succeeded in improving the free mode spectra from their STS-1 seismometers (Wielandt and Streckeisen 1982) at SSB after the Macquarie Ridge event of May 23, 1989 by correcting for local barometric pressure using a frequency-dependent complex admittance. The best results were obtained for three horizontal seismometers.

Recent results by Japanese colleagues (e. g. Suda et al. 1998) indicate, that at periods between 150 and 500 s the lowest vertical noise levels are defined by incessantly excited fundamental spheroidal free oscillations ${}_oS_l$ of the earth, probably excited by energy input from the atmosphere. This partially explains, why the procedure used successfully at longer periods ceases to work (Zürn and Widmer 1995). At shorter periods of around 100 s it is long known (e. g. Sorrels 1971; Peterson 1993) that local atmospheric turbulence correlates with noise, especially so for horizontal components. At periods of 4 to 20 s the well-known marine microseisms are dominating the noise spectrum on all components. So for periods of 500 s and shorter there is little chance for possibilities to "correct" the records in a deterministic manner.

Impressed by the observation of the atmospheric Lamb waves sent around the world by the explosion of Mount St. Helens, USA (e. g. Bolt and Tanimoto, 1981, Müller and Zürn 1983), and by rather frequent observation of wave trains simultaneously in the barometer and seismograph records, we decided to try to model these signals in order to get a better understanding of long-period seismic noise. In the following section we present results for a simple model, thereafter we apply this model to two observations.

2 Theory

We will not consider the theory of waves in the atmosphere, this subject is covered by Hines (1972), Francis (1975) and Gossard and Hooke (1975). A modern application of the linearized theory can be found in Kanamori et al. (1994), in which the authors explain seismic observations during the eruption of Mount Pinatubo in 1991. Our purpose here is to study the non-instrumental effects of atmospheric waves on seismic and deformation observations on the earth's surface or below. We will consider examples having periods between several minutes and 1.5 hours or so, because we have observations in this range. A particular solution (for zero vertical particle velocities) of the linearized wave equation for the atmosphere are the *Lamb waves*, which are trapped near the surface of the earth, travel horizontally with phase velocities equal to the speed of sound and decay vertically. They present the simplest case of gravity-acoustic waves and therefore we take those as a model, but we leave the phase velocity variable. Gravity waves in general propagate obliquely and their horizontal phase velocity is an order of magnitude less than the speed of sound (e. g. Egger et al. 1993 report speeds of 7 and 27 m/s for two cases observed in Antarctica). More details can be found in Neumann (1997). We consider a homogeneous elastic half-space with the Lamé constants λ and μ below an isothermal atmosphere (the theory for a layered half-space is

treated by Neumann 1997). The surface of the half-space is the x-y plane, the z-axis points upward. It can be shown (e. g. Gossard and Hooke 1975, Neumann, 1997) that this atmosphere supports Lamb waves with the following density distribution:

$$\rho(x,y,z,t) = \hat{\rho} \cdot exp(-\frac{z}{H\gamma}) \cdot exp(j(k_h \cdot x - \omega \cdot t), \tag{1}$$

where $\hat{\rho}$ is the peak density deviation from equilibrium, t is time, H the scale height of the atmosphere, γ the coefficient of adiabatic expansion, k_h the horizontal wave number and ω the angular frequency of the plane wave propagating horizontally in x-direction. The pressure disturbance follows a similar relation with peak pressure:

$$\hat{p} = c^2 \cdot \hat{\rho} \tag{2}$$

where c is the speed of sound, while $c_h = \omega/k_h$ is the horizontal phase velocity of the wave. The signals from such a wave on gravi-, seismo-, tilt- and strainmeters can readily be computed from the previous equations (Sorrels, 1971; Neumann, 1997). The sensor is located at positions x_a, $y_a = 0$ and $z_a \leq 0$. The r.h.s of the following equations (4) to (13) have to be multiplied by the factor

$$exp(k_h z_a) \cdot exp(j(k_h \cdot x_a - \omega \cdot t)) \tag{3}$$

where $j = \sqrt{-1}$. The results for the gravitational attraction of the sensor mass by the air are for the vertical component:

$$g_z^A(x_a, z_a) = 2 \cdot \pi \cdot G \cdot \frac{\hat{p}}{c^2} \cdot \frac{H\gamma}{1 + k_h H\gamma} \tag{4}$$

with the gravitational constant G. The horizontal component of attraction is:

$$g_x^A(x_a, z_a) = \pm j \cdot 2 \cdot \pi \cdot G \cdot \frac{\hat{p}}{c^2} \cdot \frac{H\gamma}{1 + k_h H\gamma}. \tag{5}$$

Since the horizontal phase velocities of atmospheric waves are at most of the order of the sound speed , i. e. 330 m/s, we do not include the inertial terms in the equations of motion of the elastic solid. Our solutions are therefore static solutions for the elastic medium. The displacement field was computed following Sorrels (1971) and from its components the following signals are derived. The free air gravity effect due to vertical motion of the sensor in the undisturbed gravity field of the earth at the surface:

$$g_z^F(x_a, z_a) = -\left|\frac{\delta g}{\delta z}\right| \cdot \frac{1}{2\mu} \cdot \left[\frac{\lambda + 2\mu}{(\lambda + \mu)} - k_h \cdot z_a\right] \cdot \frac{1}{k_h} \cdot \hat{p} \tag{6}$$

where g is the local gravitational acceleration and $\delta g/\delta z$ is the vertical gravity gradient. The inertial effect associated with this motion is:

$$g_z^I(x_a, z_a) = -\frac{1}{2\mu} \cdot \left[\frac{\lambda + 2\mu}{(\lambda + \mu)} - k_h \cdot z_a\right] \cdot \frac{\omega^2}{k_h} \cdot \hat{p} \tag{7}$$

The horizontal acceleration from the tilt is:

$$g_x^T(x_a, z_a) = \pm j \cdot g \cdot \frac{1}{2\mu} \cdot \left[\frac{\lambda + 2\mu}{(\lambda + \mu)} - k_h \cdot z_a \right] \cdot \hat{p} \tag{8}$$

The inertial effect from the horizontal acceleration is accordingly:

$$g_x^I(x_a, z_a) = \pm j \cdot \frac{1}{2\mu} \cdot \left[\frac{\mu}{(\lambda + \mu)} + k_h \cdot z_a \right] \cdot \frac{\omega^2}{k_h} \cdot \hat{p} \tag{9}$$

and finally we get the strains:

$$\epsilon_{xx} = -\frac{1}{2\mu} \left[\frac{\mu}{(\lambda + \mu)} + k_h \cdot z_a \right] \cdot \hat{p} \tag{10}$$

$$\epsilon_{zz} = -\frac{1}{2\mu} \left[\frac{\mu}{(\lambda + \mu)} - k_h \cdot z_a \right] \cdot \hat{p} \tag{11}$$

and

$$\epsilon_{xz} = \pm \frac{1}{\mu} \cdot k_h \cdot z_a \cdot \hat{p} \tag{12}$$

The last equation vanishes for $z_a = 0$, which satisfies the boundary condition at the free surface.

For extremely long wavelength $k_h = 0, \omega = 0, c_h = 0$ all horizontal accelerations vanish and the vertical Newtonian attraction (e. g. Müller and Zürn 1983) is described by:

$$g_z^B = 2 \cdot \pi \cdot \frac{G}{g} \cdot \hat{p} \tag{13}$$

The ratio of the vertical attraction by a Lamb wave and this "Bouguer"-plate model is:

$$\frac{g_z^A}{g_z^B} = \frac{1}{1 + \frac{\omega \cdot c^2}{g \cdot c_h}} \tag{14}$$

since $H \cdot \gamma / c^2 = 1/g$. This means that the vertical attraction by the "Bouguer"-plate is an upper limit.

3 The Mount St. Helens Lamb wave

When Mount St. Helens, U.S.A. exploded on May 18, 1980 it sent an air pressure wave around the earth, which was recorded on microbarographs, but also on seismographs and gravimeters (Ritsema, 1980; Bolt and Tanimoto, 1981; Bath, 1982; Müller and Zürn, 1983; Delclos et al., 1990). The group velocity of the first arrival was estimated from our records to be 308 m/s, a result confirmed by other authors. The peak amplitude of pressure at BFO was 0.23 hPa. The pressure wave train is shown in Figs. 1 and 2 (top traces) and in Fig. 11 of Müller and Zürn (1983). The speed of the wave and the long distances it traveled suggest it to be a Lamb wave.

Since because of BFO's efficient air-lock the wave signature in the ambient pressure was reduced by at least an order of magnitude, buoyancy and other direct influences on

the sensors can essentially be ruled out as an explanation of the observations. We used the model and equations from the previous section to determine the theoretical effects on a gravimeter (ET-19) and two horizontal seismometers (STS-0, i. e. prototypes of STS-1, e. g. Wielandt and Streckeisen 1982). The gravimeter and its installation as well as the air-lock at BFO are described in Richter et al. (1995). However, the time constant of the air-lock was later found to be longer than 20 h, rather than the 4 hours quoted by Richter et al. (1995). Fig. 1 shows the pressure signal and the gravity record (mode channel: Müller and Zürn, 1983) together with theoretical effects computed from the pressure record. These computations were performed in the frequency domain. The gravity record was instrument corrected in the frequency domain also. We used 308 m/s for the phase speed, identical Lamé constants of granite $3.37 \cdot 10^{10} kg/m/s^{-2}$, a scale height of 8 km and a surface gravity gradient of $3 \cdot 10^{-6} s^{-2}$. The Lamé constants correspond to P- and S-wave velocities of 6.18 and 3.57 km/s, respectively. If we make the rock softer (fractures,cavities etc.), the inertial and free air effects grow with respect to the attraction. Our values are most probably a bit too high. Anyway, the free air effect is essentially negligible and the inertial effect dominates the theoretical signals. The dotted curve in Fig. 1 is the total synthetic signal, however, we delayed this in time by 40 s. Even so, the fit to the data is not really good, we can only claim to obtain the order of magnitude and partial alignment of several oscillations. However, there are two difficulties with this comparison. First, the pressure record had to be hand-digitized from a chart record with a speed of 3 cm/h and a sensitivity of 15.0 mm/hPa. 40 s correspond to 0.33 mm on the chart record which was about the width of the trace. Secondly, the oscillations at the very beginning of the gravity record were identified with the Rayleigh wave R_2 (major arc) from a quake in Yugoslavia almost 3 hours earlier. This leads to the conclusion, that unfortunately our Lamb wave signal is corrupted by R_3 from the same quake (minor arc plus one full tour around the globe). Due to the proximity of the source to BFO, the amplitude of R_3 cannot be expected to be much smaller than R_2 even on a spherically symmetric earth model, and with the real 3-D earth with lateral heterogeneities it could be quite a bit larger or smaller. Neumann (1997) tried to model these wave trains with synthetic seismograms and with other earthquakes in that area, but no significant improvement of the fit could be obtained. Some of the higher frequency gravity oscillations having no counterpart in the pressure signal are probably due to this wave train.

Both problems exist for the comparison of the horizontal seismograms to the theoretical pressure signals in Fig. 2 as well. Note that the dotted traces were not shifted as in Fig. 1, because here it would make the fit worse. We have not multiplied the theoretical traces with the direction cosines corresponding to the direction of arrival $N327°E$ of 0.839 (NS) and -0.545 (EW), since there are more uncertainties in our model anyway. The polarity of the NS-seismogram is inverse to seismological convention. Tilt is clearly dominating theoretically in the case here and again with decreasing rigidity of the halfspace this and the inertial signal would be amplified with respect to the attractional part. The fit of the synthetic signal to the EW-seismogram is not bad at all, but we have to keep the timing uncertainty and the R_3 wave train in mind. However, the same is not the case for the NS-component: there is a very clear phase

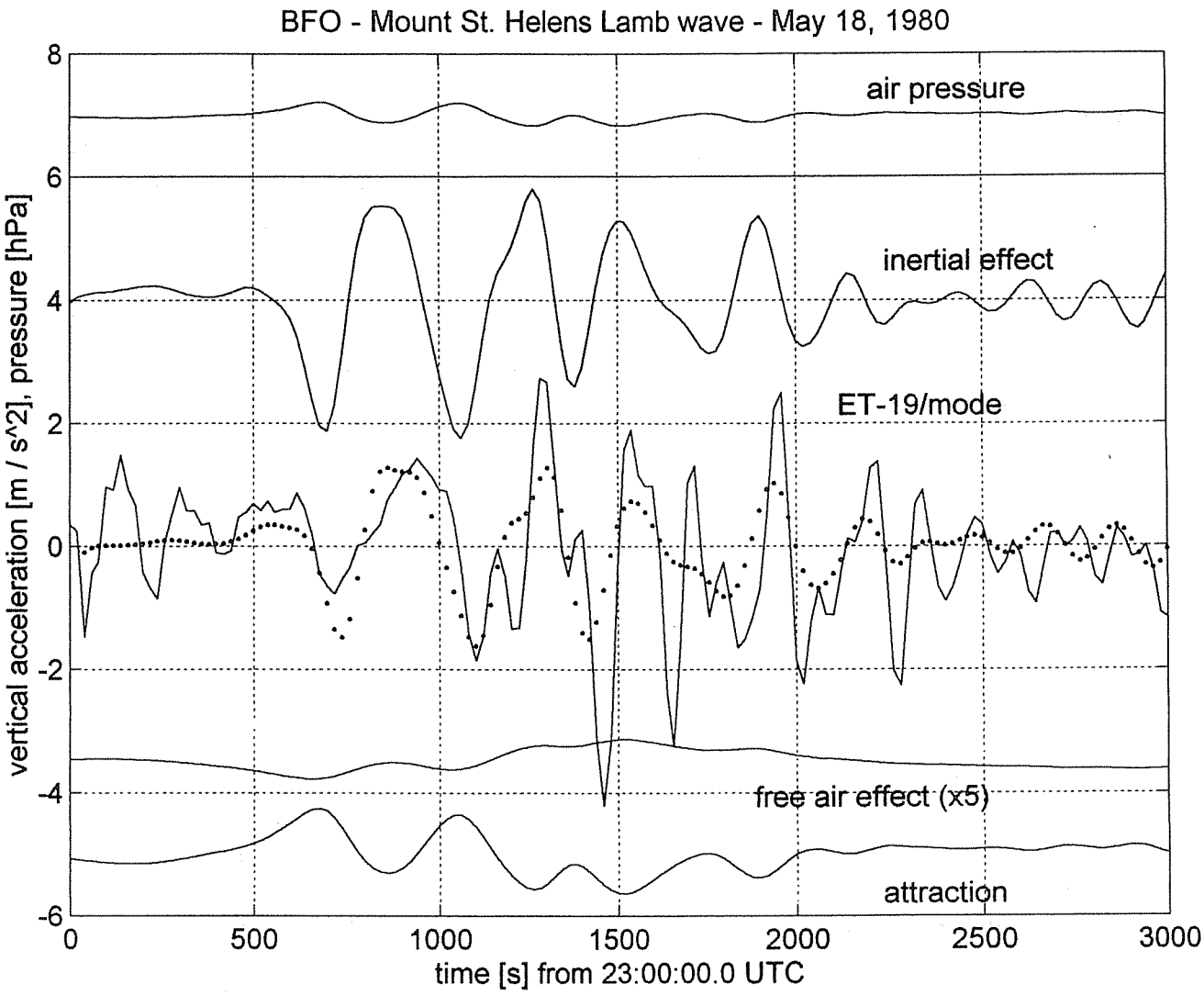

Figure 1: Time series of air pressure (top), theoretical attraction (bottom), inertial (2.) and free air (4.) effects and the gravity signal from the mode channel of ET-19. Note that the free air effect was multiplied by 5. The dotted curve corresponds to the sum of the theoretical contributions, but delayed by 40 s (two samples). See discussion in the text.

shift for this with respect to the EW-component and to the synthetics. The particle trajectory in the horizontal plane is clearly elliptical with the major axis pointing towards Mount St. Helens roughly (Neumann 1997). The NS-seismogram is much closer in phase with the direct pressure signal and there is a possible explanation. Eqs. (5) and (8) to (12) show, that all the contributions to the horizontal seismograms are out of phase with the pressure and vertical contributions, but also with the strain signal. This leads us to suspect (again) so-called strain-induced tilts (King et al. 1976), which could be quite large at these long periods and quite different for different components. The strain in the direction of propagation was multiplied by a strain-tilt coupling factor c_{st} of 2.5 $nrads/10^{-9}$ and added to the synthetics for the NS-component improving the fit considerably. Additional improvement could have been obtained by fine tuning this factor, but we feel this is not really worth while considering all the other uncer-

tainties. This strain-coupled tilt signal is also shown in the bottom trace. A serious problem arises here: the coupling factors needed for adjustment of the phase of the synthetics to the NS-data were of the order of 2.5 $nrads/10^{-9}$. If we form the ratio r of strain-coupled tilt to the direct tilt from eqs. (8) and (10) we find:

$$r = \frac{c_{st}}{2} \cdot \frac{1 - 2 \cdot \sigma}{1 - \sigma} \tag{15}$$

where σ is Poisson's ratio of the half-space (0.25 so far). Increasing Poisson's ratio reduces r and therefore fitting the phase would require c_{st} to be even larger. Of course, c_{st} is not independent of μ and λ, but depends mainly on geometry. For modeling of earth tide tilts and strains factors of up to 50 were produced in a demonstration, but even factors of one were on the large side (Emter and Zürn, 1985; Harrison, 1985). Of course, small baseline instruments like seismographs are more likely to be affected, and probably the observations of Beauduin et al. (1996) are another example of strain-tilt couling with the strains produced by loading.

4 The signal of June 28, 1994

Many times at BFO and certainly other stations wavelike oscillations in barometric pressure were observed simultaneously with similar oscillations in records of gravimeters, for example. One fine example from June 28, 1994 is the subject of this chapter (Fig. 3 to 5). In contrast to the Lamb wave discussed above, we were not able to identify the type of oscillation clearly, despite considerable efforts by Neumann (1997). A barometric record from station J9 near Strasbourg (distance to BFO about 70 km) did not show these oscillations, even considering very low speeds of the order of 10 m/s. Neither speed and backazimuth nor horizontal or vertical wavenumbers could be derived from additional observations or information. The oscillations were observed clearly at BFO with the gravimeter ET-19, 3 STS-1 and 1 STS-2 seismometers and on 3 invar-wire strainmeters (Widmer et al. 1992).

For lack of better information we chose the average value of the two cases recorded by Egger et al. (1993), 17 m/s, for our models. Since the periods of the oscillations were about 1000 s, this corresponds to a wavelength of 2.7 km. Other model parameters were identical to the ones used for the case of Mount St. Helens. Fig. 3, 4 and 5 show the data from the ET-19 gravimeter, the two horizontal components of the STS-1 station and the three invar-wire strainmeters at BFO, together with the atmospheric pressure record, theoretical signals derived from it using the Lamb wave and Bouguer models for comparison. All observations were digitally recorded at 5 s intervals (after low-pass filtering) with a resolution of 22 bits. The time series were band-pass filtered between 0.3 and 8 mHz using a single-pole Butterworth filter to remove the tides and high frequency noise. The data were converted to hPa, nm/s^2 and 10^{-9} and corrected for instrumental response (frequency domain).

Fig. 3 shows the vertical components with upward accelerations positive. The inertial and free air effects from the Lamb wave model were multiplied by factors of 5 and 20, respectively, before plotting. Newtonian attraction is clearly dominating. However, when the total Lamb wave model is compared to the observations, it is clearly

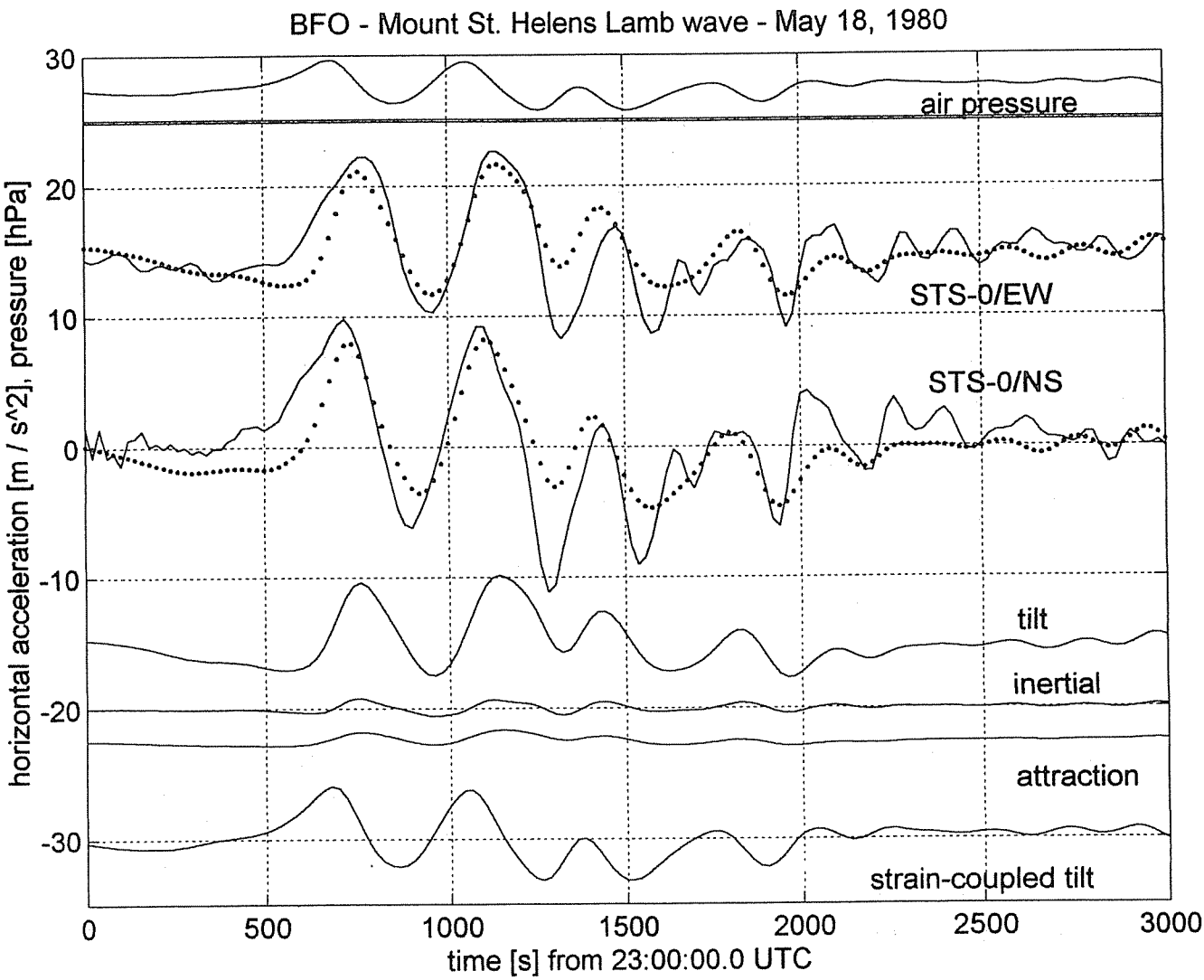

Figure 2: Time series of (top to bottom) air pressure (in dPa), the EW- and NS-seismograms from the STS-0 seismometers after instrumental correction and the tilt, inertial, attraction and strain-coupled tilt effects computed from the air pressure signal. The dotted traces represent the sums of three (EW) and four (NS) theoretical contributions. See discussion in text.

underpredicting the observed gravity variations, while the simple Bouguer model explains them very well, not only during the stronger oscillations but through the full time span. We conclude that the corresponding Lamb wave would need a much larger horizontal phase velocity to account for the observed gravity signal.

Fig.4 shows the air pressure, the theoretical horizontal accelerations derived from it using the Lamb wave model and the EW- and NS-seismograms after modification. The synthetic models (dotted lines) do by far not fit as well as for the vertical component, although conspicuous phase shifts were partially removed by introducing an additional strain-induced tilt as in the case of the Mount St. Helens wave above. The STS-1 and STS-0 seismometers were located on different piers in the same vault, which could make a significant difference in strain-tilt coupling (e. g. Beauduin et al. 1996). The

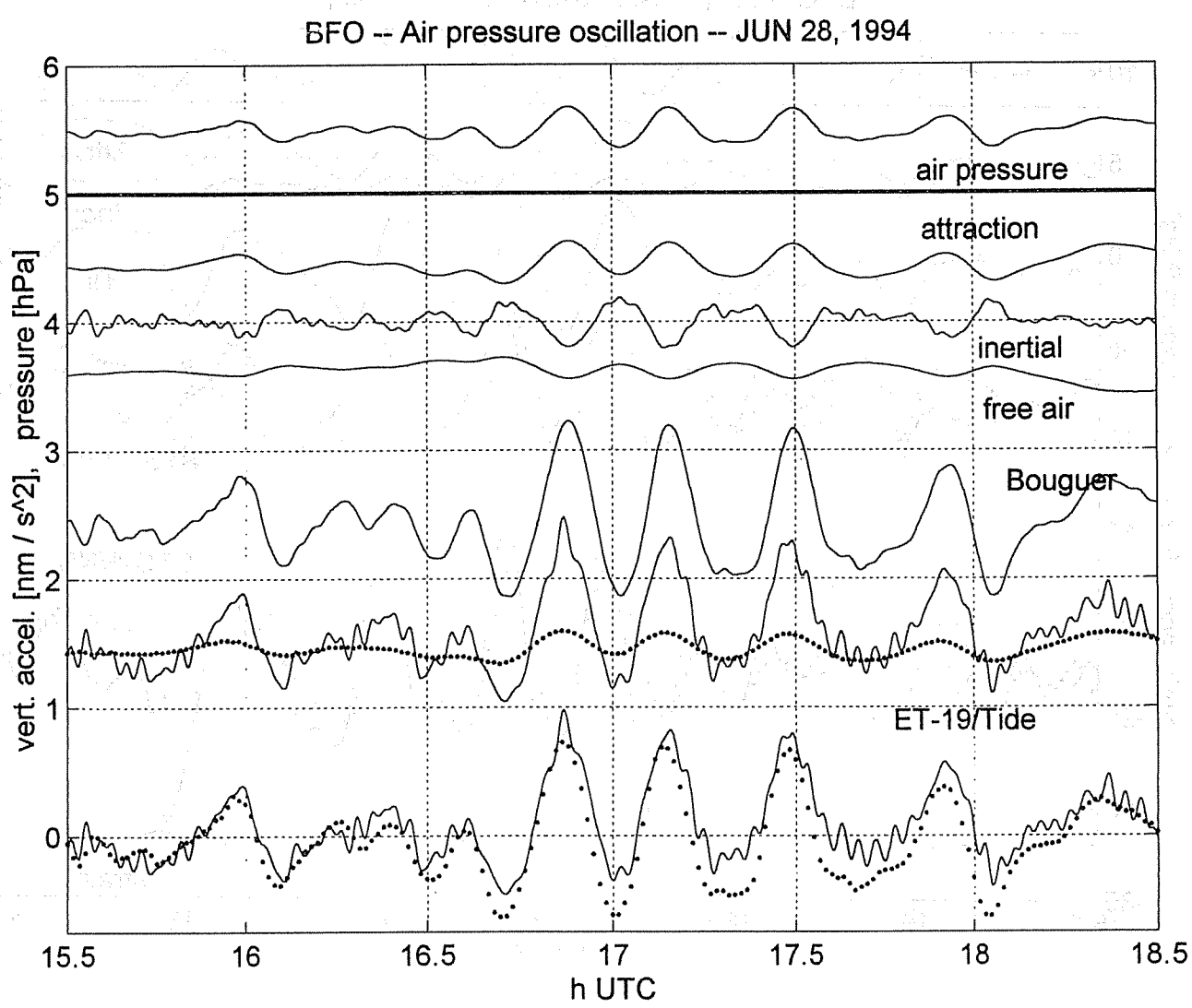

Figure 3: Time series (top to bottom) of air pressure, attraction, inertial and free air effects computed from the pressure using the Lamb wave model, the attraction effect from the Bouguer model and the gravity record compared to the two models (dotted lines) without any adjustment. The inertial and free air effect were multiplied by factors of 5 and 20, respectively. See text for details.

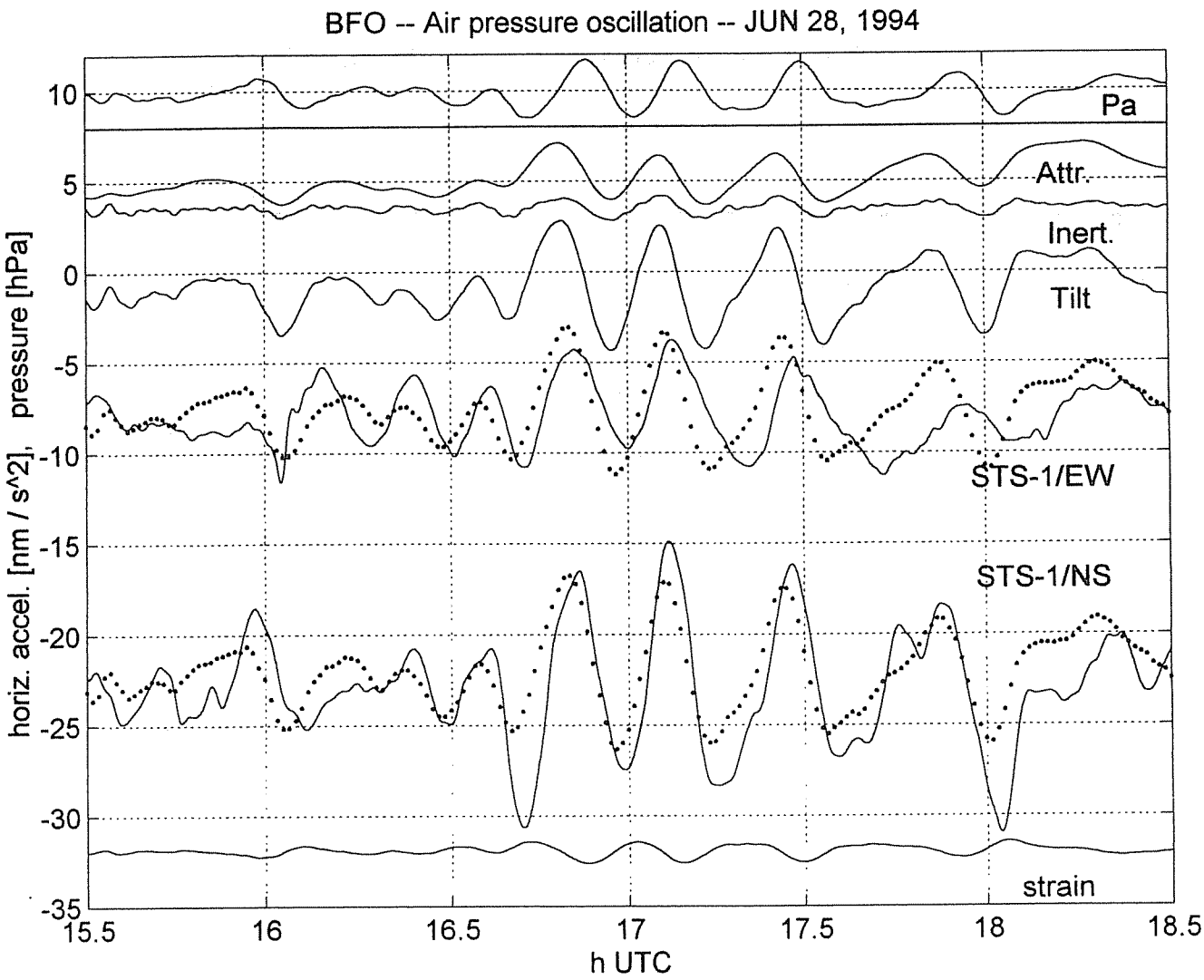

Figure 4: Time series (top to bottom) of air pressure (in dPa), the attraction, inertial and tilt effects from the Lamb wave model and the horizontal accelerograms in EW- and NS-direction. The strain in direction of propagation of the wave is plotted at the bottom (in 10^{-9}, but multiplied by 5). The attraction and inertial effects were multiplied by factors of 10 and 50, respectively before plotting. The synthetic seismograms (dotted lines) comprise attraction, inertial and tilt effects as well as strain-coupled tilts with factors of 2.5 (NS) and 2.1 $nrads/10^{-9}$ (EW), respectively.

factors used were 2.5 and 2.1 $nrads/10^{-9}$ for the NS- and EW- component, respectively. Only brief attempts were made to improve the fits by trial-and-error, since too many uncertainties exist concerning the atmospheric wave itself. No direction cosines were applied to the model, since the backazimuth of the wave is not known. Because of the phase shifts between the observed components due probably to strong strain-tilt coupling the arrival direction cannot be determined from the observations with any confidence. It appears that changing the strain-coupling factors only did not allow to adjust phase and amplitude of the oscillations simultaneously. So the modeling of horizontal accelerations is again much more difficult than for vertical ones.

Finally in Fig. 5 we show the air pressure, the strain computed for the Lamb wave model and the three straingrams from the BFO-array (Widmer et al. 1992). Without any adjustment the computed synthetic fits the recorded strain very nicely. For a traveling plane Lamb wave there should be much stronger variation with strainmeter azimuth no matter what the propagation direction would be. Actually the amplitude would vary with $cos^2(\phi)$, where ϕ is the angle between propagation direction and strainmeter azimuth. Since the strain signals are very clear we must draw the conclusion, that either the atmospheric phenomenon responsible for them was not a traveling plane wave, or that local modification of the strain tensor destroys the $cos^2(\phi)$ pattern. Actually, we fitted the barometric pressure to the observed strains and obtained regression factors of 0.61, 0.71 and 0.83 $10^{-9}/hPa$ for St-0, St-3 and St-4, respectively. The theoretical value for our model (direction cosines neglected) would be 0.7425 $10^{-9}/hPa$ with the same polarity: higher pressure causing rock compression.

5 Conclusions

Two quite different cases of atmospheric oscillations with periods from 5 minutes to about half an hour were producing signals on gravity-, seismo- and strainmeters. These variations were highly suppressed in the immediate vicinity of the instruments by the air-lock at BFO. A simple model of a Lamb wave was used to model these effects and we present comparisons of model calculations and observations. In the first case, the Lamb wave generated by the explosion of Mount St. Helens on May 18, 1980, modeling was handicapped by a tertiary wave train from an earthquake and lack of timing precision in the pressure record. Nevertheless the gravity signal could be explained in magnitude by mainly the inertial effect, but the waveform was not really well matched. The horizontal seismograms could only be explained in magnitude and phase by invoking strain-induced tilts. A second clear oscillation on June 28, 1994 was very well modeled in gravity and strain, not so well in horizontal accelerations. Again strain-induced tilts had to be added in the latter case to get even close to the signals. Lack of information on the atmospheric phenomenon (we only have the local barometric data) prevents us to constrain the models to a higher degree.

Acknowledgements: We thank Jacques Hinderer for providing pressure records from station J9 (near Strasbourg). We also use this occasion to thank the colleagues at Stuttgart (E. Wielandt) and Fürstenfeldbruck (M. Beblo, E. Schmedes, M. Feller) for

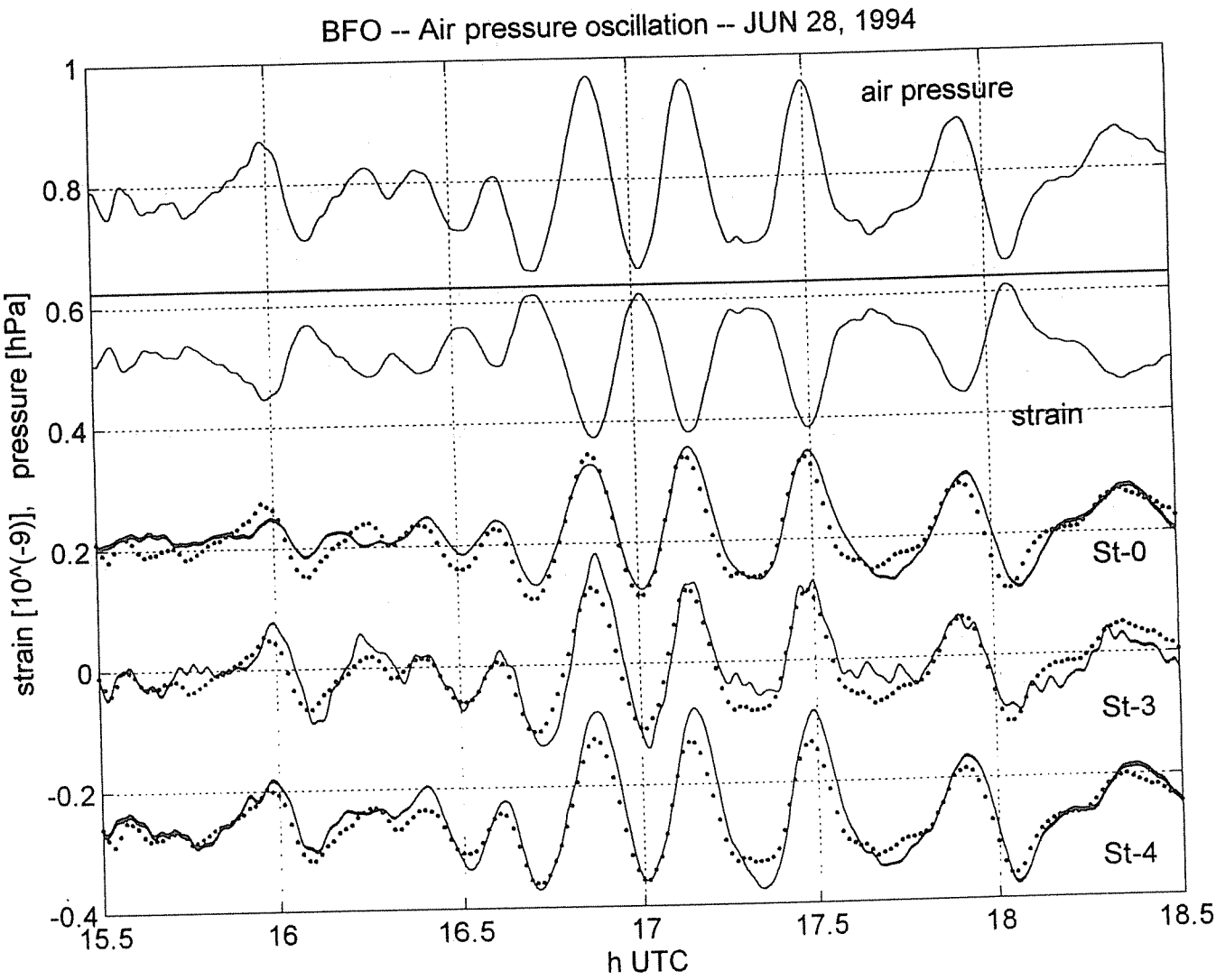

Figure 5: Time series of (top to bottom) air pressure, extensional strain in propagation direction computed from the Lamb wave model and observed linear extensions for the three invar-wire strainmeters St-0 (azimuth $N2^oE$), St-3 ($N33^oE$ and St-4 ($N60^oE$). The dotted lines correspond to the computed strain without any adjustment. Positive excursion corresponds to rock compression, so increasing air pressure compresses the rocks in all three directions

running microbarographs now. Many discussions with Erhard Wielandt and Rudolf Widmer-Schnidrig are appreciated. We also benefitted from the work Axel Roehm did during his Diploma thesis.

References

Bath, M. (1982). Atmospheric waves from Mount St. Helens. *EOS (Trans. Am. Geophys. Union)*, **63**: 193.

Beauduin, R. (1996). Étude du bruit de fond sismique à l'aide des données GEOSCOPE et des données de l'expérience OFM/SISMOBS. Thèse de doctorat, Université de Paris VII, pp. 130.

Beauduin, R., P. Lognonné, J. P. Montagner, S. Cacho, J. F. Karczewski and M. Morand (1996). The Effects of Atmospheric Pressure Changes on Seismic Signals or How to Improve the Quality of a Station. *Bull. seism. Soc. Am.*, **86**: 1760 - 1769.

Bolt, B. A., Tanimoto, T. (1981). Atmospheric Oscillations after the May 18, 1980 Eruption of Mount St. Helens. *EOS (Trans. Am. Geophys. Union)*, **62**: 529 - 530

Crossley, D., Jensen, O., Hinderer, J. 1995. Effective barometric admittance and gravity residuals. *Phys. Earth planet. Inter.*, **90**: 221 - 241.

Delclos, C., Blanc, E., Broche, P., Glangeaud, F., Lacoume, J. L. 1990. Processing and Interpretation of Microbarograph Signals Generated by the Explosion of Mount St. Helens. *J. Geophys. Res.*, **95**: 5485 - 5494.

Egger, J., Wamser, C., Kottmeier, C. 1993. Internal atmospheric gravity waves near the coast of Antarctica. *Boundary-Layer Meteorology*, **66**: 1 - 17.

Emter,D., Zürn,W. (1985). Observation of local elastic effects on earth tide tilts and strains. In: *Earth Tides* (ed. J. C. Harrison), pp. 309-327, *Benchmark Papers in Geology*, Van Nostrand Reinhold, New York.

Francis, S. H. (1975). Global propagation of atmospheric gravity waves: a review. *J. Atmos. Terr. Physics*, 37: 1011 - 1054.

Gossard, E. E., Hooke, W. H. (1975). *Waves in the Atmosphere.* Elsevier, Amsterdam, 456 pp.

Grosse-Brauckmann, W. (1979). Untersuchungen der Bodenunruhe im Periodenbereich von 2 min bis 1 h mit dem Askania-Bohrlochneigungsmesser. Dissertation, Techn. Univ. Clausthal, 130 pp.

Harrison, J. C. (ed.)(1985). Earth Tides. *Benchmark Papers in Geology Series*, 419 pp., Van Nostrand Reinhold, New York.

Hines, C. O. (1972). Gravity waves in the atmosphere. *Nature*, **239**: 73 - 78.

Kanamori, H., Mori, J., Harkrider, D. G. (1994). Excitation of atmospheric oscillation by volcanic eruptions. *J. Geophys. Res.*, **99**: 21,947 - 21,961.

King, G. C. P., W. Zürn, R. Evans and D. Emter (1976). Site Correction for Long Period Seismometers, Tiltmeters and Strainmeters. *Geophys. J. R. astr. Soc.*, **44**, 405 - 411.

Müller, T. and W. Zürn (1983). Observation of gravity changes during the passage of cold fronts. *J. Geophys.*, **53**: 155 - 162.

Neumann, U. (1997). Langperiodisches seismisches Rauschen durch atmosphärische Wellen. Diploma thesis, Geophysics, University of Karlsruhe, 137 p.

Peterson, J. (1993). Observations and Modeling of Seismic Background Noise. U. S. Geol. Surv., Open-File Rep. 93-322, 1 - 45.

Ritsema, A. R. (1980). Observations of St. Helens eruption. *EOS (Trans. Am. Geophys. Union)*, **61**: 1201.

Richter, B., H.-G. Wenzel, W. Zürn and F. Klopping (1995). From Chandler wobble to free oscillations: comparison of cryogenic gravimeters and other instruments in a wide period range. *Phys. Earth planet. Inter.*, **91**, 131 - 148.

Sorrells, G. G. (1971). A preliminary investigation into the relationship between long-period seismic noise and local fluctuations in the atmospheric pressure field. *Geophys. J. R. astr. Soc.*, **26**: 71 - 82.

Suda, N., Nawa, K., Fukao, Y. (1998). Earth's Background Free Oscillations. *Science*, **279**: 2089 - 2091.

Van Camp, M. (1998). Comparison between the Tide and Gravity Signal output of the GWR superconducting gravimeter C021. In: Proc. 13th Int. Symp. Earth Tides, Brussels 1997 (B. Ducarme, P. Paquet, Eds.), pp. 565 - 572, Observatoire Royal de Belgique, Brussels.

Virtanen, H. (1996). Observations of free oscillations of the Earth by superconducting gravimeter GWR T020. *Acta Geod. et Geophys. Hung.*, **31**: 423 - 431.

Warburton, R. J., Goodkind, J. M. (1977). The influence of barometric pressure variations on gravity. *Geophys. J. R. astr. Soc.*, **48**: 281 - 292.

Widmer, R., W. Zürn and T. G. Masters (1992). Observation of Low Order Toroidal Modes from the 1989 Macquarie Rise Event. *Geophys. J. Int.*, **111**: 226 - 236.

Wielandt, E. and G. Streckeisen (1982). The Leaf-Spring Seismometer: Design and Performance. *Bull. seism. Soc. Am.*, **72A**: 2349 - 2368.

Zürn, W. and R. Widmer (1995). On noise reduction in vertical seismic records below 2 mHz using local barometric pressure. *Geophys. Res. Lett.*, **22**: 3537 - 3540.

Zürn, W., Widmer-Schnidrig, R., Bourguignon, S. 1999. Efficiency of air pressure corrections for the BFO records of the Balleny Islands earthquake, March 25, 1998. *Bull. Inf. Marées Terrestres*, : submitted (this volume).

ESTIMATES OF ENVIRONMENTAL EFFECTS IN SUPERCONDUCTING GRAVIMETER DATA

Jürgen Neumeyer, Franz Barthelmes, Detlef Wolf
GeoForschungsZentrum Potsdam (GFZ), Division 1 „Kinematics and Dynamics of the Earth"
Telegrafenberg, D-14473 Potsdam, Germany
e-mail: neum@gfz-potsdam.de

1. Introduction

Because matter has the properties of gravity and inertia, the sensor inside the gravimeter (a test mass) reacts to time variations of

a) gravitational forces (Newtonian attraction) caused by redistribution and density variations of all the surrounding gravitating masses
b) inertial forces caused by the accelerations, i.e. the second time derivative of the vertical position, of the gravimeter site.

The gravimeter integrates gravity changes of the different sources and it cannot separate them.

In most cases research is concentrated on geophysically induced gravity effects such as Earth, tides, seismic normal modes, core gravity modes, earthquakes, Chandler wobble etc. To investigate one special effect, all the others have to be separated and removed from the data.

One disturbing part consists of accelerations (vibrations) usually considered as noise (seismic, industrial and ocean noise), which can be reduced by low-pass or by band-pass filtering (if the particular frequencies are known). Very important in this connection is the hardware damping of the signal according to the transfer function of the gravimeter. Supplementary instrumental effects (drift, offsets, instrumental noise) superimpose the gravimeter signal. These instrumental effects can be reduced by a new design of the gravimeter *(Richter and Warburton 1997)*.

It is difficult or even impossible to separate geophysically induced parts of the signal from noise, if they have the same frequencies. That is why for high resolution gravity measurements a site should be selected with low noise and also the instrumental drift and noise should be as low as possible.

Another part usually treated as disturbing signal are environmental effects. To remove them, they have to be modeled and hence the environmental parameters (e.g. temperature, atmospheric pressure, precipitation) must be measured precisely. The contributions to the gravimeter signal are summarized schematically in Table 1.

Geophysical gravity effects	Earth tides, seismic normal modes, core gravity modes, earthquakes, Chandler wobble etc.
Environmental gravity effect	Gravity induced by atmosphere and hydrosphere
Noise at the site	Seismic, industrial and ocean noise
Instrumental effects	Drift, offsets, instrumental noise

Table 1: Contributions to the gravimeter signal

In this paper the magnitudes of some environmental effects are roughly estimated. For this purpose, they are calculated by empirical (admittance function) and physical models.

2. Main sources of environmental effects

Mass redistribution and density variations in the atmosphere and hydrosphere induce gravity changes. In addition to this the gravimeter records environmentally generated vibrations. Table 2 gives an overview of the different sources which affect the gravity signal.

Atmosphere	*Hydrosphere*
Pressure	Ground water
Air-humidity	Soil moisture
Air-temperature	Rainfall
Wind	Snow
	Ocean

Table 2: Main sources in the atmosphere and hydrosphere affecting the gravity signal

The redistribution and density variations of the masses in the atmosphere and hydrosphere affect the gravimeter reading in two different ways:
a) Newtonian attraction term (gravity changes due to the direct attraction of the masses)
b) Deformation term with two parts
   b1) Gravity changes due to the vertical displacement of the gravimeter on the deformed Earth (in a first approximation according to the free-air gravity gradient)
   b2) Gravity changes due to the redistribution and density variations of the masses inside the Earth caused by deformation (in a first approximation according to the Bouguer plate of adequate thickness)

2.1 Atmosphere

The traceable Newtonian attraction term of the atmospheric masses acts at the sensor within a radius of about 50 km and the traceable deformation term acts up to a distance of about 1000 km *(Rabbel and Zschau 1985).* The deformation term has the opposite direction to the dominant Newtonian attraction term. For estimating the gravity effect induced by the atmosphere on principle the atmospheric pressure is used. The frequency range of the atmospheric pressure reach from minutes to years. Atmospheric pressure changes may reach +/-60 hPa for periods of days, which cause gravity changes of about +/-20 µgal. This is about 10 per cent of the short-period tidal gravity effect. Annual atmospheric pressure changes are in the order of +/-10 hPa, which cause gravity changes of about +/-3 µgal *(Merriam 1992, Sun 1995).*

Wind generates vibrations at the surface, which increase the noise in the gravimeter reading. Most of this noise can be eliminated by low-pass filtering.

2.2 Hydrosphere

The water circulation *(Boppard 1979)* in the surroundings of the gravimeter causes variation in the gravitational attraction and deformation at the surface similar to that due to the atmosphere. Precipitation (rain and snow) at the surface causes changes in soil moisture and groundwater level. One part of this precipitation evaporates at the surface and in the ground. Another part increases the groundwater level or drains off.

The ocean gives rise to noise at the site and causes the ocean loading effect, which can be modeled and adjusted for the tidal parameters according to an ocean model (*Schwiderski 1980*). By low-pass filtering, the ocean noise can be drastically reduced.

3. Modeling of the environmental effects.

The accurate modeling of the Newtonian attraction and deformation terms require:
a) knowledge of the density distribution in space and time
b) knowledge of the loading distribution in combination with a suitable local Earth model.

Unfortunately, not all this information is available. Therefore, the modeling can only be approximated using the available environmental parameters at the surface.

It is well known that the atmospheric surface pressure changes are highly correlated with the gravity variations induced by the atmosphere. In the past, different methods based on atmospheric pressure were developed, which generally fall into two categories: the empirical and physical approaches.

The empirical methods *(Warburton and Goodkind 1977, Crossley et al. 1995, Neumeyer 1995)* using the local atmospheric pressure determine the single and the complex admittance based on regression and cross-spectral analysis. The physical approaches *(Merriam 1992, Sun 1995; Boy et al. 1997; Neumeyer et al. 1997; Kroner and Jentzsch 1997; Vauterin 1997)* based on atmospheric models determine the attraction and deformation terms according to the Greens function *(Farrell 1972)*. Global atmospheric pressure and temperature changes measured at the surface are inputs of these models.

The empirical approaches yield good correction results in the short-period tidal band. An improvement of the correction can be obtained in the long-periodic tidal band with physical approaches.

Similar to the atmosphere, the influence of groundwater level, soil moisture, rain and snow can be accounted for by empirical or physical approaches. For the attraction term, the model of a Bouguer plate provides a first approximation for uniform changes in homogeneous horizontal layers. If we assume groundwater-level variations of 1 m and consider a water filled pore space of 10%, the gravity effect is 4.2 µgal. In the same way, soil-moisture changes can be calculated. If we assume a thickness of the layer of 1 m and soil-moisture changes of 1%, the gravity effect is 0.42 µgal. In reality, there are no homogeneous layers but geological materials of different structures whose dimensions are usually not well known. This limits the accuracy.

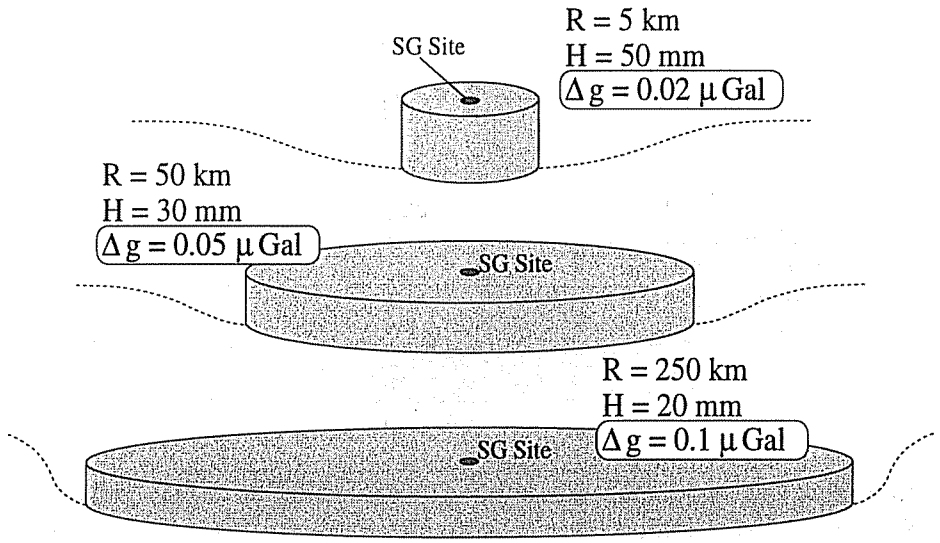

Figure 1: Modeling of gravity changes caused by deformation due to rainfall
R = radius of the load, H = thickness of the load, Δg = associated gravity contribution

The deformation due to rainfall and snow is calculated using the Hankel-transform method (Wolf 1985, Neumeyer et al. 1997). The Earth model employed is a laterally homogenous, incompressible, layered elastic half space. Each layer of the half space is characterized by the parameters shear modulus, density and layer thickness according to the PREM model (Dziewonkski and Anderson, 1981), which was used here in a simplified version. A constant density is assumed because of the small contribution of internal density discontinuities. The effective shear modulus is decreased by 30 % to simulate effects due to compressibility. Since the contribution of any point load only depends on the distance to the gravimeter site, the load distribution of snow and rain water at the Earth's surface was simplified to an axis-symmetric and time-dependent disc load.

Figure 1 shows three assumptions of rain-water loading around the gravimeter site with different radii R and heights H. The contribution is very small in comparison to the direct attraction and can be neglected.

To estimate the order of contributions due to snow loading three simplified snow load geometries are assumed, which serve as approximations of snow in the low mountain ranges Harz and Thuringian Forest and in the Alps. Figure 2 shows their deformation contributions at the gravimeter site. The influence on gravity is small and can be neglected for the GFZ Potsdam site. However, if the site is e.g. near or in the Alps, this contribution becomes larger and should be considered.

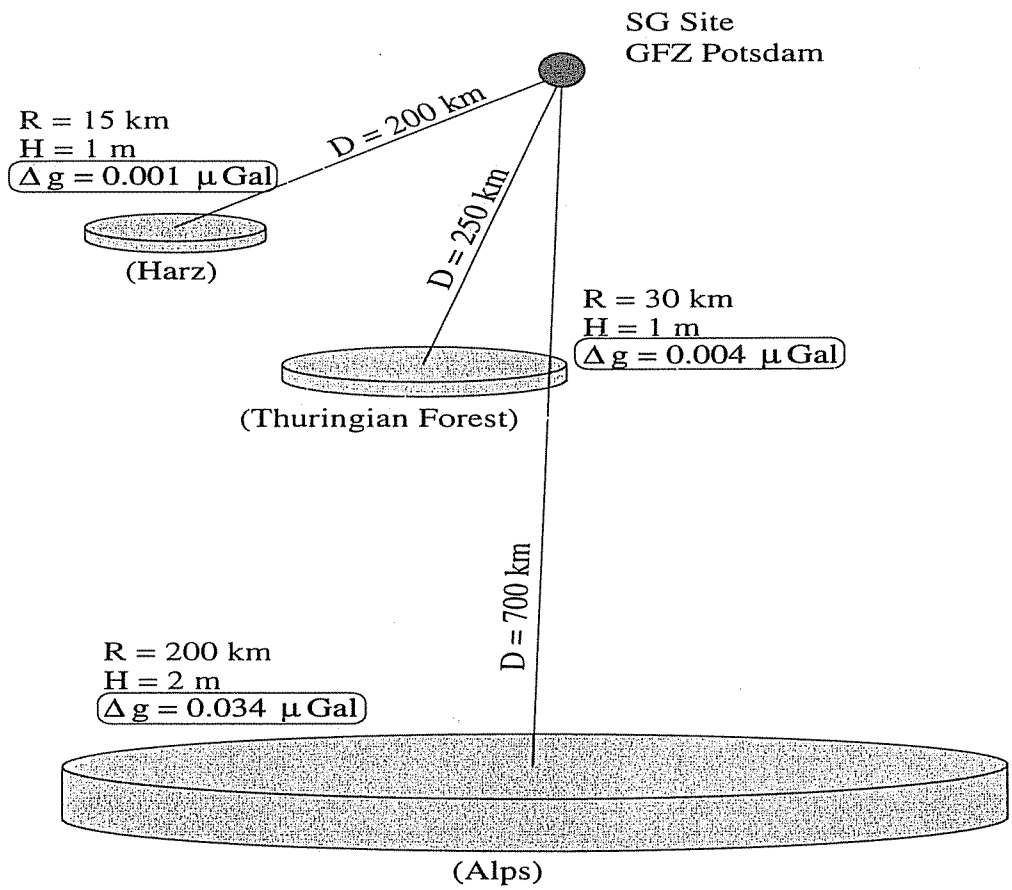

Figure 2: Modeling of gravity changes caused by deformation due to snow loading
R = radius of the load, H = thickness of the load, Δg = associated gravity contribution

The empirical model of a pseudo groundwater aquifer thickness *(Crossley 1997)* is based on the assumption that the rain charges the ground with water and discharges it according to an exponential function. The charge and discharge time can be empirically determined.

4. Analysis of data from Superconducting Gravimeter TT70

During a period of 660 days beginning on 9 January 1996, gravity data of the Superconducting Gravimeter (SG) TT 70 and environmental data (atmospheric pressure, groundwater level and rainfall) have been recorded at the GFZ Potsdam site. The groundwater level data have been collected with a sampling rate of 10 minutes in a borehole about 200 m distant from the SG site. The daily rain fall data are from the Deutscher Wetterdienst Potsdam.

These data are used for estimation of the environmental gravity effects. For this purpose the Earth tides and the pole tide are extracted from the gravity data using the PRETERNA program *(Wenzel 1994)*. The gravity residuals as result of this calculation are used in a multiple-regression analysis together with the atmospheric-pressure and the groundwater-level data for the determination of the associated admittance coefficients. Table 3 concentrates the coefficients. The atmospheric-pressure coefficient has a typical value of -0.29 µgal per hPa. The good correlation to gravity is expressed by the correlation coefficient of 0.72. The calculated groundwater-level admittance is 2.5 µgal per m. It is smaller than the calculated value for the Bouguer-plate assumption and the correlation to gravity is small with a coefficient below 0.4.

Environmental parameters	*Admittance coefficients*
Atmospheric pressure	-0.29 µgal per hPa
Groundwater level	2.5 µgal per m
Rainfall	0.08 µgal per mm

Maximum effects	*Variation*	*Gravity effect*
Atmospheric pressure	56.8 hPa	16.5 µgal
Groundwater Level	0.56 m	1.4 µgal
Rainfall	32.2 mm	2.6 µgal

Table 3: Admittance coefficients and maximum gravity effects of atmospheric pressure, groundwater level and rainfall

Figure 3 shows the estimated gravity variations using environmental data. For better demonstration, the gravity residuals are additionally corrected for atmospheric pressure (curve A). The gravity changes due to groundwater-level changes have been determined with the calculated admittance coefficient (curve B). According to a rainfall function (Crossley 1997), the gravity variations due to rainfall (curve D) have been calculated with a charge time of 3 hours and a discharge time of 21 days (curve C). The gravity changes induced by groundwater and rainfall temporally correlate well, e.g. during the days 60 to 330. The gravity changes induced by rainfall are greater. Curve C possibly includes soil-moisture and groundwater-level changes. The rainfall can be an indicator as well of the soil moisture as of the groundwater. Likewise, there is a good correlation between the rainfall and the atmospheric pressure. Curve E represents gravity variation by atmospheric pressure.

In general, there is poor agreement between the gravity residuals (curve A) and the gravity variations due to groundwater level and rainfall (only during short intervals e.g. between days 150 and 210, a correlation is visible). The effects are small and superimposed by instrumental effects. On the other hand the aquifer is not well known and the model assumption may not be

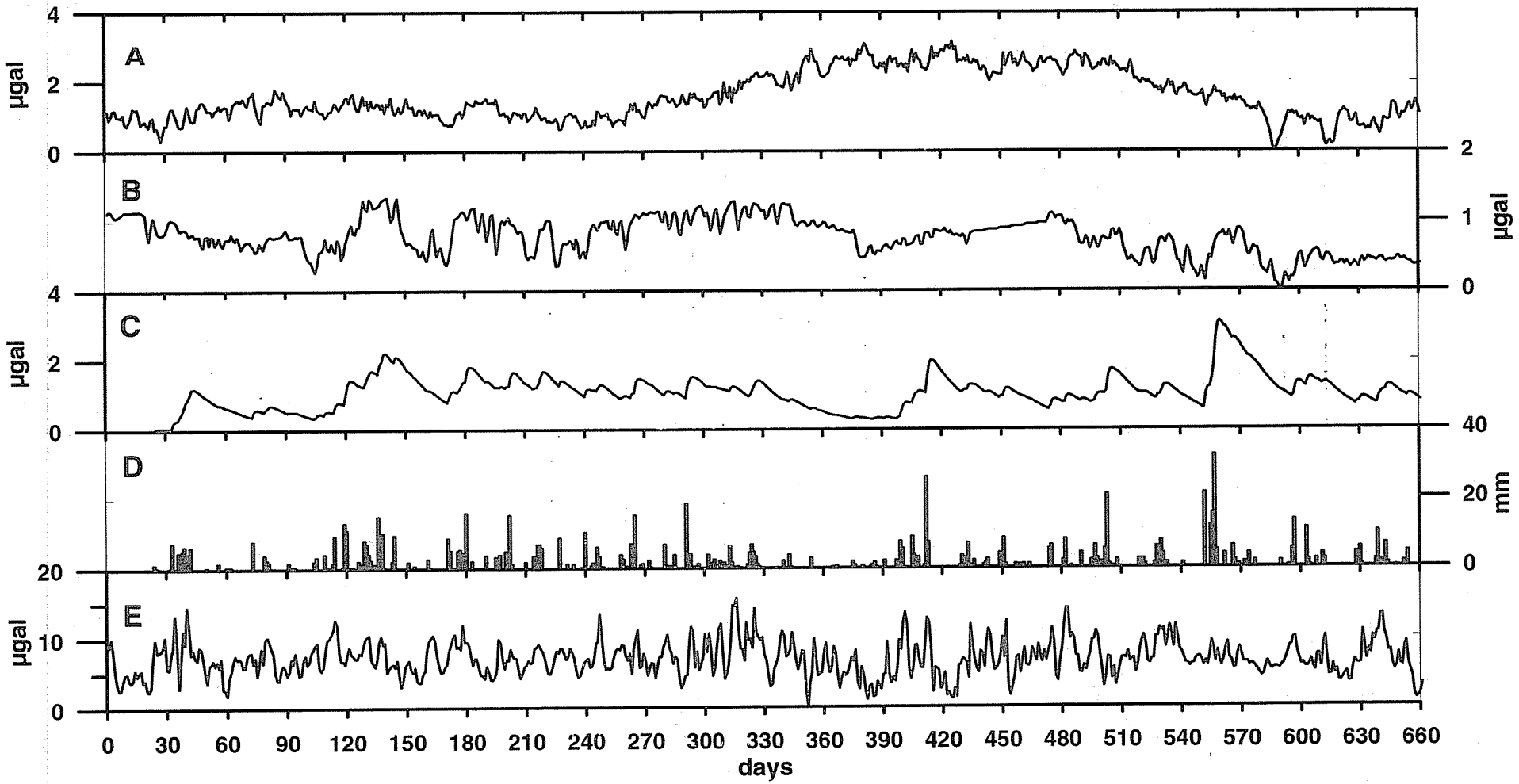

Figure 3 Residuals and environmental parameters

A = Gravity residuals (Earth tides and pole tide extracted, atmospheric pressure corrected)

B = Gravity variations due to groundwater level changes (borehole about 200m distant from the site)

C = Gravity variation due to pseudo groundwater aquifer thickness induced by rainfall

D = Rainfall

E = Gravity changes due to atmospheric pressure changes

appropriate. Table 3 also includes the maximum variations of atmospheric pressure, groundwater level and rainfall and the associated maximal gravity effects.

5. Conclusions

- The gravitational effect of deformation due to rainfall can be neglected.
- For a time series of 660 days at the GFZ Potsdam site, the modeling of a pseudo groundwater aquifer due to rainfall is temporally in good agreement with the groundwater-level changes. It gives a very crude estimate of the gravity changes induced by soil moisture and groundwater changes.
- The snow loading should be considered at the surrounding of the gravimeter site only and if the snow height is greater than about 2 m.
- If the environmental effects are in the order of a few μgal, it is difficult to separate them from instrumental effects (offsets, drift) which have the same order for the SG TT 70.

6. Aknowledments. We would like to thank Dr. Dehne Deutscher Wetterdienst Potsdam for providing the rainfall data and Dr. H.-J. Dittfeld GFZ for preprocessing of the SG data.

7. References

Boppard, Hydrologischer Atlas der Bundesrepublick Deutschland (1979) In Wie funktioniert das Wetter? Klima und Wetter, Meyers Lexikonverlag Mannheim/Wien/Zürich/ 1989.

Boy J.-P. Hinderer J. Gegout P. (1997) The effect of atmospheric loading on gravity. Proceedings of the Thirtheenth International Symposium on Earth Tides, Brussels, 1997, Eds.: B. Ducarme and P. Paquet, pp. 439-446.

Crossley D. J. Jensen O. G. Hinderer J. (1995) Effective barometric admittance and gravity residuals. Phys. Earth Planet. Int., 90, 221-241.

Dziewonkski A.M. Anderson D.L. (1981) Preliminary reference earth model. Phys. Earth Planet. Inter. 25, 297-356.

Farrell W. E. (1972) Deformation of the Earth by surface loads. Rev. Geophys., 10, 761-797.

Kroner C. Jentzsch G. (1997) Comparison of Air Pressure Reducing Methods and Discussion of other Influences on Gravity. Proceedings of the Thirtheenth International Symposium on Earth Tides, Brussels, 1997, Eds.: B. Ducarme and P. Paquet, pp. 431-438.

Kroner C. (1997) Reduktion von Luftdruckeffekten in zeitabhängigen Schwerebeobachtungen, Dissertation Mathematisch - Naturwissenschaftliche Universität Clausthal

Merriam J. B. (1992) Atmospheric pressure and gravity. Geophys. J. Int., 109, 488 - 500.

Neumeyer J. (1995) Frequency dependent atmospheric pressure correction on gravity variations by means of cross spectral analysis. Marees Terrestres Bulletin d'Informationes, Bruxelles, 122, 9212-9220.

Neumeyer J. Barthelmes F. Wolf D. (1997) Atmospheric Pressure Correction for Gravity Data Using Different Methods. Proceedings of the Thirtheenth International Symposium on Earth Tides, Brussels, 1997, Eds.: B. Ducarme and P. Paquet, pp. 431-438.

Richter B. Warburton R.J. (1998) A New Generation of Superconducting Tides Gravimeter. Proceedings of the Thirtheenth International Symposium on Earth Tides, Brussels, 1997, Eds.: B. Ducarme and P. Paquet, pp. 545-555.

Rabbel w. Zschau J. (1985) Static deformations and gravity changes at the earth´s surface due to atmospheric loading. J. Geophys. ,56, 81-99

Schwiderski E. W. (1980),Ocean tides: I. Global ocean tidal equations; II A hydrodynamic interpolation model. Mar.Geod., 3, 161-217 and 219-255.

Sun H.-P. (1995) Static Deformation and Gravity Changes at the Earth's Surface due to the Atmospheric Pressure. Observatoire Royal des Belgique, Serie Geophysique N° Hors-Serie, Bruxelles.

Vauterin P. (1997) The correction of the pressure effects for the superconducting gravimeter in Membach (Belgium). Proceedings of the Thirtheenth International Symposium on Earth Tides, Brussels 1997, Eds.: B. Ducarme and P. Paquet, pp. 447-454.

Warburton R. J. Goodkind J. M. (1977) The influence of barometric-pressure variations on gravity. Geophys. J. R. astr. Soc., 48, 281-292.

Wenzel H.-G. (1994) PRETERNA - a preprocessor for digitally recorded tidal data. Marees Terrestres Bulletin d'Informationes, Bruxelles, 118, 8724-8734.

Wolf D. (1985) The normal modes of a layered, incompressible Maxwell half space. J. Geophys. 57, 106-117.

Hydrological Influences in the Registrations of Superconducting Gravimeters and Ways to their Elimination

Martina Harnisch, Günter Harnisch
Bundesamt für Kartographie und Geodäsie (BKG), Aussenstelle Potsdam
Michendorfer Chaussee 23, PF 600 808, D-14408 Potsdam

1. Introduction

While the correction of air pressure influences became a more or less standard procedure within the processing of gravimeter data, hydrological influences are neglected in most cases. One of the reasons may be, that hydrological data have until now been available only to a limited extent. But in contrast to the more or less short-time air pressure influences, variations of the hydrological regime in the ground may act over long times and in this way may influence all investigations of long-time gravity variations, which constitute one of the main aims of the use of superconducting gravimeters. Therefore, with growing accuracy and stability of the superconducting gravimeters also hydrological influences are studied and considered to an increasing extent in the recent past.

2. Meteorological, hydrological and physical background

The problem of hydrological influences on gravity measurements finally may be reduced to the determination of the gravity effect of density variations in the underground, arising from the changing moisture content within the different soil layers. The changes of soil moisture may be produced by supply of water both from above (rainfall, melting snow) and from below (changing height of the groundwater level in combination with capillarity). However, changes of the groundwater level are not only influenced by superficial hydrological processes, they may happen also independently due to inflow and run-off of water in the underground.

In the simplest case, the moisture induced gravity variations may be described by the model of a homogeneous plane layer of thickness D (Bouguer plate):

$$\delta g_B = 2\pi f \sigma D,$$

with $2\pi f = 4.191\ 10^{-7}$ g^{-1} cm^3 s^{-2}. From this it follows, that a water layer (σ = 1 g cm^{-3}) with a thickness of D = 1 cm has a gravity effect of 4.2 nm s^{-2}. If the gravity effects of variations of the soil moisture or of the groundwater level are considered, effective densities have to be used, which take into consideration the density of the dry material, the pore volume, the density of the liquid inside the pores and the degree up to which the pores are filled with the liquid.

An example of the direct way to correct hydrological influences is the procedure, utilized for high precision gravity measurements on the west-east gravity profile between Magdeburg and Frankfurt/Oder [2]. During each measuring campaign around each of the seven observation pillars soil moisture and the height of the groundwater level were measured and converted into gravity corrections by the formulae

$$\Delta g_{gw}\ (\text{nm s}^{-2}) = 112 \ldots 142\ \Delta h_{gw}\ (\text{m})$$

$$\Delta g_F\ (\text{nm s}^{-2}) = 11.9 \ldots 13.1\ F\ (\%),$$

where Δh_{gw} are the changes of the groundwater level, measured in m, and F the soil moisture in percent. The numerical constants in the formulae have been derived from the soil parameters at each measuring site.

In most cases due to the very complicated and inhomogeneous geological and hydrological situation around the gravimetric observatories, reliable hydrological parameters not have been available. Therefore during the processing of measurements of superconducting gravimeters corrections for the influence of hydrological effects are derived - if really done at all - by the formal procedure of regression analysis. Regression coefficients may be estimated simply by inclusion of additional hydrological information (e.g. groundwater level) into the multichannel tidal analysis (e.g. the ETERNA program). Experience shows, that the better way would be an independent regression analysis before the tidal analysis itself. But in any case it has to be kept in mind, that groundwater is only one of the possible influences, the other comes from variations of the soil moisture. Because both are correlated, the resulting regression coefficients are effective ones, representing different combinations of the influences of soil moisture and groundwater.

Soil moisture is strongly governed by the precipitation activity throughout the year. Therefore precipitation measurements may be used as an alternative, simple and cheep method to describe the hydrological regime within the ground. But the penetration of water into the ground is a very complicated process, depending not only on different parameters of the soil, but also on the counteracting processes of superficial run-off of the rain and of the of evapotranspiration.

Recently by different authors models were developed to transform precipitation data into variations of soil moisture [1, 4, 6]. In principle all these models use two exponential functions to consider the slowly beginning of infiltration into the ground and the long-term decrease of moisture due to evapo-transpiration. For example CROSSLEY, XU and VAN DAM [1] used the empirical formula

$$D_i = \sum_{j=1}^{i} r_j (1 - e^{-(i-j)/\tau_1}) e^{-(i-j)/\tau_2}$$

$$g_i = 2\pi f \sigma D_i$$

where r_j = amount of rain at hour number j, D_i = thickness of an equivalent water layer at hour number i and $\sigma = 1$ g cm^{-3}. g_i gives the gravity disturbance at hour number i. The decay constants $\tau_1 = 4$ hours ("recharge time constant") and $\tau_2 = 91$ days ("discharge time constant") were derived by comparison of the modeled gravity data with the data, measured at the TMGO (search for maximum correlation). Therefore these values are valid only for the special geological and hydrological situation around the TMGO. For each other station they have to be estimated in an correspondent way, regarding the different local situation.

Precipitation shows, like all meteorological phenomena, a distinct seasonal variation. Therefore also the hydrological influences on gravity measurements must vary seasonally and in this way they affect all investigations in the long-term period range. Fig. 1 shows monthly averages of the rainfall at Potsdam, Boulder and Miami. The values of Potsdam are based on the data series 1893 - 1992, registered at the Meteorological Observatory at Potsdam [5], while for the other two stations only rainfall data during the registration period of the gravimeters have been available (in both cases about two years)[1]. The maximum at early summer is most clearly expressed in the Miami data set (1043.6 mm in May 1991). Due to the longer data series the yearly variations at Potsdam are much more smoothed than the variations at the other two stations, however the values of single months may deviate considerably (202.3 mm in July 1907). The yearly mean of the total rainfall at Miami (subtropics) is about three times as the value at Potsdam (146.5 mm and 49.0 mm). With refer to the three examples under consideration, the least rain falls at Boulder (32.8 mm), but in special cases also there heavy rainfall may occur (154.0 mm in June 1995). From the comparison of the precipitation at Boulder and Potsdam it may be concluded, that also in Central Europe significant hydrological influences are to be expected. On the other hand the high yearly rainfall at Miami, the very clear geological situation and the flat topography make the data from this station particularly suited for the investigation of hydrological influences on gravity measurements.

---

[1]The rainfall data from the Miami airport were kindly made available by Deutscher Wetterdienst, Seewetteramt, Hamburg

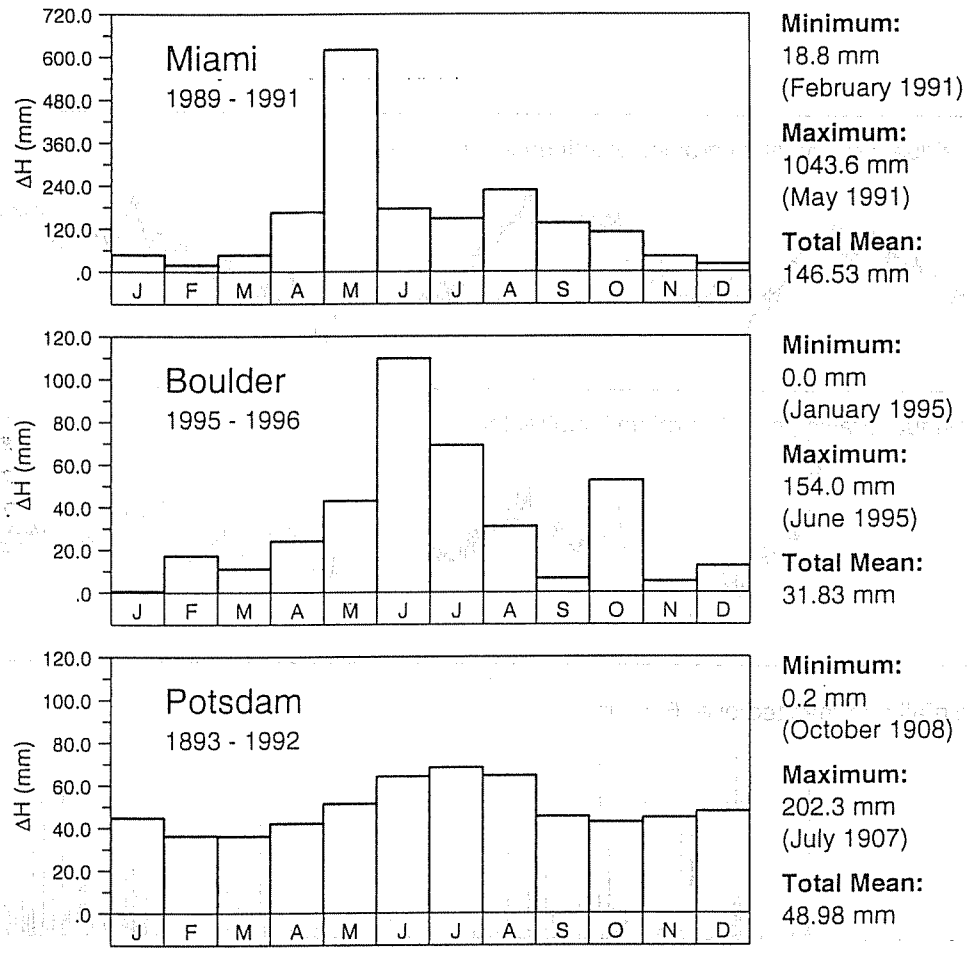

Fig. 1: Mean values of monthly rainfall at Miami, Boulder and Potsdam

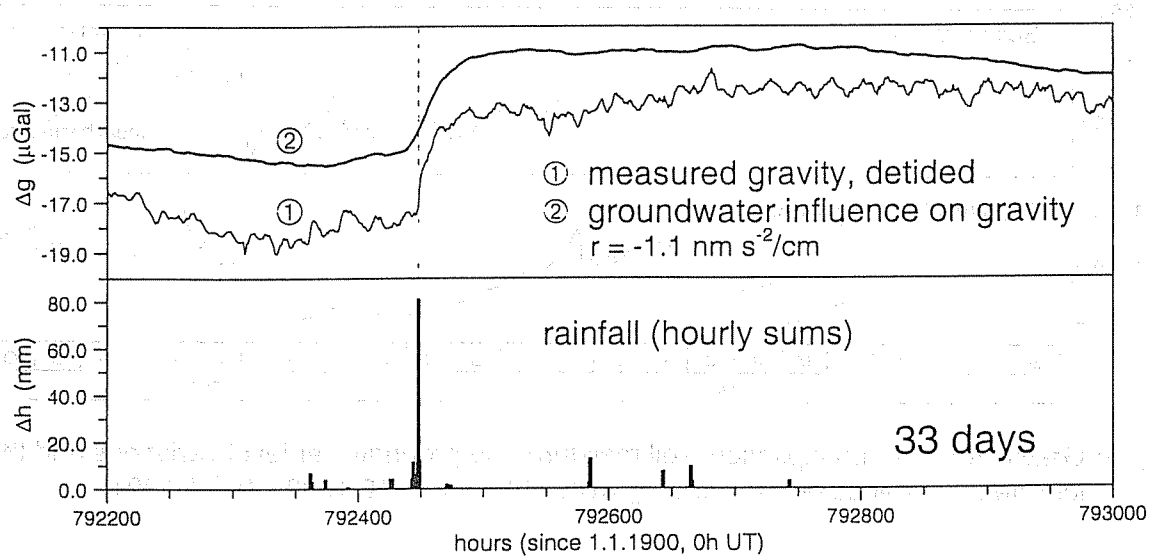

Fig. 2: Influence of a single heavy rainfall on the groundwater level and the measured gravity at Miami (17.5. - 19.6.1990)

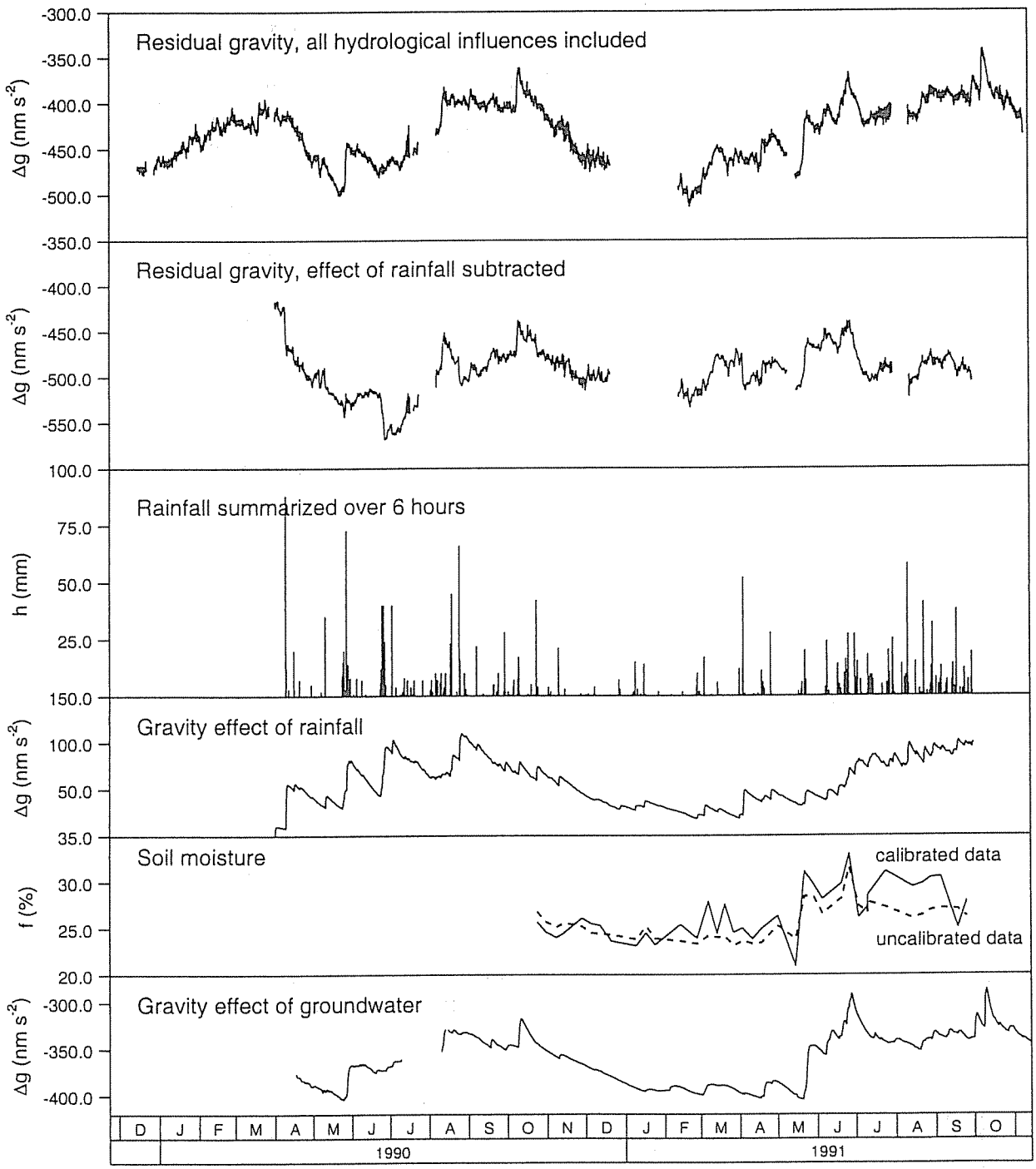

Fig. 3: Gravity effect of precipitation, soil moisture and groundwater level variations and their long-term influence on measured gravity at Miami (6.12.1989 - 10.11.1991)

The foregoing more principal considerations shall be illustrated in the following by three examples of measurements with superconducting gravimeters, at which instruments of the BKG (the former IfAG) participated.

3. US Naval Observatory Richmond, near Miami, Florida, U.S.A.

Between November 1989 and November 1991 the gravimeters SGB of the University San Diego, California and TT40 of the former IfAG (now BKG) were running side by side at the Richmond station [4, 6]. The meteorological as well as the hydrological situation at Richmond is very extreme: Due to the subtropical climate in the early summer there are very heavy rainstorms. The underground of the station consists of carstic limestones with a very high "porosity" (up to 30 - 40 percent). Therefore the rain water penetrates into the ground very quickly and after a very short time of only a few hours it reaches the groundwater level. The hydrological influences on the gravity measurements are so large, that a reliable processing of the gravimeter data is not possible without additional hydrological information.

In order to monitor the changes of the groundwater level 4 groundwater gauges were established around the gravimeter building in distances of up to 100 m. The depth of the groundwater table varied with time between 2.5 and 3.5 m. Within a few cm the changes were the same in all 4 wells. Though it is clear that there is a strong correlation between rainfall and changes of the groundwater level, influences of artificial water regulations in the swampy area of the nearby Everglades are possible. Because of the fast penetration of the rainfall to the groundwater level only a small part of the rain is stored as soil moisture over longer times.

Additionally to the groundwater data 37 single values of soil moisture have been available as well as precipitation data for the period 1.4.1990 to 30.9.1991 from the meteorological station at the nearby Miami airport (distance ca. 10 km). The soil moisture was measured about weekly with a neutron probe. But corrections were derived by regression analysis of the groundwater measurements alone, yielding a groundwater regression coefficient of -1.1 nm s^{-2}/cm. However, due to the correlation between the three different influences this value must contain also contributions of precipitation and soil moisture.

Fig. 2 shows the effect of a heavy rainfall on the 27th of May 1990 with an amount of 80 mm/h. Immediatly after the beginning of the rainfall a sharp rise of the groundwater level and of the residual gravity curve are visible in the graph. The change of the residual gravity may be explained by the rise of the groundwater level using the regression coefficient -1.1 nm s^{-2}/cm.

Fig. 3 gives a general idea of the hydrological situation (six-hourly sums of precipitation, measurements of the soil moisture, height of the groundwater table) during the whole registration period of the gravimeters. A certain correlation between precipitation and soil moisture becomes evident as well as between groundwater level and rainfall in summertime.

In the fourth field of fig. 3 the modeled gravity effect of rainfall is given, following the exponential model of CROSSLEY et al. [1]. The first decay constant was assumed to be $\tau_1 = 6$ hours with regard to the six-hour rainfall data, for the second a value of $\tau_2 = 30$ days was chosen, in order to ensure that the cumulative gravity effect of rainfall tends to zero in times without or with low rainfall. The shape of the modeled gravity effect of rainfall over the whole timespan is very similar to the gravity effect of the groundwater level variations, determined by the linear regression model (see the lowermost field of fig. 3). This similarity indicates again, that rainfall commonly reaches very fast the groundwater level and in this way acts indirectly on the measured gravity by variations of the groundwater level. However, some details within the figure seem to indicate a shift of about 2 months between the gravity effects of rain and groundwater. From the fast infiltration of the rain into the ground it is to be expected, that only a small fraction remains in the ground and gives rise to soil moisture variations.

Because there are only a few measurements of soil moisture and due to the very high porosity of the carstic limestone the results of these measurements are not very reliable [6], and the estimation of soil moisture regression coefficients is not very useful. As may be seen from the fifth field of fig. 3, the common trend of the soil moisture values seems to be similar as well to the precipitation model as also

to the gravity effect of the groundwater variations. This - on the other hand - means, that the soil moisture is correlated with the other hydrological influences, and the regression analysis on the basis of the groundwater variations alone results in an effective regression coefficient, which more or less reflects also all the other hydrological influences. The steep rise of soil moisture at the end of May and the peak at the end of June 1991 seem to be directly connected with groundwater variations.

4. Table Mountain Gravity Observatory (TMGO), near Boulder, Colorado, U.S.A.

Between April 1995 and July 1996 the two compact type gravimeters C023 and C024 were running side by side at the TMGO [3]. The residual gravity curves, derived for both instruments, are of very similar shape with nearly the same deflections from the theoretical gravity effect of the observed polar motions (fig. 4). Obviously, there is a connection to heavy rainfalls during this time as may simply be seen from the corresponding rainfall data. For a more detailed investigation the gravity perturbations caused by the rainfall were estimated, using the formula and the parameters $\tau_1 = 4$ hours and $\tau_2 = 91$ days from the paper of CROSSLEY et al. [1]. The value of τ_2 was derived by a fit of the gravity residuals of the observed data to the mathematical model. If the observed gravity is corrected by the modeled gravity effect of the rainfall at first a much better correspondence with the polar motion curve results, very clearly to be seen in the initial part of the time series under consideration. But also other parts of the residual gravity curve are changed after the rainfall correction has been applied, while some smaller details are fully eliminated. As a very instructive example the small steplike perturbation of the gravimeter C024 in mid-September 1995 should be mentioned, which vanishes after the rainfall correction. This underlines the importance of rainfall corrections or - more generally - of corrections of hydrological influences: If no rainfall data had been available, probably a step correction would have been applied, leading to a systematic falsification of the whole residual gravity curve.

The influence of rainfall corrections becomes evident not only in the shape of the residual gravity curve but also by significant changes of the estimated parameters of long-term gravity effects. In table 1 the influences on the gravity effect of the annual wave and of the Chandler wave of the polar motions are summarized. As a consequence of the rainfall correction the δ-factor of the Chandler wave changes from 1.32 ± 0.01 to 1.66 ± 0.01. The second value, resulting from the corrected data, lies more in the common trend than the first one, derived before.

Table 1: δ-factors, derived from gravimeter data and observed polar motions (IERS data).

Gravimeter C024, Boulder 11.4.1995 - 19.3.1997	m_0	Annual Wave T = 365.25 days		Chandler Wave T = 439.3 days	
		a nm s^{-2}	$\delta_{a,pole}$	a nm s^{-2}	δ_{Ch}
uncorrected for rain	±13.2	28.18 ±0.31	2.48 ±0.03	40.42 ±0.01	1.32 ±0.01
influence of rain eliminated	±7.9	17.79 ±0.25	1.56 ±0.02	50.72 ±0.25	1.66 ±0.01

5. Fundamental Station Wettzell, Bavarian Forest, Germany

The observatory Wettzell was founded on a flat mountain top in the German Low Mountains. It was equipped with several astronomical and geodetic instruments, among them the superconducting gravimeter SG103. The underground of the station consists of gneiss, superficially weathered to a depth varying from place to place. The solid rock in a greater depth is crossed by a multitude of faults and clefts. From the hydrological point of view we have a very inhomogeneous situation, which may be modeled only by formal mathematical methods, integrating over a large area.

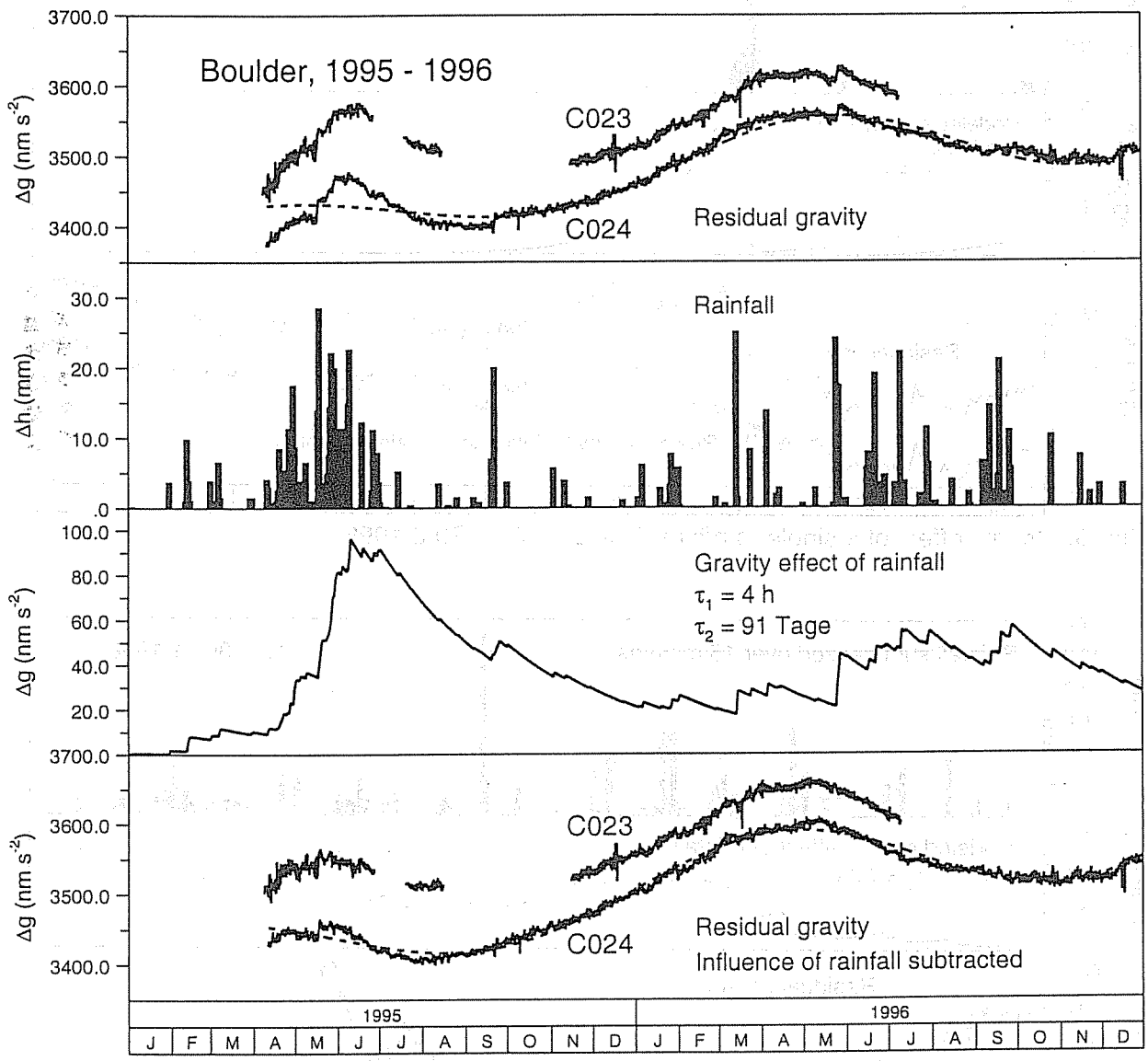

Fig. 4: Gravity effect of precipitation and its long-term influence on the measured gravity at Boulder (1.1.1995 - 31.12.1996)

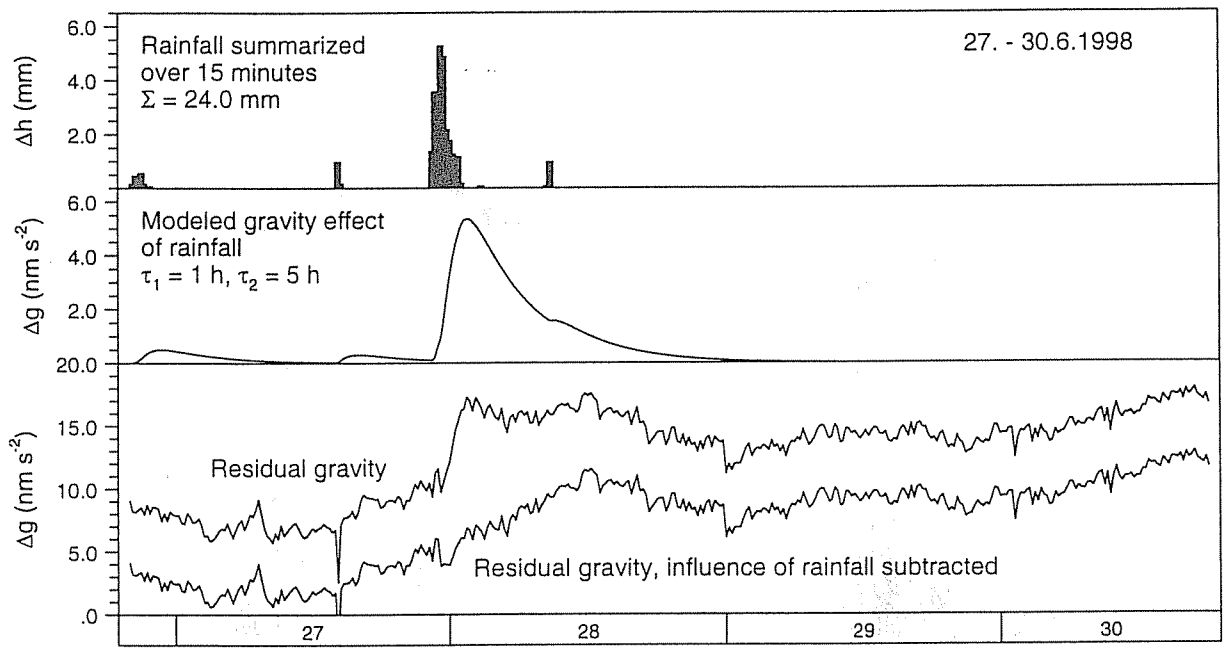

Fig. 5: Gravity effect of a single rainfall at Wettzell (27. - 30.6.1998)

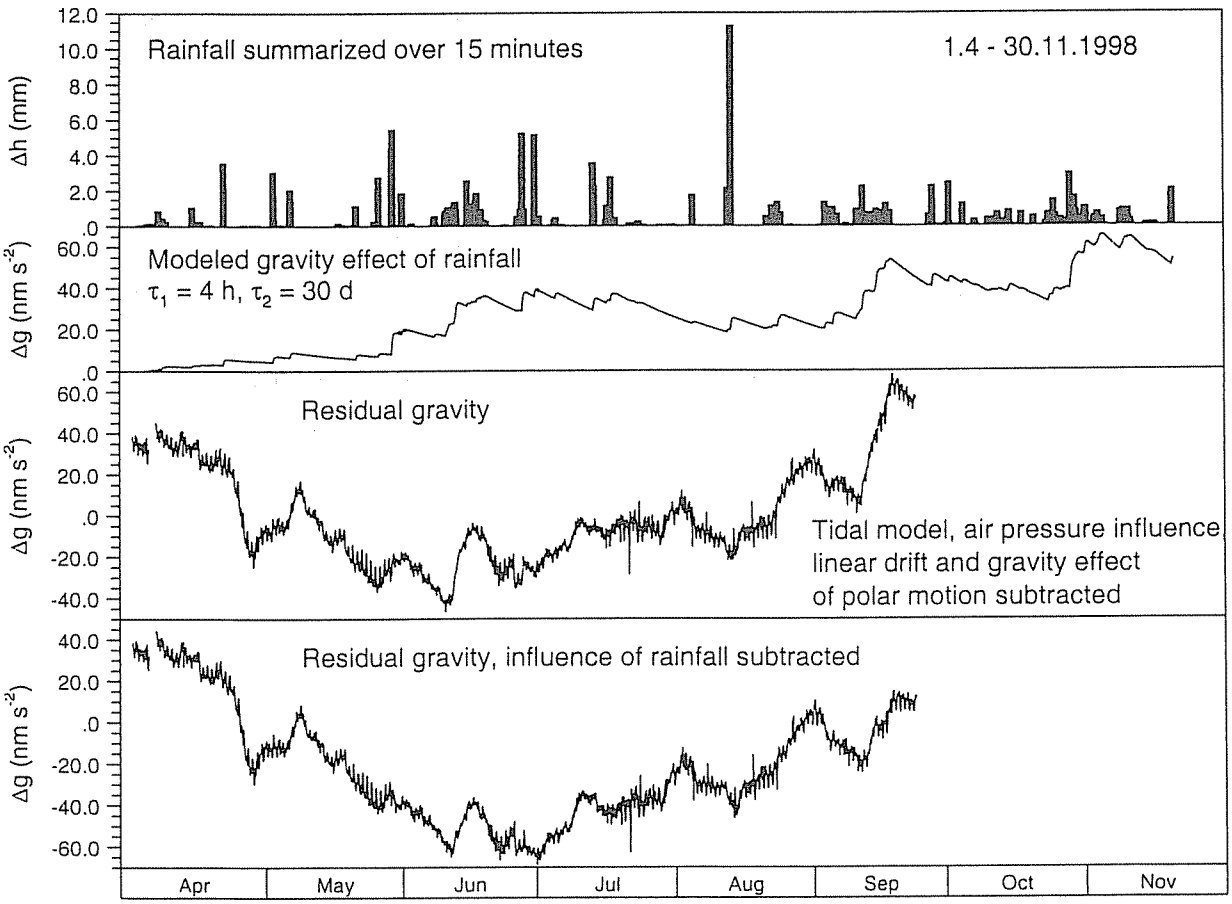

Fig. 6: Gravity effect of precipitation and its long-term influence on the measured gravity at Wettzell (1.4. - 30.11. 1998)

From the described geological situation it is to be expected, that after rainfall the changes of moisture in the superficial weathered soil layer will produce gravity variations, measured by the superconducting gravimeter. Groundwater gauges, established in the last time show, that also significant variations of the groundwater level may occur, which also may produce perturbations of the gravity recorded by the superconducting gravimeter. Unfortunately, continuous groundwater data are not available as yet.

The time series of the superconducting gravimeter SG103 at Wettzell started in April 1996, continuous rainfall data have been available since April 1998.

The rainmeter, used at Wettzell, records the time when a tipping device inside the instrument changes its equilibrium position. Each of such events corresponds to an amount of rainfall of 0.1 mm. If the single events are summed up over 15 minutes and compared with the residual gravity at the same time short-time gravity changes after strong rainfalls become evident (fig. 5). Using the formula of CROSSLEY et al. [1] with the modified decay constants τ_1 = 1 hour and τ_2 = 5 hours, it seems to be possible to model the short-time gravity effect of the rainfall, produced by soil moisture variations near the earths surface. Such a procedure is suited to reduce the noise of the residual gravity and the root mean square of the tidal analysis. If long-term gravity effects of the rainfall are to be modeled, decay constants are needed in the same order of magnitude as used and described by CROSSLEY et al. [1]. In this way rainfall data may be considered as a substitute for measurements of the soil moisture. Figure 6 shows the modeled gravity effect of the rainfall at Wettzell between April and September 1998 using the roughly estimated decay constants τ_1 = 4 hours and τ_2 = 30 days. The time series of rainfall measurements at Wettzell is not long enough to serve for deriving reliable constants, especially in the long-term range. Keeping in mind, that from the residual gravity curve also the gravity effect of polar motions was eliminated, a similar tendency of the modeled gravity effect of the rainfall and of the residual gravity curve is evident. That means, that despite the roughly estimated decay constants the modeled gravity changes seem to reflect at least parts of the long-term influence of rainfall and changes of the soil moisture on the recorded gravity signal. Continuing this idea one can see, that the elimination of long-term hydrological influences (e.g. precipitation) is unavoidable, if the investigations are aimed at long-term gravity variations, e.g. on the gravity effect of polar motions. And this is true also for mountain stations such as Wettzell.

6. Conclusions

- In all cases where hydrological data and parameters (groundwater, soil moisture, rainfall) could be included into the data processing of superconducting gravimeters more or less significant influences were found.
- The influences of variations of the hydrological regime are at least of the same order of magnitude as the influence of air pressure variations. They may act both in the short-time and in the long-time range. Especially seasonal variations of the groundwater level and of the soil moisture may considerably influence the investigation of long-term effects (e. g. polar motions).
- To make better use of the very high information content of modern superconducting gravimeters, at each station the continuous registration of the gravity signal and of the local air pressure variations should be completed by continuous registrations of groundwater level, soil moisture, and rainfall. If measurements of groundwater level and soil moisture are either not possible or too expensive (note the price of the gravimeter!), at least the rainfall should be registered.
- The influences of variations of the groundwater level and of the soil moisture may be eliminated by empirical regression coefficients, obtained directly from regression analysis in the context of tidal analysis. The use of rainfall data needs further model studies and the development of procedures to obtain locally representative model parameters.
- The estimation of reliable model parameters and regression coefficients, and especially the development of adequate models need long-time series of the gravimeter signal as well as of hydrological data.

Acknowledgements

We (the authors) like to express our thanks to all the many peoples, mostly unknown for us by name, which are engaged to maintaine the instruments in operation and to collect the data, which are the basis of our studies. Above all we thank B. RICHTER for his support of the investigations, P. WOLF, who looks after the instruments of the BKG and last, but not least T. VAN DAM, who made available for us the data from the TMGO, especially the rainfall data.

References

1. Crossley, D.J., Xu, Su, van Dam, T.
   Comprehensive Analysis of 2 years of SG Data from Table Mountain, Colorado.
   Proc. 13th Intern. Symp. Earth Tides Brussels 1997. Brussels 1998, pp. 659-668.

2. Harnisch, G.
   Systematic Errors Affecting the Accuracy of High Precision Gravity Measurements
   7th Intern. Symp. „Geodesy and Physics of the Earth" Potsdam 1992. Berlin, Heidelberg 1993, pp. 200-204.

3. Harnisch, M., Harnisch, G., Richter, B., Schwahn, W.
   Estimation of polar motion effects from time series recorded by superconducting gravimeters
   Proc. 13th Intern. Symp. Earth Tides Brussels 1997. Brussels 1998, pp. 511-518.

4. Klopping, F.J., Peter, G., Berstis, K.A., Carter, W.A., Goodkind, J.M., Richter, B.
   Analysis of two 525 day long data sets obtained with two side-by-side, simultaneously recording superconducting gravimeters at Richmond, Florida, U.S.A.
   Proc. Second Workshop: Nontidal Gravity Changes. Intercomparison between absolute and superconducting gravimeters. Sept. 6th to 8th, 1994, Walferdange (Luxembourg). Cah. Centre Europ. Géodyn. et Séismol., Vol. 11. Luxembourg, 1995, pp. 57-69.

5. Lehmann, A., Kalb, M.
   100 Jahre meteorologische Beobachtungen an der Säkularstation Potsdam 1893 - 1992
   Deutscher Wetterdienst, Offenbach a.M. 1993, 32 p.

6. Peter, G., Klopping, F.J., Berstis, K.A.
   Observing and modeling gravity changes caused by soil moisture and groundwater table variations with superconducting gravimeters in Richmond, Florida, U.S.A.
   Proc. Second Workshop: Nontidal Gravity Changes. Intercomparison between absolute and superconducting gravimeters. Sept. 6th to 8th, 1994, Walferdange (Luxembourg). Cah. Centre Europ. Géodyn. et Séismol., Vol. 11. Luxembourg, 1995, pp. 147-159.

THE HYDROLOGIC INDUCED STRAIN-TILT SIGNAL – A REVIEW

Carla Braitenberg
Department of Earth Sciences, University of Trieste, via Weiss 1, 34100 Trieste, Italy.
berg@univ.trieste.it

Abstract

A discussion of the ambient factors influencing deformation measurements undertaken with strain-tilt gauges is made. The factors which are mostly disturbing are determined, which turn out to be the hydrologic agents. The induced signals are first qualitatively described, relying on published observations and those of the NE-Italy strain-tiltmeter network. A quantification of the maximum expected signals is made. Different types of statistical and physical models which attempt to model the induced signals are discussed and tested. Among them a new approach, which relies on the techniques of predictive filtering is introduced. The methods applied for the modeling of the strain/tilt induced signals are valid also for the study of the induced signals in gravimeters.

Introduction

The deformation measurements being made at or not far from the earth's surface, they always suffer from disturbing ambient factors as temperature, hydrologic agents and air pressure. Among these agents the temperature is the most predictable, as it is closely tied to the position of the earth with respect to the sun. A well-defined yearly cycle and a periodicity of the solar day are thus an obvious consequence on the measurements. Much more complex is the time variation of the latter two agents. The hydrologic agents comprise the rainfall and its surface or subsurface runoff and the watertable variations. The two quantities are not independent. The hydrologic agents are largely aperiodic, and influence deformation measurements on a broad band of frequencies ranging from short-term variations (days) to long term variations (several years). Apart from coseismic deformation steps, the deformation which should accompany the preparation of a seismic event, according to theoretical considerations (Lorenzetti and Tullis, 1989; Scholz et al., 1973; Scholz, 1990: ff 362), covers the entire range from long period (several years) to short period deformation (days) shortly

before the event. The similarity in the time constants involved makes the hydrologic induced signals particularly disturbing in deformation studies aiming at detecting tectonic movements.

The influence of air pressure compared to the hydrologic induced signals has been studied for time variations slower than two days. Nine months of borehole tilt in the English Lake District (Edge et al., 1981) were studied together with air pressure and water table level measurements. The tilt was recorded at 12-m depth with two Askania tiltmeters. The regression coefficients gave 2 msec/hPa (0.01 microrad/hPa) for pressure and 200 msec/m (1 microrad/m) for watertable variations. These values translate to maximum induced signals of approximately 20 msec (0.1 microrad) and 200 msec (1 microrad), for pressure and watertable respectively.

A study of the strain measurements of three horizontal strainmeters installed at 60-m depth in a cave in NE-Italy gave a similar ratio of the barometric and hydrologic induced effects. In this case the hydrologic agent was measured in the quantity of rainfall, and the regression analysis found 4-5 nstrain/mm rainfall, which amounted to a maximum value of several 100 nstrain (Dal Moro and Zadro, 1998). The effect of pressure on strain gave a coefficient of 2 nstrain/hPa, which amounts to a maximum value of about 20 nstrain. These values are not very different from those found for the Cambridge-type extensometer array at the Black Forest Observatory (BFO) in SW Germany at higher frequencies. According to Dr. Walter Zürn (personal communication) at periods between 1000s and 3000s coefficients between 0.5-0.8 nstrain/hPa were found. As also for the tilt in the English Lake district, the hydrologic induced signal in NE-Italy is at least 10 fold greater than the air pressure induced effect at frequencies lower than 0.5 cpd.

In the present paper we intend to study only the hydrologic induced deformation, giving a characterization of and presenting the different models which attempt to reproduce the signals. There are some uncertainties regarding the physical nature of the induced deformation. Evans and Wyatt (1986) attribute the deformation to changes in the aperture of subsurface hydraulically conductive fractures due to pore pressure changes and to compaction due to porosity changes induced by changing pore pressure. A different model considers the deformation of the rock matrix due to pore pressure gradients leading to groundwater flow in the pore space (Kümpel, 1986; Kümpel, 1989).

Characterization of the hydrologic induced deformation

The hydrologic induced deformation is characterized by a typical time evolution, which is found both in extensometer and in tiltmeter records. The onset is rapid, almost steplike with a

near to exponential recovery. The azimuth of the tilt signal is typical for each station. Edge et al. (1981) find the induced tilt to be oriented perpendicular to the strike of the cleavage planes of the slate forming the bedrock. Peters and Beaumont (1981) find a strong dependence of the tilt signal on the orientation of the structures at depth permeated with water.

The extensometric signal may be either compressive or dilatational, which can depend at a certain station on the azimuth. The sign of the deformation is though generally constant (Wolfe et al., 1981; Yamauchi, 1987). Tanaka et al. (1989) find compression for two strainmeters and extension or compression for a third extensometer in accordance to a rain threshold.

Long term fluctuations in annual precipitation may lead to slow variations in the watertable level, which have been made responsible of long term influences on the deformation measurements (Kasahara et al., 1983).

Modeling of the induced signals

An important task is the modeling of the induced signals, with the scope of cleaning the observations from the hydrologic influence. Two different approaches can be made, which is to create statistical models that describe the signals or to reproduce the physical nature of the problem as close as possible. In the following we present various statistical methods together with some examples.

The most straight forward way to detect the influence of rainfall is to compare rainfall with some component of deformation, as the tilt or extensometric record, or composite quantities as the areal deformation, total tilt, etc. This method, although widely used, is not convenient as it does not compare the correct quantities. The induced signal depends on the entire history of rainfall, whereas the rainfall histogram considers the rainfall over definite limited time intervals (for example day or half a day). The rainfall series is different also from a statistical point of view, as it has only positive or zero values, which is not the case for the time series of a deformation component. The consequence is that the correlation coefficient between rainfall and a deformation record appears to be low, although by visual inspection it is evident that the onset of rainfall is responsible for a deformation signal.

With a simple mathematical procedure it is possible to obtain two time series which can be compared. The first is to integrate the rainfall over the entire time interval and subtract an average linear trend. Be $p(n)$ the sampled rainfall, $\bar{\dot{p}}$ the average time derivative of rainfall, then the rainfall function I $r(n)$ is defined by:

$$r(n) = \sum_{k=0}^{n} p(k) - \bar{\dot{p}}\, n\, \Delta t \qquad (1)\,,$$

with Δt the sampling interval.

Another procedure is to evaluate the time derivative of the observed deformation (or a composite quantity as areal strain, total tilt, etc.) and compare it with rainfall. In Fig. 1

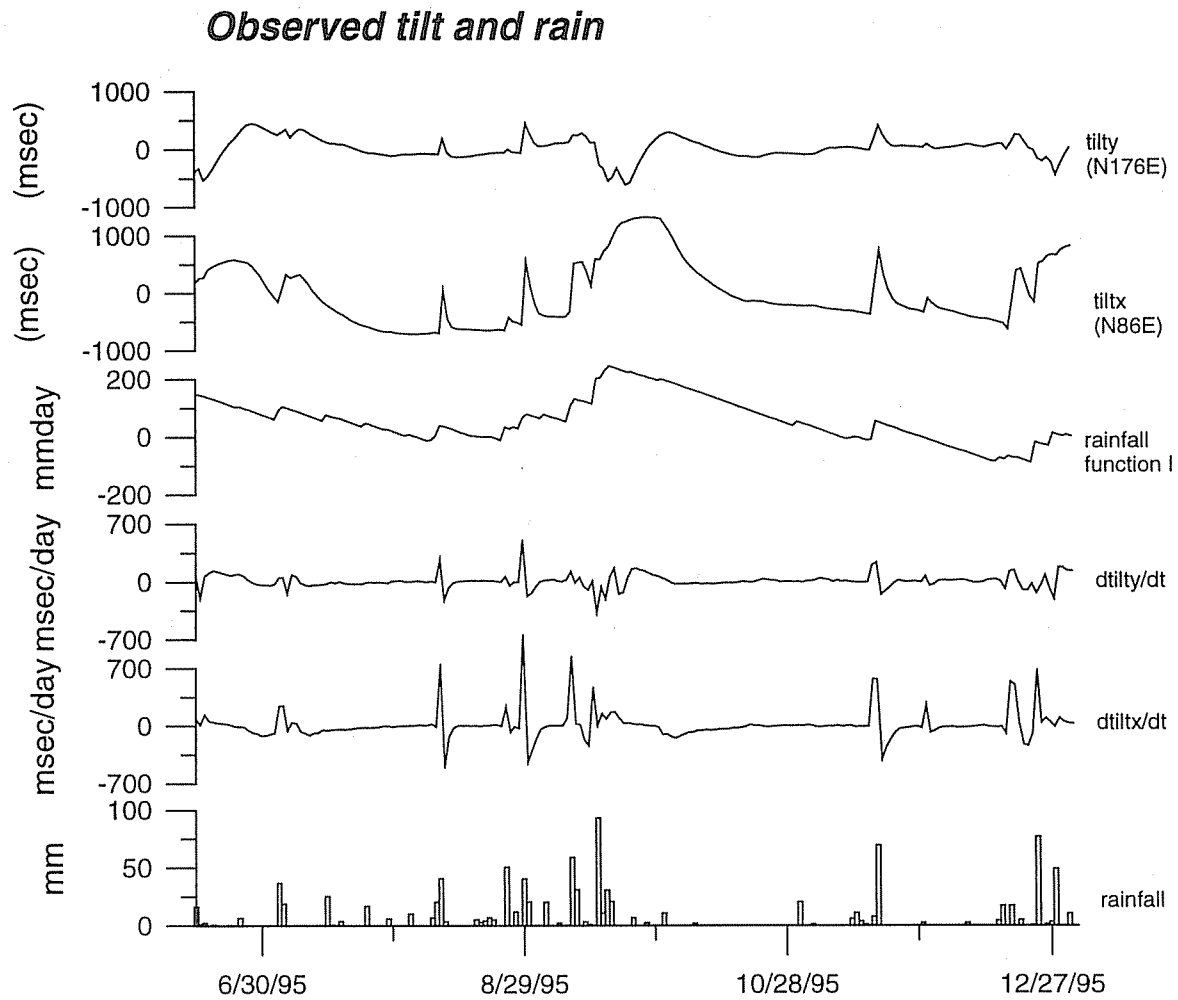

Fig. 1 – Different ways to evaluate the influence of rainfall on tilt observations by visual inspection. For the second half of the year 1995 the rainfall, the time integral of rainfall minus a linear trend (rainfall function I), the time derivative of tilt and the tilt observations are shown. The tilt observations refer to a reference system aligned with the orientation of the induced tilt (N86E).

rainfall, the rainfall function I (Eq. 1), the time derivative of the two tilt components and the two tilt components are graphed for the second half of year 1995. The rainfall and tilt measurements refer to the Friuli (NE-Italy) strain-tiltmeter network installed in 1977 (Zadro, 1978). Rainfall is furnished by the Italian Government service (Magistrato delle Acque, station Vedronza) with daily sampling. The relative distance between the tilt and rainfall station is 9 km.

The tilt observations are made in a natural cave at the Gemona station with Zöllner type horizontal pendulums. Details about the station and the network are described in Braitenberg (1998). The tilt data have been reduced from hourly to daily sampling, after having applied an antialiasing filter. The long term drift and yearly thermoelastic deformation have been taken off by least squares adjustment with the sum of a fourth order polynomial and a sine and cosine function of 1 year period. Remaining long period signals have been taken off by high pass filtering with cut off period of 30 days. The reference system of tilt has been rotated so as to align one axis with the orientation of maximum hydrologic induced deformation. This orientation was obtained from the principal direction of the ellipse describing the angular distribution of the mean square tilt amplitude (tilt cleaned from long period time variations). For the year 1995 the mean orientation of the greatest and least square tilt amplitude is oriented N86E and N176E, respectively. The correlation coefficients of rain or the rainfall function I (Eq. 1) with the tilt observations and the tilt time derivatives are given in Table I. The values refer to the second half of year 1995.

The Table I shows that the correlation coefficients of rainfall with the tilt components would erroneously demonstrate that the tilt measurements were independent from rainfall. Use of the rainfall function I or the time derivative of the tilt measurements for the correlation analysis reveals that hydrologic influence does exist.

Langbein et al. (1990) considered the influence of rainfall on repeated length measurements of geodetic baselines near Parkfield, California. They introduce a rainfall function II that has great similarities with the above rainfall function I. It is a cumulative function of rainfall, but rainfall is convolved with an exponential function with a time constant (τ). The rainfall function II is defined as:

$$r(n) = \sum_{k=1}^{n} p(k) e^{-\left((n-k)\Delta t/\tau\right)} - \bar{p}\, n\Delta t \qquad n \geq k \qquad (2)$$

As in eq(1) a linear trend given by the average time derivative $\bar{p}$ is subtracted. The method has been applied successively by Bella et al. (1995) for correcting observed tilt variations.

	Tilt x	Tilt y	Time derivative Tilt x	Time derivative Tilt y
rain	0.002	-0.000	0.525	-0.018
Rain function I	0.703	-0.147		

Tab. I – The correlation coefficients of rain or the rainfall function I and the tilt observations or their time derivatives are reported. The time interval is the second half of year 1995. The time series refer to those graphed in Fig. 1. The tilt components refer to the reference system rotated by 86° clockwise, which is the direction of greatest amplitude for the induced deformation.

Wolfe et al. (1981) find strong influence of hydrologic agents in strain data from a Benioff type gauge installed in the Kipapa tunnel (Oahu, Hawaii). The tunnel is located at 30m depth beneath weathered basalt. An empirical model for the rain-strain relationship is developed that uses two known hydrologic mechanisms, infiltration and recession (outflow of water from the ground). They find the following expression for the rain-induced strain (*e(t)*):

$$\begin{aligned} e(t) &= \alpha f t & 0 \le t \le t_c \\ e(t) &= \alpha f t e^{-(t-t_c)/\tau} & t_c \le t \le \infty \end{aligned} \qquad (3)$$

with

α = transfer value from rainfall to strain

f = infiltration rate

t_c = duration of rainfall

τ = time constant

The time constant (τ) takes inflow of water through the porous aquifer and exponential recession into account. The application of the model to observed data gives transfer values (α) in the order of 10 nstrain/mm. The time constant of the exponential decay ranges from 20 to 50 hours.

Yamauchi (1987) studies the effect of rainfall on 10 years of crustal strain (extensometer and tiltmeter) at Mikawa crustal movement observatory, Central Japan. The induced strain is modelled by a simulated outlet of a series of 3 concatenated tanks, which has a nonlinear response to the incoming rainfall. The tank model has been used also in the simulation of groundwater flow. Each tank obeys the differential equation:

$$\dot{H}(t) = P(t) - \alpha H(t) - a_1(H(t) - H_1) - a_2(H(t) - H2) \qquad (4)$$

with

$$a_i = \begin{cases} \text{constant } (\neq 0) & H(t) \ge H_i \\ 0 & H(t) < H_i \end{cases}$$

where $H(t)$ is the waterlevel in the tank at time t, $\dot{H}(t)$ is the time derivative of $H(t)$, and H_1, H_2 are two levels at which the outlets are set. The input flow to the successive tank is given by:

$$O(t) = \begin{cases} a_1(H(t) - H_1) & H(t) \ge H_1 \\ 0 & H(t) < H_1 \end{cases}$$

The second tank behaves in analogous way, its outlet being fed into a third tank. The waterlevel of the third tank simulates the strain response to rain. The equations must be numerically solved and the parameters adapted by trial and error. The examples shown are

promising and partly reproduce the induced signals well; the authors claim that they were able to correct 90% of the effects of rainfall over a 10 years observation period. One problem in the general application of the method is that the determination of the parameters is made with trial and error, which is a time consuming approach.

An innovative method is given by the techniques of predictive filtering. The subclass of the autoregressive (AR) time series model is defined by

$$x(n) = -\sum_{1}^{m} a(k)x(n-k) + u(n) \qquad (5).$$

in which $x(n)$ is the output sequence of a causal filter modeling the observed data and $u(n)$ is an input driving sequence (Marple, 1987; p.174). The parameter m defines the order of the AR-model. The $a(k)$ parameters define the filter, and can be obtained as solutions to linear equations. Marple (1987) gives an ample discussion on the different algorithms with which the $a(k)$ parameters can be calculated, given the model order m and the sequence to be modeled $x(n)$.

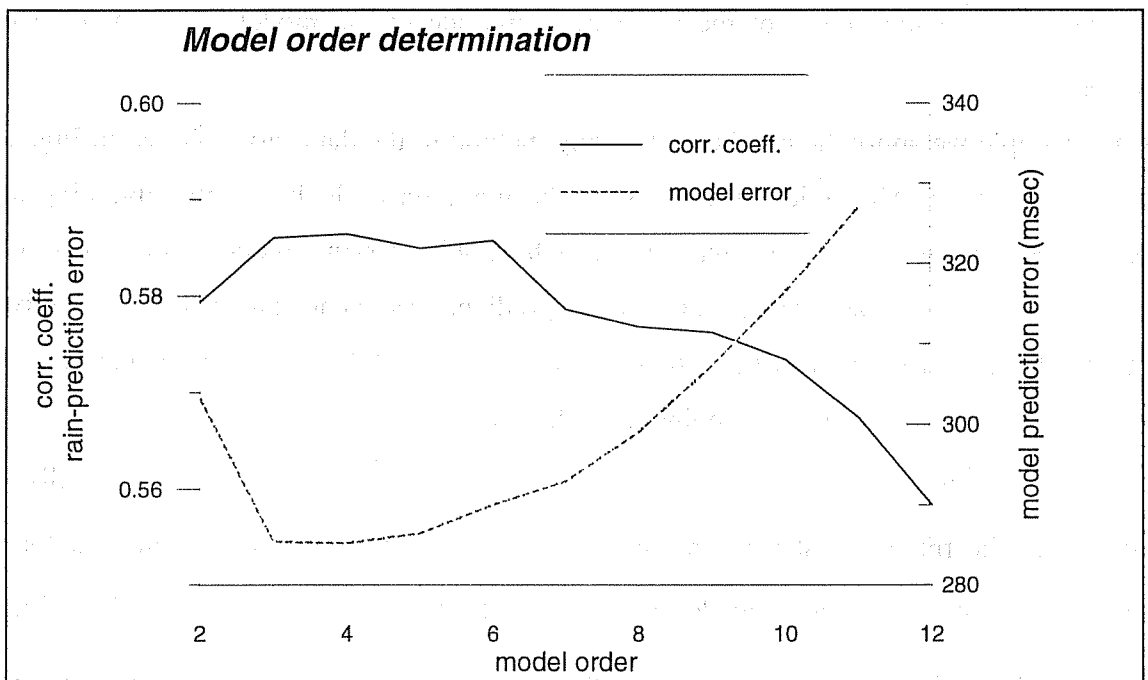

Fig. 2 – Two statistical quantities for determining the model orders: 1) correlation coefficient of rainfall and the theoretical driving sequence (fpe) obtained for different orders of the AR model, 2)model error, equal to the root mean square of the difference of the observed and predicted rain induced tilt for different model orders. The quantities are extreme for model order equal to 4.

The choice of the model order m constitutes a problem, for which we propose two solutions. Both solutions base on the postulate that the AR-model obtained should represent the portion of observed data which is rain induced. Consequently the driving sequence $u(n)$, should be equal to the rainfall multiplied by an appropriate scaling factor (units msec/mm),

$S\ p(n)$. Given the AR model, we may calculate for the first solution a theoretical driving sequence, which is equal to the forward prediction error (fpe):

$$e_m(n) = \sum_{k=1}^{m} a(k)x(n-k) + x(n) \qquad (6).$$

We apply the criteria of maximizing the correlation coefficient of rainfall and the theoretical driving sequence ($e_m(n)$) for different model orders m.

The second criterion bases on the postulate that the modeled data sequence should be as close as possible to the observed data, given the rainfall as the driving sequence. With $\overline{p}$ the time average over the studied period of rainfall, we define the error of the induced signal by

$$\Delta_m(n) = x(n) - \left[S_m\left(p(n) - \overline{p}\right) - \sum_{k=1}^{m} a_m(k)x(n-k) \right] \qquad (7),$$

in which S_m is a scaling factor. The scaling factor (S_m) is equal to the ratio of the mean square root amplitude of the fpe ($e_m(n)$) and the rainfall ($p(n)$). We choose that particular model order m for which the root mean square amplitude of the model error ($\Delta_m(n)$) is minimized.

As an example we apply the predictive filtering method to the data series shown in Fig. 1. The estimation of the AR-model parameters can be made on a block of data, obtaining an average model, or in an adaptive way, by which slowly varying model parameters are obtained. For the present case we have applied the gradient least mean square (LSM) adaptive algorithm, which is a robust adaptive method (see e.g. Marple, 1987), in which the parameters are recursively corrected at each data point, according to

$$a_k(n) = a_k(n) - u\nabla\left(e_m^2(n)\right) \qquad k = 1, m \qquad (8)$$

with $e_m(n)$ the fpe at the step n, and u a convergence factor. The convergence factor u adjusts the amount of correction made at each step. In order to guarantee stability of the algorithm, it should be chosen as $u < \frac{1}{m\,w}$, with w the mean square amplitude of the fpe and m the model order (Marple, 1987).

The gradient LMS method has been applied to 6 months of tilt recordings of the Gemona station (see Fig.1). As explained above, the data have been reduced to daily sampling rate and freed from long period signals. The component aligned with the preferential orientation of the induced signal was modeled (tiltx). The most appropriate model order has been obtained from the two criteria of maximum correlation coefficient of the fpe and rainfall and the minimum root mean square amplitude of the error on the predicted rain induced tilt. The two quantities

are graphed in Fig. 2 for different model orders, and are seen to obtain extreme values (maximum and minimum, respectively) for a model order equal to 4. The scaling factor S_4 resulted to be 13 msec/mm (63 nrad/mm) rainfall. The convergence factor was chosen u = 5 10^{-8} for all orders examined in Fig.2. The modeled rain induced tilt (light trace), the observed tilt (heavy trace) and the fpe are graphed in Fig. 3. Comparison with Fig. 1 reveals the great similarity between the fpe and the time derivative of the tilt signal (dtiltx/dt). The agreement between the fpe and rainfall is partial, which may have different reasons. First, the observed tilt signal is a combination of tectonic and ambient factors, and each of these parameters constitutes a driving sequence to the signal. Second, in the particular case of the Gemona station, the pluviometer is located 9 km away from the observation station, which in mountainous areas can lead to significant differences in the observed rainfall. Nonetheless, in Fig. 3. one can see that the algorithm is apt to identifying the portions of the observed tilt which are rain induced.

The time variation of the four autoregressive parameters is shown in Fig. 4. The parameter of first order is almost five times greater in amplitude than the parameter of second order and

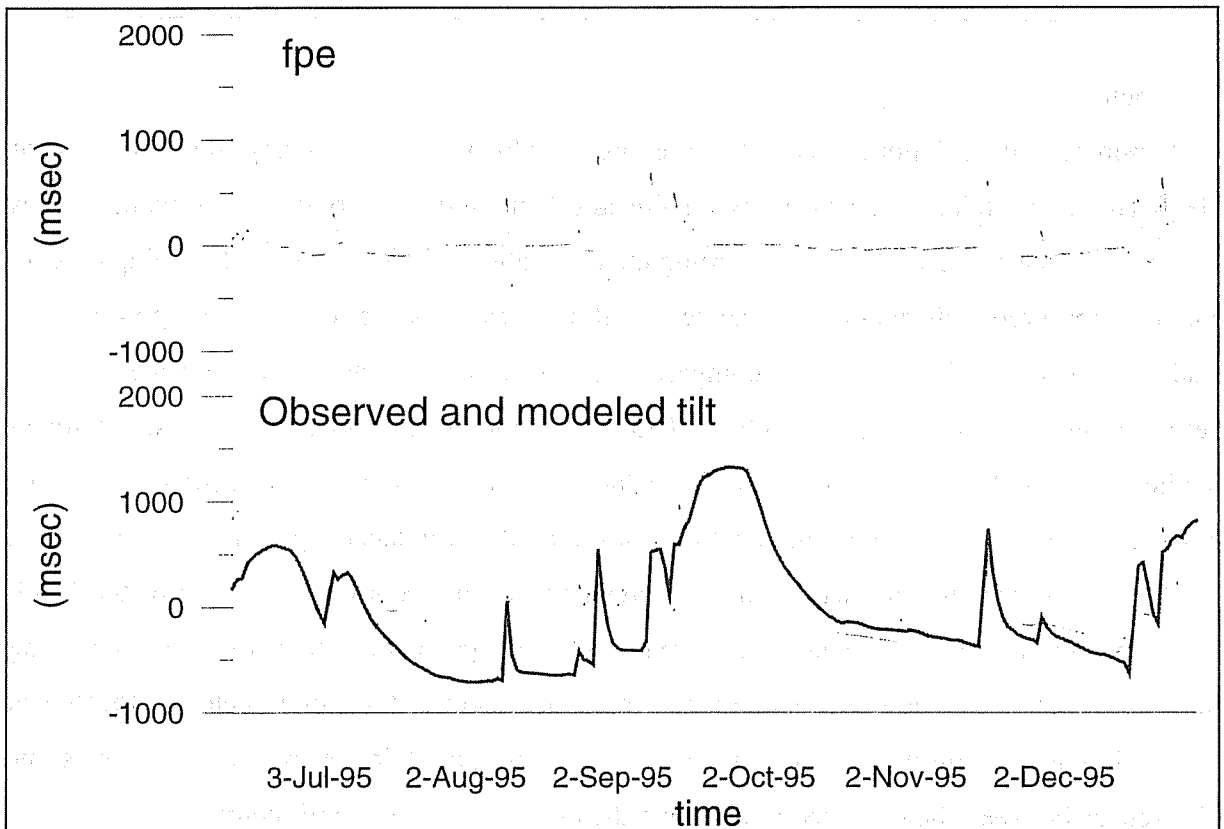

Fig. 3 – Modeled (light trace) and observed (heavy trace) hydrologic induced deformation of tilt at GE - station. Original records freed from long period signal and reduced to daily sampling. Also shown is the forward prediction error (fpe)

nearly an order of magnitude greater than the parameters of third and fourth order. This explains the great similarity between the fpe and the time derivative of tilt.

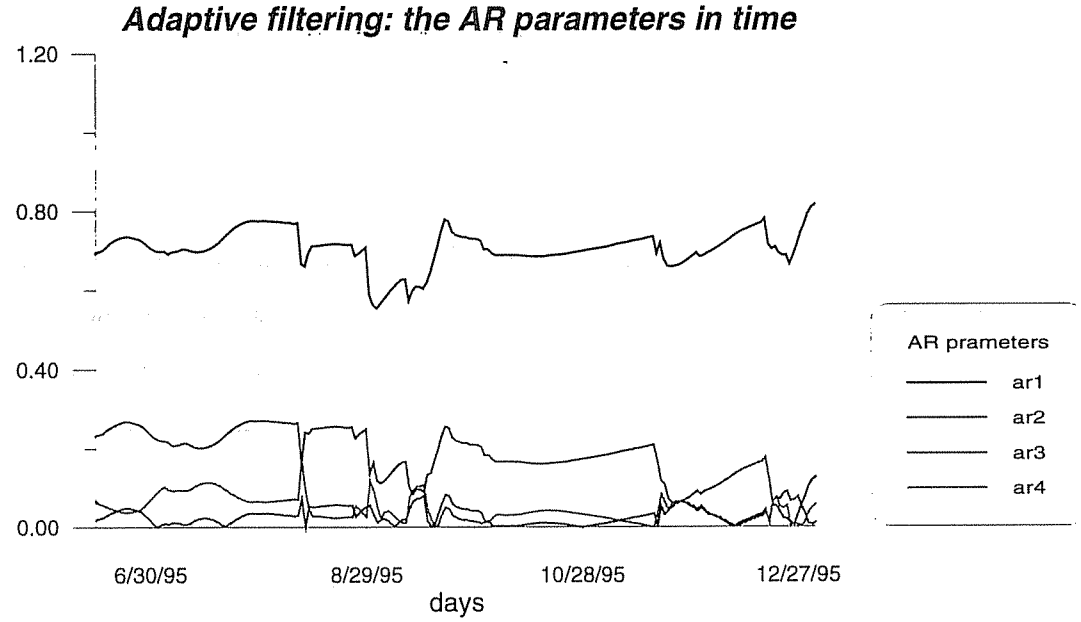

Fig. 4 – The time variation of the AR-model of the tilt recorded at Gemona station.

Conclusions

A number of techniques have been exposed which aim at solving the problem of identifying and modeling the hydrologic induced effects in deformation measurements. It has been shown that erroneous results regarding the correlation coefficient of the hydrologic agent and the observed deformation are achieved, if the two time series are not appropriately analyzed. The rainfall is to be compared to the time derivative of deformation, the deformation to a time integral function of rainfall. Among the statistical models, the linear prediction filters have given good results for the modeling of the hydrologic induced signals. In the example shown though, the reliability of the modeled induced signal is not such, that it can blindly be used to subtract the induced signals from the records. In the case of the Friuli measurements two main reasons can be made responsible for this: first, the daily sampling rate of rainfall is too low and should be increased. Second, the pluviometer is located at several km away from the observation station, which in mountainous areas could cause some differences between the observed rainfall and the one influencing the tiltmeter.

Acknowledgements - the work was partly financed by EC research grant no. IC15 CT96-0205 and CNR 98.00159/97.00121. I wish to thank Prof.M.Zadro for suggestions and the critical review of the paper and Prof.C.Ebblin for discussions during the development of the study.

References

Bella, F., Biagi, P.F., Caputo, M., Della Monica, G., Ermini, A., Manjgaladze, P.V., Sgrigna, V. and Zilpimiani, D.O., 1995. Possibile creep-related tilt precursors obtained in the Central Apennines (Italy) and in the Southern Caucasus (Georgia). PAGEOPH, 144: 277-300.

Braitenberg C. (1998) The Friuli (NE Italy) tilt/strain gauges and short term observations. Submitted to Annali di Geofisica.

Dal Moro G. and Zadro M., (1998) Subsurface deformations induced by rainfall and atmospheric pressure: tilt/strain measurements in the NE-Italy seismic area, Earth and Planetary Science Letters, in press.

Edge, R.J., Baker, T.F. and Jeffries, G., 1981. Borehole tilt measurements: aperiodic crustal tilt in an aseismic area. Tectonophysics, 71: 97-109.

Evans, K. and Wyatt, F., 1984. Water table effects on the measurement of earth strain. Tectonophysics, 108: 323-337.

Kasahara, M., Shichi, R. and Okada, Y., 1983. On the cause of long-period crustal movement. Tectonophysics, 97: 327-336.

Kümpel, H.J., 1986. Model calculations for rainfall induced tilt and strain anomalies. In: Vieira R. (Editor), Proceedings of the Tenth International Symposium on Earth Tides. Madrid, pp. 889-901.

Kümpel, H.J., 1989. Verformungen in der Umgebung von Brunnen. Habil. thesis, Univ. of Kiel, Faculty of Mathematics and Natural Sciences, 198 p.

Langbein, J.O., Burford, R.O. and Slater, L.E., 1990. Variations in fault slip and strain accumulation at Parkfield, California: initial resul using two-color geodimeter measurements, 1984-1988. J. Geophys. Res.,95, B3: 2533-2552.

Lorenzetti, E. and Tullis, T.E., 1989. Geodetic predictions of a strike-slip fault model: Implications for intermediate-and short-term earthquake prediction. J.Geophys. Res., 94: 12343-12361.

Marple, S.L., 1987. Digital spectral analysis with applications. Prentice-Hall, Inc., Englewood Cliffs, New Jersey.

Peters, J. and Beaumont, C., 1981. Preliminary results from a new borehole tiltmeter at Charlevoix, Québec. Proceedings of the Ninth International Symposium on Earth Tides. New York City, pp. 69-77.

Scholz C.H., 1990. The mechanics of earthquake faulting, Cambridge University press, Cambridge. 439 pp.

Scholz, C.H., Sykes, L.R., and Aggarwal, Y.P., 1973. Earthquake prediction: a physical basis. Science, 181: 803-809.

Tanaka, T., Shimojima, E., Mitamura, K., Hoso, Y. and Ishihara, Y., 1989. Precipitation, groundwater and ground deformation. In: "Global and regional geodynamics", Edinburgh, Scotland, August 3-5 1989, Editors Vyskocil P., Reigber C. & Cross P.A., Springer-Verlag, pp. 132-139.

Wolfe, J.E., Berg, E. and Sutton, G.H., 1981. "The change in strain comes mainly from the rain": Kipapa, Oahu.. Bull. Seismol. Soc. Am., 71: 1625-1635.

Yamauchi, T., 1987. Anomalous strain response to rainfall in relation to earthquake occurrence in the Tokai area, Japan. J. Phys. Earth, 35: 19-36.

Zadro, M. , 1978. Use of tiltmeters for the detection of forerunning events in seismic areas. Boll. Geod. Sc. Aff., 2-3: 597-618.

Efficiency of Air Pressure Corrections in the BFO-Records of the Balleny Islands Earthquake, March 25, 1998

by

Walter Zürn, Rudolf Widmer-Schnidrig and Sandra Bourguignon

Black Forest Observatory Schiltach, Heubach 206
D-77709 Wolfach, Germany,
Institute of Geophysics and Planetary Physics, University of California at San Diego,
La Jolla, CA 92093, U. S. A.
and
Geophysical Institute, Karlsruhe University, Hertzstr. 16
D-76187 Karlsruhe, Germany

Abstract

It is well known that in the period range of the tides a simple subtraction of local barometric pressure data with regression factors of 3 to 4 $nm/s^2/hPa$ does a lot for variance reduction in gravity records. Zürn and Widmer (1995) demonstrated the efficiency of the identical procedure up to about 1.5 mHz. Several records of the Magnitude 8.2 Balleny Islands earthquake from BFO were analysed with the goal to improve the signal-to-noise ratio of low order free oscillations of the earth using local records of atmospheric pressure. In addition we corroborate the result obtained by Japanese scientists that between 2 and 7 mHz the lowest noise level in gravity records is defined by incessantly excited spheroidal free oscillations.

1 Introduction

In the analysis of modern gravity tide observations of high quality a simultaneous record of the local atmospheric pressure is included in the functional model for the least squares solution (e. g. Wenzel, 1997). With regression factors in the vicinity of 3.5 $nm/s^2/hPa$ the variance of the post-fit residuals is reduced appreciably (for example by 86 % in the record by Polzer et al. 1996). Introduction of frequency dependence of this gravity-pressure admittance especially at very long periods further reduces the variance, but by far not as much (Crossley et al. 1995; Neumeyer and Dittfeld, 1997). The efficiency of this simple prodedure at frequencies between the tides and the seismic free oscillations is well known by people searching for the Slichter modes (e. g. Smylie, 1992; Hinderer et al. 1995). Zürn and Widmer (1995) and Van Camp (1998) demonstrated, that using this correction in gravity records after large earthquakes improves the signal-to-noise ratio (SNR) below 1.5 mHz to the extent, that modes like ${}_oS_2$ and ${}_oS_3$ become visible in the spectra. Virtanen (1996) identified ${}_oS_2$ in the corrected record of the Finnish superconducting gravimeter of the Shikotan earthquake (October 4, 1994), but without showing the uncorrected record. Newtonian attraction by the local atmosphere explains most of the effect, with additional contributions from

the vertical motion due to surface loading by the atmosphere. Many theoretical models support this theory (see Neumann and Zürn, this volume; e. g. Müller and Zürn, 1983; Rabbel and Zschau, 1985).

Beauduin (1996) and Beauduin et al. (1996) demonstrated the efficiency of barometric corrections on free oscillation spectra from vertical and horizontal STS-1 seismometers (Wielandt and Streckeisen, 1982) located in Central Europe and the Sahara (Africa). These authors determined a complex frequency dependent transfer function between seismic noise and local barometric pressure in the frequency range between 0.1 and 10 mHz. Interesting features of their results for the horizontals are, that the corrections worked especially well for installations showing higher noise than others at the same location and that there was a strong and constant linear polarization of the pressure-induced signal over a full year. Considering also the fact that local pressure was efficient and not the pressure gradient for example, we propose the following mechanism: pressure deforms the surrounding of the station resulting in a tilt proportional to pressure in a fixed direction and magnitude which strongly depends on the very local geometry and geology of station and pier. This mechanism is very similar to the one producing the infamous local elastic effects in tidal tilt and strain records (Harrison, 1985). Beauduin (1996) suggested other physical models which we think do not explain all the observations.

In the following section below we test the possibility to correct long period records using local barometric pressure again using the data following the great Balleny Islands earthquake of March 25, 1998. We emphasize that the effects corrected for in the gravity records are not of instrumental nature. This was demonstrated by Müller and Zürn (1983) in their study of gravity signals from cold fronts. Of course, such corrections could also be effective at much higher noise levels if the instruments are sensitive to ambient pressure. Therefore it is important to show the improvement of the data either on an absolute scale or in comparison to some hard to observe modes (e. g. Zürn and Widmer, 1995; Beauduin et al. 1996)

Japanese scientists (Nawa et al. 1998; Suda et al. 1998; Tanimoto et al. 1998; Kobayashi and Nishida, 1998) have shown with the records from STS-1 seismometers, IDA- gravimeters (Agnew et al. 1986) and superconducting gravimeters, that the fundamental spheroidal modes ${}_oS_l$ are observable by stacking the spectra of seismically quiet intervals, i. e. intervals where earthquake excitation can be ruled out. These authors suggest that the larger number of smaller quakes cannot be held responsible for the observed excitation levels (about 1 ngal), but that turbulence in the global atmosphere interacting with the solid earth could be the cause. In the last section we show, that with the data from the gravimeter at BFO these incessantly excited free oscillations of the earth between 2 and 7 mHz can also be observed.

2 Barometric Pressure Corrections between 0.2 and 1.5 mHz

We inspected the data from the different long period instruments at BFO Schiltach (48.°33 N, 8.°33 E, 589 m amsl) for low order mode excitations after the quake. Diffe-

rent record lengths for the different signals were found to show the best SNRs. Then sequences of regression factors to be multiplied with barometric pressure data subsequently subtracted from the seismic records were used to find the value producing minimal noise levels in the neighbourhood of ${}_oS_2$, avoiding theoretical mode frequencies. This was done simultaneously for both barometric pressure signals in front of (P_a) and behind (P_i) the efficient air-lock at BFO (Richter et al. 1995). This air-lock acts as a simple low-pass filter for barometric pressure variations with P_a as input and P_i as output. While Richter et al. (1995) reported a time constant of 4 h for this filter, a later analysis showed that it is higher than 20 h. So far we have not attempted to use complex admittances, mainly because our physical models for the effects are very simple, as discussed below.

2.1 Gravity

The ET-19 gravimeter and its installation were also described by Richter et al. (1995). However, the insensitivity of the instrument to P_i proven by Müller and Zürn (1983) and maintained and tested throughout the years that followed, no longer exists since August 1996, probably due to aged seals. Changes in P_i affect the instrument since that time and therefore both pressures were used for corrections here in contrast to the procedure used by Zürn and Widmer (1995). Fig. 1 shows two spectra of a 132 h time series starting about 3 h after the quake (instrument saturation occurred for the first arrival of Rayleigh waves). The time series were multiplied by a hanning window before spectra were computed. Details are presented in the caption. Of course, P_a was also used alone and most of the improvement is already produced by just subtracting the outside pressure, as in earlier cases. As pointed out by Zürn and Widmer (1985), this pressure correction has never been successful for the vertical STS-1 and the vertical component of the STS-2 seismometer at BFO at this low level of noise. The reason for this must be an instrumental one and is not understood as yet. The vertical STS-1 and the STS-2/Z show ${}_oS_3$ with SNRs of 4 and 2, respectively. A comparison of those channels for the deep North Bolivia quake of 1994 without pressure corrections can be found in Richter et al. (1995).

The outside pressure P_a acts from the distance by Newtonian attraction. The regression factor and its sign show high consistency with earlier results, with many results from tidal work at this and other stations all over the world, and with many theoretical models for this physical effect. A minor contribution is due to the free air effect and inertial force due to vertical motion of the gravimeter, both with opposite sign to the attraction. In contrast, the much smaller effect of inside pressure is instrumental, clearly, because it did not exist more than 2 years ago. The regression factor is 5 - 6 times as high as for outside pressure, but because of the high time constant of the air-lock the inside pressure signal is reduced by a factor of about 50 in this frequency range resulting in a minor contribution to the correction. The possibility of a complex admittance to P_i still needs investigation, because the suspected leak could produce a time constant.

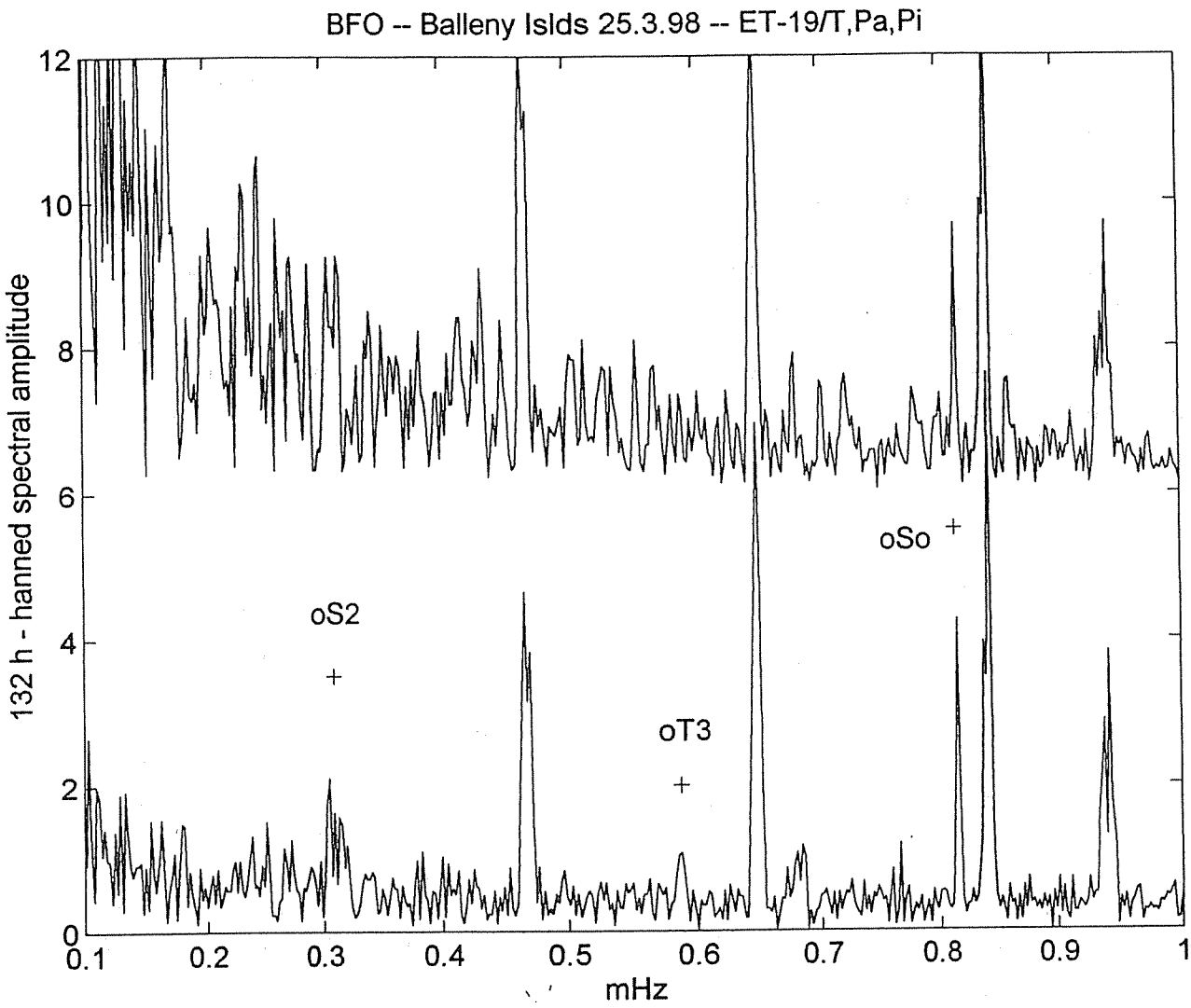

Figure 1: Spectra of a 132 h time series (hanned) from the LaCoste-Romberg ET-19 gravimeter with (bottom) and without (top) correction of atmospheric pressure. Upper spectrum shifted by 6 units for clarity. Note clear improvement of signal-to-noise ratio for ${}_oS_3$, ${}_oS_4$, ${}_oS_o$ and ${}_oS_5$ and the appearance of modes ${}_oS_2$ and ${}_oT_3$ just above the noise level after the correction. Plus signs indicate theoretical mode frequencies. The torsional mode ${}_oT_3$ shows up in this vertical record probably due to the Coriolis force associated with horizontal motion. The outside and inside barometric pressure records were multiplied by factors of 3.63 and 20 $nm/s^2/hPa$, respectively and subtracted from the gravity record. These regression coefficients were obtained simultaneously by minimizing the noise in the immediate neighbourhood of mode ${}_oS_2$. Note that in August 1996 this gravimeter first started to be sensitive to ambient (i. e. inside the air-lock) barometric pressure, but the pressure fluctuations inside the mine are reduced by almost two orders of magnitude in this frequency band due to the air-lock.

2.2 Strain

Widmer et al. (1992) could identify the fundamental torsional mode ${}_oT_2$ clearly in the records from the strainmeter array in BFO after the Macquarie Ridge event of May 23, 1989. Since the Balleny Islands quake was a similarly energetic (nearly) strike-slip event, we decided to try this again. 30 h records appeared to provide the best SNR for the low order modes, so this window length was chosen and as for gravity, noise around the frequency of ${}_oS_2$ was minimized by subtraction of P_a multiplied by a regression coefficient from the records of the individual linear strain meters St-0, St-3 and St-4. In the case of the Macquarie Ridge event the SNRs could not be improved in this manner, probably because the atmosphere was extremely quiet in Southwestern Germany after that quake. Here variance reductions of the order of 85 to 90 % resulted. The three linear strains were then combined to obtain areal and shear strain signals. The direction of the shear plane was varied to find the optimal signal, which turned out to occur for shear-planes with azimuths between $N30°E$ and N45°E. Fig. 2 shows the spectra for 6 strain signals (see caption for details). At least one of the raw linear strains and the two shear strains clearly show energy at the frequencies of the torsional fundamental modes ${}_oT_l$ for l = 2 and 3, while l = 4 is only very weakly visible if at all. Clearly the SNR in these observations is at best 2 to 3, nevertheless such observations are really rare.

The sign of the estimated regression factors is such that increasing outside barometric pressure P_a results in apparent extension of the strainmeter, i. e. compression of the rock. The factors are very similar to the ones found by Neumann and Zürn (1999, this volume) for the effect of waves in the atmosphere and show the same tendency across the array. Since these factors are very close to each other across the array and no delay with respect to P_a could be observed, we conjecture deformation of the hill containing the tunnels by the local atmospheric pressure, leading to shortening of the tunnels with increasing pressure. For P_a no instrumental effects can be responsible. So far we have not investigated the influence of P_i very carefully, several instrumental effects are expected physically. However, the level of P_i-fluctuations is very low in this frequency range due to low-pass effect of the air-lock.

2.3 Tilt

The success with identification of the lowest order torsional modes in the strain spectra led to an investigation of our other horizontal seismic records. However, complex pressure admittances analog to the work by Beauduin et al. (1996) were not tested as yet. We did not expect to see modes clearly on the record from our 120 m - differential pressure fluid tiltmeter (Otto et al. 1998). Fig. 3 shows the spectrum of a 48 h record from this instrument. While peaks exist at the frequencies of ${}_oT_2$ and ${}_oT_3$ they really do not stick out of the noise level and therefore are probably fortuitous. However, starting with l = 4 many fundamental torsional modes with higher l show up clearly. To our knowledge this is the first free oscillation spectrum of some quality from a fluid tiltmeter and it demonstrates the overall quality of this sensor of tilt. P_a was subtracted with a factor from this record as well before taking the spectrum, but the improvement is insignificant and probably just accidental.

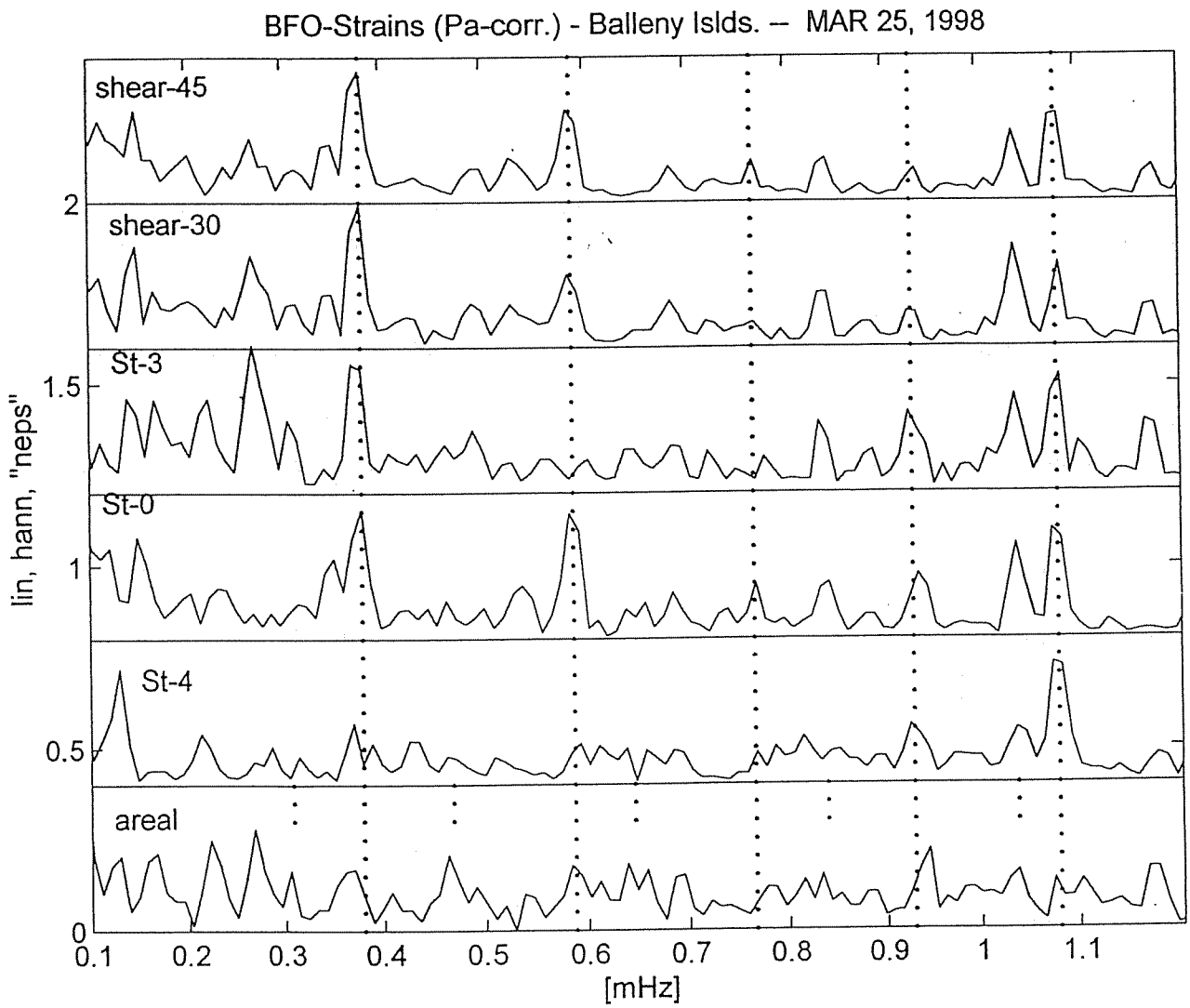

Figure 2: Spectra of 30 h time series (hanned) from the Invar wire strainmeter array at BFO (King and Bilham, 1976; Widmer et al., 1982). From bottom to top these represent in absolute units: areal strain, linear strain $N60°E$ (St-4), linear strain $N0°E$ (St-0), linear strain $N300°E$ (St-3), shear strains on vertical planes striking $N30°E$ and $N45°E$. Torsional (spheroidal) fundamental mode eigenfrequencies for Earth model 1066A are indicated by long (short) vertical dotted lines: energy is clearly present at ${}_oT_2$, ${}_oT_3$, ${}_oT_5$, ${}_oT_6$ and ${}_oS_6$, marginally at ${}_oS_4$ and ${}_oS_5$. Note that the lowest torsional modes are not present in the areal strain, which corroborates the interpretation from the frequencies alone. Outside barometric pressure with regression coefficients 0.535, 0.755 and 0.763 $10^{-9}/hPa$ was subtracted from the strain records from St-0, St-3 and St-4, respectively.

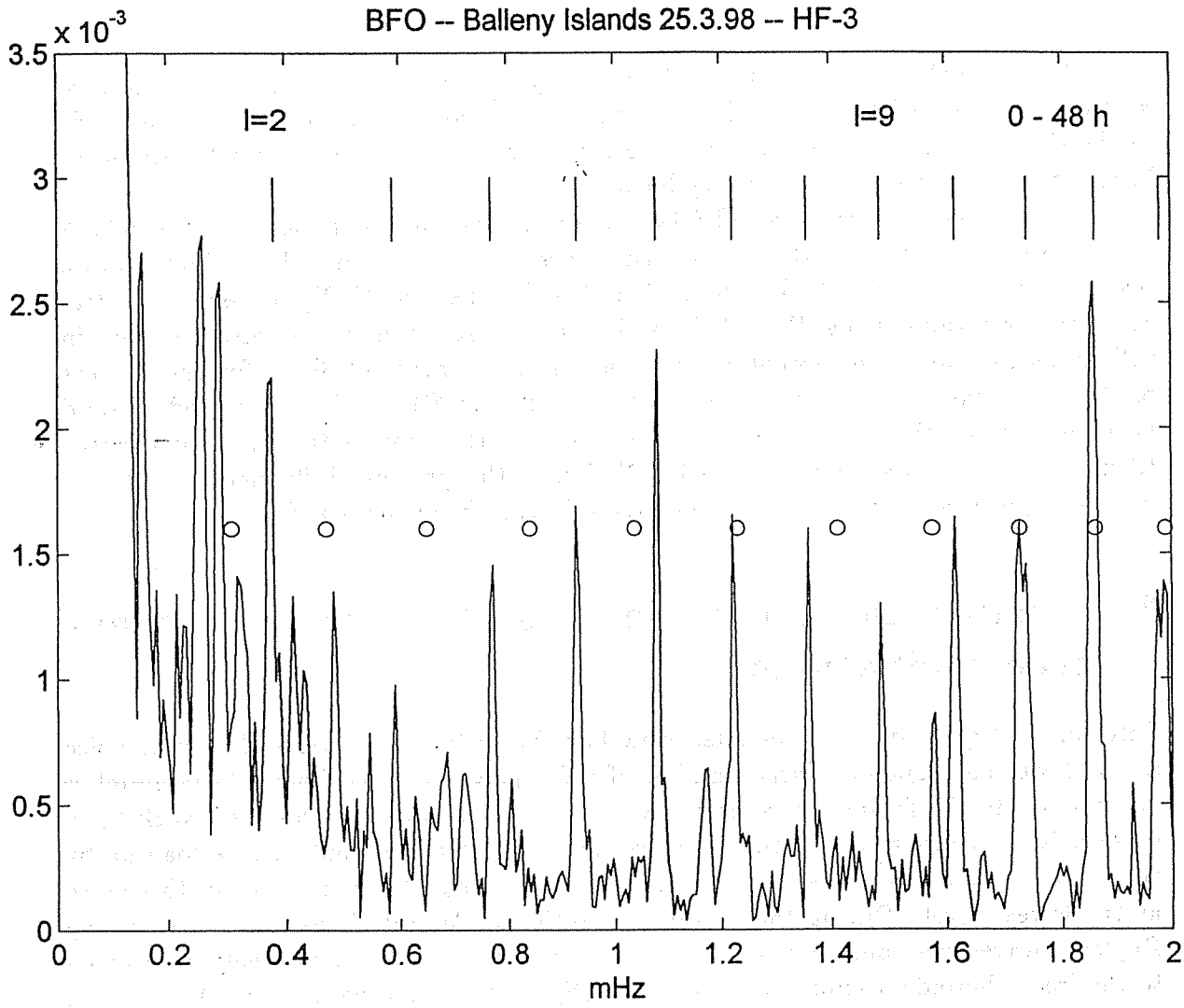

Figure 3: Spectrum of a 48 h record (hanned) from the 120 m - differential pressure fluid - tiltmeter at BFO (Otto et al., 1998). Theoretical eigenfrequencies of fundamental toroidal (spheroidal) modes for model 1066A are indicated by short vertical lines (open circles). Energy is present at the frequencies of ${}_oT_2$ and ${}_oT_3$, but there are other peaks in their neighbourhood which cannot be identified with modes .The peaks near ${}_oS_2$ and ${}_oS_3$ can also not be identified with these modes, since they are too far off in frequency. Mode identification starts to become possible for toroidal modes with l = 4 and above, clearly. However, these are the first observations of low order modes with such an instrument, which demonstrates the quality of the data. The mode just below the peak at ${}_oS_7/{}_oT_7$ can be identified with the higher mode ${}_1S_4$. This record was also corrected for outside atmospheric pressure, but the improvement of the SNR is insignificant

Note that if the earth would be spherically symmetric torsional modes would have no tilt associated with them (Gilbert, 1980). So the appearance of a torsional mode in the tiltmeter signal is either due to horizontal acceleration, or to effects related to lateral heterogeneities (possibly very local ones).

The uncorrected horizontal STS-1s and the horizontal components of the STS-2 showed peaks at some of the lowest order torsional modes, but clear identification became possible for $l = 3$ ($l = 5$) and higher for the NS- (EW)-components. Barometer corrections using P_a and P_i with simple regression factors also resulted in rather insignificant (and probably fortuitous) improvements of SNRs for the records of the two components from the Askania-Tiltmeter at BFO. The same modes could be identified for the same components as for the other horizontal seismometers (or tiltmeters in this frequency interval). Obviously the pressure influences on tilt are more complicated than on gravity and strain in this frequency band.

3 Vertical noise between 2 and 7 mHz: incessant free oscillations

Peterson (1993) derived the so-called New Low Noise Model for vertical seismic noise as the lower envelope of a large number of noise power spectra from a large number of stations. In the frequency range below 1.5 mHz it is apparent from the work by e. g. Zürn and Widmer (1995), that the gravitational attraction and surface loading by the atmosphere above the station is responsible for a significant amount of this noise at the lowest level. During the powerful eruption of Mount Pinatubo globe-circling Rayleigh waves were observed for about 6 to 8 hours, which constructively interferred to the free spheroidal oscillations ${}_oS_{28}$, ${}_oS_{36}$, ${}_oS_{37}$ and ${}_oS_{38}$ (Kanamori and Mori, 1992; Widmer and Zürn, 1992). Vertical oscillations of the atmosphere above the volcano with high probability were the source of these signals, the amplitude of which at BFO was 0.5 $\mu gals$. In a sense this was a clear case of seismic "noise" (in the form of free oscillations) produced by the atmosphere at great distance from most stations.

Very recently Japanese colleagues (Nawa et al. 1998; Suda et al. 1998; Tanimoto et al. 1998; Kobayashi and Nishida, 1998) detected that even without large earthquakes the fundamental spheroidal modes ${}_oS_l$ can be observed at very quiet stations in the vertical components. By stacking the spectra for many windows of identical length they found perfect alignment of the peaks in these stacks with the frequencies of the ${}_oS_l$-modes between 2 and 7 mHz. Note that this is the frequency range just above the range, where the barometric correction works for gravimeters. This range also corresponds to the lowest part of the New Low Noise Model. These colleagues favor atmospheric turbulence as the mechanism to produce these oscillations at amplitudes of about 1 ngal. The major task of course is to rule out the large number of small earthquakes or silent earthquakes.

We selected 96 windows far away from the large earthquakes in the Harvard CMT catalog. These windows started 16 h and 240 h after quakes of moment magnitudes of 6 and 8, respectively, with a logarithmic dependence in between. This way we intend to avoid the free oscillations excited by large quakes. All of our windows were 12 h

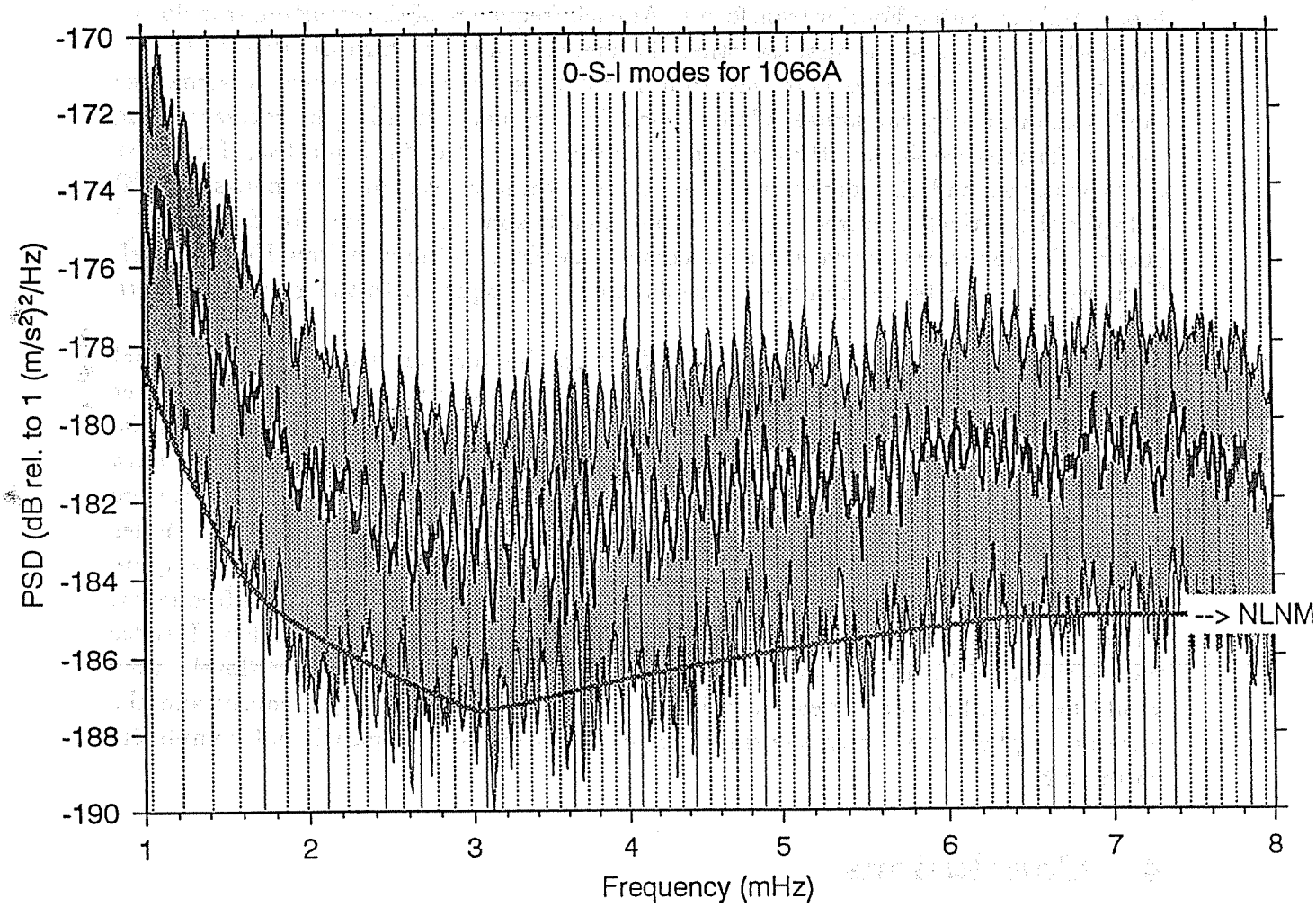

Figure 4: Pseudo power spectra obtained from 96 selected 12 h records from the ET-19 gravimeter are compared with the New Low Noise Model (NLNM) for vertical seismic noise constructed by Peterson (1993). At each frequency, the first quartile, the median and the third quartile of the 96 spectra is plotted. Dotted vertical lines represent the 1066A spheroidal fundamental mode frequencies. The windows were selected such that mode excitation by large earthquakes in the Harvard catalog is not possible: windows start no earlier than 16 (240) h after quakes of moment magnitude 6 (8), with a logarithmic dependence in between those two. This robust spectral estimation was used to avoid "contamination" by some large earthquake, which possibly sneaked into our windows. Between 2 and 7 mHz every peak in those robust "spectra" coincides with the frequency of an ${}_oS_l$-mode, thus confirming the observations of Japanese colleagues. The averaged first quartile curve essentially coincides with the NLNM.

long. We multiplied the data from the ET-19 gravimeter in these windows by Hanning tapers and computed Fourier transforms. At each frequency of the resulting transforms we plotted in Fig. 4 the first quartile, the median and the third quartile of the 96 power estimates. The idea here was, to have robust spectra with respect to some free mode excitations by earthquakes left in our selection inadvertently (the corresponding free oscillations would put the Fourier transform above the third quartile, if at most a few windows had this property. Note that the three curves all show peaks aligned with the theoretical eigenfrequencies of fundamental spheroidal modes for Earth model 1066A. The lowermost curve averaged comes very close to the New Low Noise Model. Thus we corroborate the findings of the Japanese colleagues with the gravimeter data from BFO.

The identical 96 windows from the ET-19 gravimeter were used in an additional study. Since the "correction" using local atmospheric pressure was allowing to extract low order fundamental spheroidal modes after very large quakes from the noise we tried this for these windows using a regression factor of 3.5 nm/s^2. Again the data were afterwards multiplied by hanning windows (12 h) and the resulting spectra were stacked. However, it was not possible to identify the spectral peaks with the modes except for one or two alignments, which we ascribe to chance. This was not quite unexpected, since the noise level below 1.5 mHz rises quickly with decreasing frequency, while the incessant mode spectrum appears to be almost constant in frequency. If those modes would be excited as much as the ones above 2 mHz (at the 1 ngal-level), they would be buried in the increasing noise probably due to instrumental causes and the local atmosphere, for which the simple model used in the first part is not completely correcting.

4 Conclusions

It appears from this and the referenced work that the low frequency part of the NLNM for vertical components is at least partially understood. Below 1.5 to 2 mHz a major part of the noise is caused by Newtonian attraction of the sensor mass by the atmosphere overhead of the station, with some contribution from the free air and inertial effects due to vertical displacement. Clearly the simplistic model used cannot account for all atmospheric phenomena, so some amount of atmospheric noise is left after the correction. Probably many instruments also contribute instrumental noise in this period band, even some of the best ones. In contrast, in the frequency band between 2 and 7 mHz the lowest noise levels are showing incessant free oscillations of the Earth probably excited by loading by the global atmosphere. In this band therefore corrections using local pressure will not help to lower the noise below the NLNM, as they do below 1.5 mHz. However, we think we are close to instrumental sources of noise here too, because the modes cannot be seen as well in individual windows. The mechanism of excitation at present is poorly understood and more work needs to be done to clarify this point. For the strainmeters and probably also some horizontal components local deformations by the local air pressure may dominate, but this could be very different from station to station, and as Beauduin et al. (1996) have shown, from installation

to installation.

Acknowledgements: Discussions with Erhard Wielandt and Udo Neumann are highly appreciated. The air-lock at BFO is serviced efficiently by Heinz Otto.

References

Agnew, D.C., Berger, J., Farrel, W.E., Gilbert, J.F., Msters, G., Miller, D., 1986 : Project IDA: A Decade in Review. *EOS (Trans. AGU)* **67**: 203 - 211

Beauduin, R. (1996). Étude du bruit de fond sismique à l'aide des données GEOSCOPE et des données de l'expérience OFM/SISMOBS. Thèse de doctorat, Université de Paris VII, pp. 130.

Beauduin, R., P. Lognonné, J. P. Montagner, S. Cacho, J. F. Karczewski and M. Morand (1996). The Effects of Atmospheric Pressure Changes on Seismic Signals or How to Improve the Quality of a Station. *Bull. seism. Soc. Am.*. **86**: 1760 - 1769.

Crossley, D., Jensen, O., Hinderer, J. 1995. Effective barometric admittance and gravity residuals. *Phys. Earth planet. Inter.* **90**: 221 - 241.

Gilbert, F., 1980. An introduction to low-frequency seismology. In: Physics of the Earth's Interior (A. M. Dziewonski and E. Boschi, Eds.), North-Holland, Amsterdam, 41 - 81.

Harrison, J. C. (ed.)(1985). Earth Tides. *Benchmark Papers in Geology Series*, 419 pp., Van Nostrand Reinhold, New York.

Hinderer, J., Crossley, D., Jensen, O. (1995). A search for the Slichter triplet in superconducting gravimeter data. *Phys. Earth planet. Inter.* **90**: 183 - 195.

Kanamori, H., Mori, J. (1992). Harmonic excitation of of mantle Rayleigh waves by the 1991 eruption of Mount Pinatubo, Philippines. *Geophys. Res. Lett.* **19**: 721 - 724.

King, G. C. P., Bilham, R. (1976). A Geophysical Wire Strainmeter. *Bull. seism. Soc. Am.* **66**, 2039 - 2047.

Kobayashi, N., Nishida, K. (1998). Continuous excitation of planetary free oscillations by atmospheric disturbances. *Nature* **395**: 357 - 360.

Müller, T. and W. Zürn (1983). Observation of gravity changes during the passage of cold fronts. *J. Geophys.*. **53**: 155 - 162.

Nawa, K., Suda, N., Fukao, Y., Sato, T., Aoyama, Y., Shibuya, K. (1998). Incessant excitation of the Earth's free oscillations. *Earth Planets Space* **50**: 3 - 8.

Neumann, U., Zürn, W. (1999). Gravity signals from waves in the atmosphere and their modeling. *Bull. Inf. Marées Terrestres*, submitted, this volume.

Neumeyer, J., Dittfeld, H.-J. (1997). Results of three years observation with a superconducting gravimeter at the GeoForschungsZentrum Potsdam. *J. Geodesy* **71**: 97 - 102.

Otto, H., Wenzel, H.-G., Zahran, K., Zürn, W. (1998). Tidal Analysis of the DFP Tiltmeter in the Black Forest Observatory (BFO), Schiltach. In: Proc. 13th Int. Symp. Earth Tides, Brussels 1997 (B. Ducarme, P. Paquet, Eds.), pp. 141 - 148, Observatoire Royal de Belgique, Brussels.

Peterson, J. (1993). Observations and Modeling of Seismic Background Noise. U. S. Geol. Surv., Open-File Rep. 93-322, 1 - 45.

Polzer, G., Zürn, W., Wenzel, H.-G. (1996). NDFW Analysis of Gravity, Strain and Tilt Data from BFO. *Bull. Inf. Marées Terrestres* **125**: 9546 - 9557.

Rabbel, W., Zschau, J. (1985). Deformations and Gravity Changes at the Earth's Surface Due to Atmospheric Loading. *J. Geophysics* **56**: 81 - 99.

Richter, B., H.-G. Wenzel, W. Zürn and F. Klopping (1995). From Chandler wobble to free oscillations: comparison of cryogenic gravimeters and other instruments in a wide period range. *Phys. Earth planet. Inter.* **91**, 131 - 148.

Smylie, D. E. (1992). The inner core translational triplet and the density near the Earth's center. *Science* **255**: 1678 - 1682.

Suda, N., Nawa, K., Fukao, Y. (1998). Earth's Background Free Oscillations. *Science* **279**: 2089 - 2091.

Tanimoto, T., Um, J., Nishida, K., Kobayashi, N. (1998). Earth's continuous oscillations observed on seismically quiet days. *Geophys. Res. Lett.* **25**: 1553 - 1556.

Van Camp, M. (1998). Comparison between the Tide and Gravity Signal output of the GWR superconducting gravimeter C021. In: Proc. 13th Int. Symp. Earth Tides, Brussels 1997 (B. Ducarme, P. Paquet, Eds.), pp. 565 - 572, Observatoire Royal de Belgique, Brussels.

Virtanen, H. (1996). Observations of free oscillations of the Earth by superconducting gravimeter GWR T020. *Acta Geod. et Geophys. Hung.* **31**: 423 - 431.

Wenzel, H.-G. (1997): Analysis of Earth Tide Observations. In: Tidal Phenomena (H. Wilhelm, W. Zürn and H.-G. Wenzel, Eds.). *Lecture Notes in Earth Sciences* **66**: 59 - 75. Springer, Heidelberg.

Widmer, R., Zürn, W. (1992). Bichromatic excitation of long-period Rayleigh and air waves by the Mount Pinatubo and El Chichón volcanic eruptions. *Geophys. Res. Lett.* **19**: 765 - 768.

Widmer, R., W. Zürn and T. G. Masters (1992). Observation of Low Order Toroidal Modes from the 1989 Macquarie Rise Event. *Geophys. J. Int.*. **111**, 226 - 236.

Wielandt, E. and G. Streckeisen (1982). The Leaf-Spring Seismometer: Design and Performance. *Bull. seism. Soc. Am.* **72A**, 2349 - 2368.

Zürn, W. and R. Widmer (1995). On noise reduction in vertical seismic records below 2 mHz using local barometric pressure. *Geophys. Res. Lett.* **22**, 3537 - 3540.

Air pressure signatures in the SG data of Vienna

Bruno Meurers
Institute of Meteorology and Geophysics, University of Vienna
Central Institute of Meteorology and Geodynamics, Vienna

Abstract

Three case studies of short term (< 120 min) air pressure variations and their gravity response are investigated by comparing the air pressure signal and the residual gravity in high temporal resolution. All events are connected with front passages partly accompanied by vertical convection activity. Even very short (< 20 min) pressure perturbations are visible in the gravity residuals and can be removed by applying the admittance factor obtained when investigating the diurnal and semidiurnal tidal frequencies. An attempt is made to estimate the gravity effect of vertical air mass exchange that probably causes a temporary residual offset observed in one of the case studies while the air pressure returns to its initial level.

Introduction

A three years' time series of high resolution gravity and air pressure data is now available in Vienna (Austria) obtained by the superconducting gravimeter GWR C025 that has been operating since August 1995 in the seismic laboratory of the Central Institute of Meteorology and Geodynamics. Main goal of this study is the investigation of some short term (< 120 min) air pressure variations with respect to their gravity response by comparing the air pressure and the residual gravity in high temporal resolution.

Data processing

The data acquisition system of GWR C025 offers high resolution gravity data (HR-GRAV) sampled with 1 Hz and the air pressure signal sampled with 0.1 Hz respectively. In a first step a tidal model for the Vienna station was derived by analysis of the gravity data. Preprocessing of the raw data consisted of calibrating, degapping, despiking, destepping and decimating to 1 h samples. Manual offset corrections were necessary only in three cases up to now. Otherwise despiking and destepping was done automatically applying thresholds of 2 and 5 nms^{-2} respectively for spike and step detection. The analysis of the three years' hourly data using the Tamura (1987) tidal potential defines the tidal model applied afterwards for detiding the 1 min gravity data. The results are given in Table 1. The pressure admittance factor results to -3.533 ± 0.004 nms^{-2}/hPa. There is no significant difference to the results for the main tidal constituents formerly obtained by an about two years' data analysis (Meurers 1998). All processing steps have been performed by applying the ETERNA v3.3 software package of Wenzel (1996) and the programming module GSOFT of Vauterin (1997).

In the second step both the gravity and air pressure data were decimated to 1 min samples for those intervals that include interesting short term air pressure variations using appropriate FIR filters offered by the ETERNA package. The residuals were then calculated by removing the tidal effect from one minute data and compared with the air pressure signal. In most cases a narrow correlation can be found even for pressure variations of less than 1-2 h duration although the latter are often caused by very local meteorological processes. This can be demonstrated by removing the air pressure effect from the residuals. For that purpose the mean

wave group	amplitude [nms^{-2}]	amplitude factor	standard deviation	phase lead [deg]	standard deviation
Q1	67.6815	1.14514	0.00021	−0.0961	0.0106
O1	354.5013	1.14839	0.00004	+0.1129	0.0022
M1	28.0205	1.15417	0.00043	+0.0827	0.0215
P1	164.7973	1.14734	0.00008	+0.1509	0.0040
S1	3.7291	1.09790	0.00484	+9.1668	0.2514
K1	492.4664	1.13434	0.00003	+0.1935	0.0015
PSI1	4.2994	1.26583	0.00343	+0.8462	0.1552
PHI1	7.2404	1.17118	0.00184	+0.1752	0.0900
J1	28.0425	1.15512	0.00056	+0.1090	0.0279
OO1	15.2896	1.15101	0.00129	+0.2231	0.0641
2N2	11.8720	1.16538	0.00047	+1.7659	0.0233
N2	75.1972	1.17880	0.00010	+1.4987	0.0048
M2	393.9489	1.18237	0.00002	+1.0765	0.0009
L2	11.1044	1.17912	0.00053	+0.1928	0.0255
S2	182.8437	1.17952	0.00004	+0.0923	0.0021
K2	49.7479	1.18052	0.00020	+0.3031	0.0095
M3M6	4.6716	1.07099	0.00068	+0.1792	0.0365

Tab. 1: Tidal parameters obtained by analyzing the GWR C025 data between 1995 08 01 and 1998 12 17.

admittance factor obtained from tidal analysis has been applied. Of course, this is an oversimplified correction method, as the pressure admittance function is frequency dependent and not constant in time. Only a few case studies are discussed here.

Case studies

The first event on 1998 06 22 is caused by a cold front passage connected with convective activity (Fig. 1). The air pressure signal shows a +1.5 hPa increase over a period of about 40 min only with small undulations superimposed. Air pressure returns back to its former level after the passage. The same is true for the residual gravity curve. The air pressure corrected residuals indicate the applied admittance factor to be too small. During the cold front passage the noise is increasing due to heavy storm. This has been controlled by inspecting the raw 1 s gravity signal and probably is the reason for the fact that air pressure perturbations at noise frequencies are less well reflected in the residuals.

Another cold front passage could be observed on 1998 07 27 (Fig. 2a). Again it was accompanied by heavy storm inducing high frequency noise into the 1 s gravity data. However, while the air pressure returns back to its former level the gravity residual does not. An temporary offset of about 8 nms^{-2} remains. It needs more than 5 hours to bring the residuals back into their long term trend function (Fig. 2b). Obviously this event was connected with a convective process resulting in a vertical exchange of air of different density. This example shows that even refined admittance functions would not be able to remove all atmospheric effects from the gravity residuals.

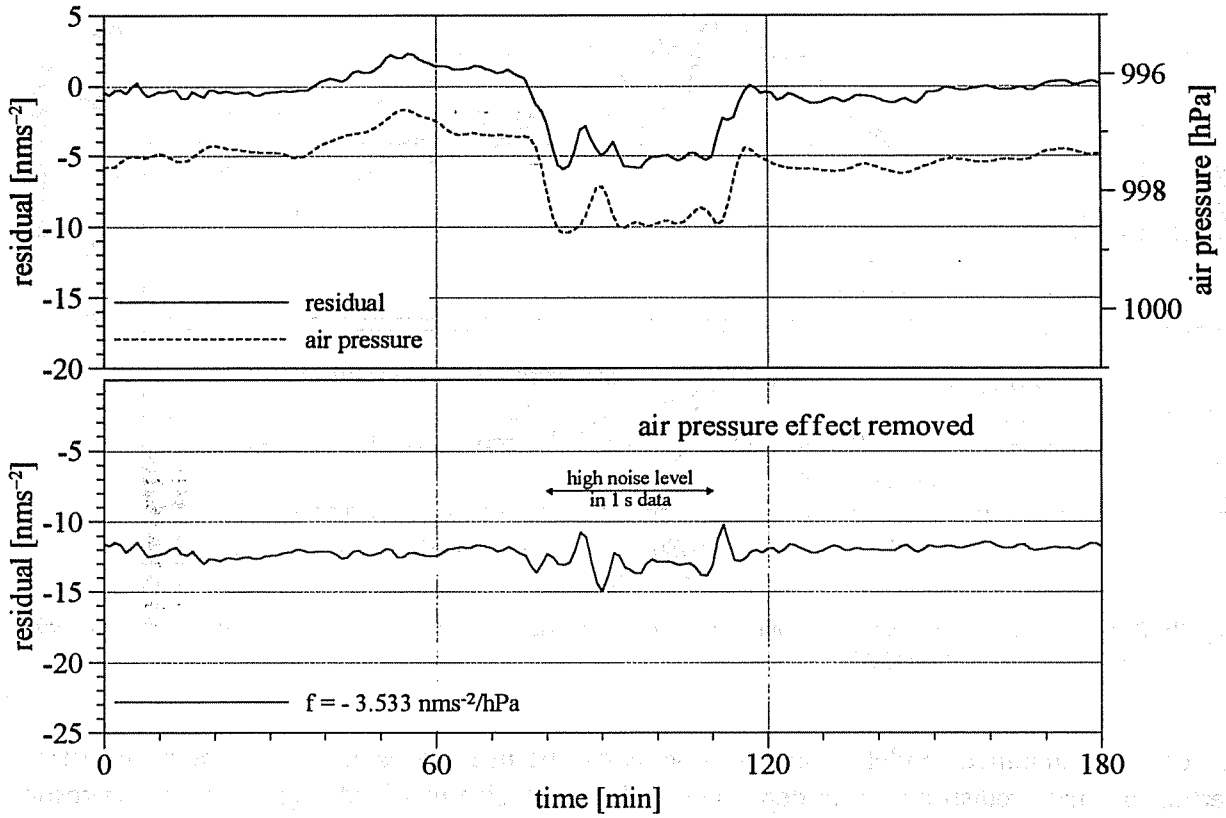

Fig.1: Residuals and air pressure effect due to a cold front passage connected with convective activity on 1998 06 22. Time axis starts at 13:00 UTC.

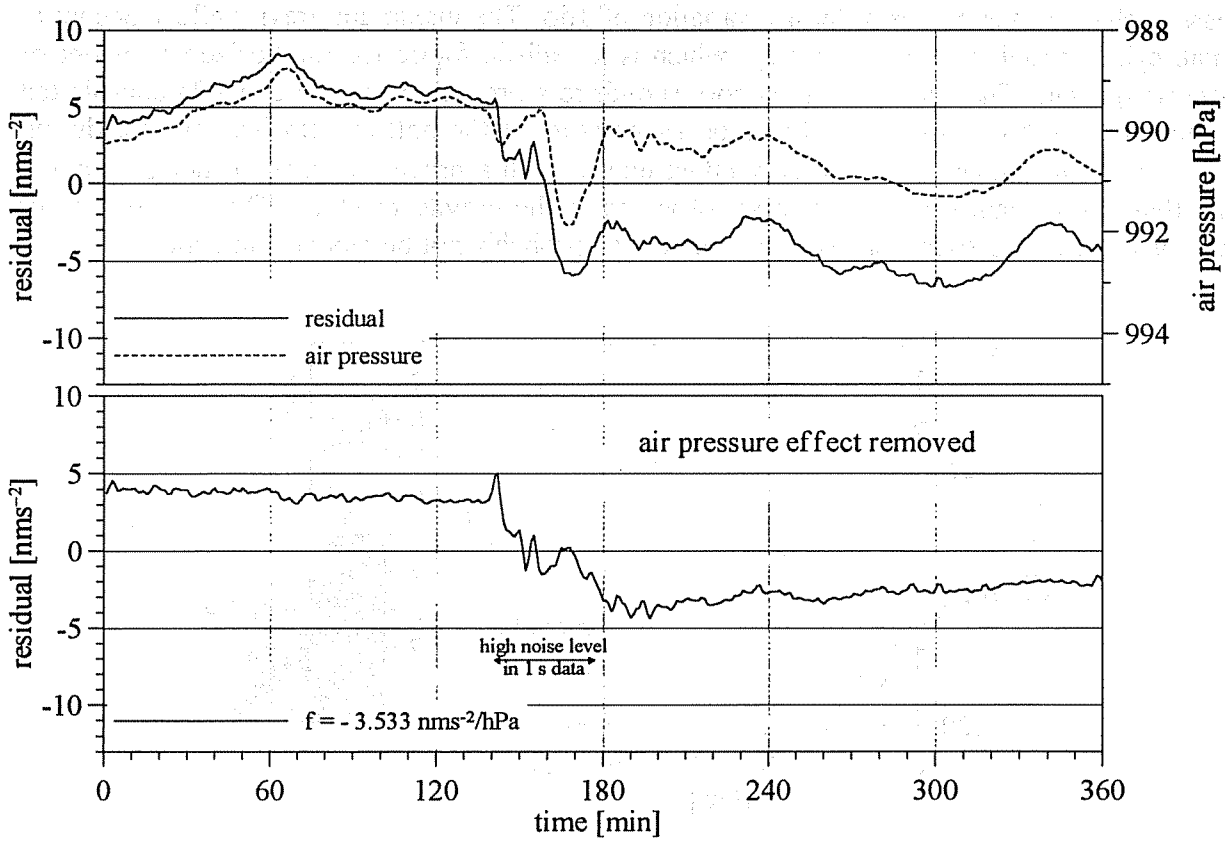

Fig. 2a: Residuals and air pressure effect due to a cold front passage connected with convective activity on 1998 07 27. Time axis starts at 15:00 UTC.

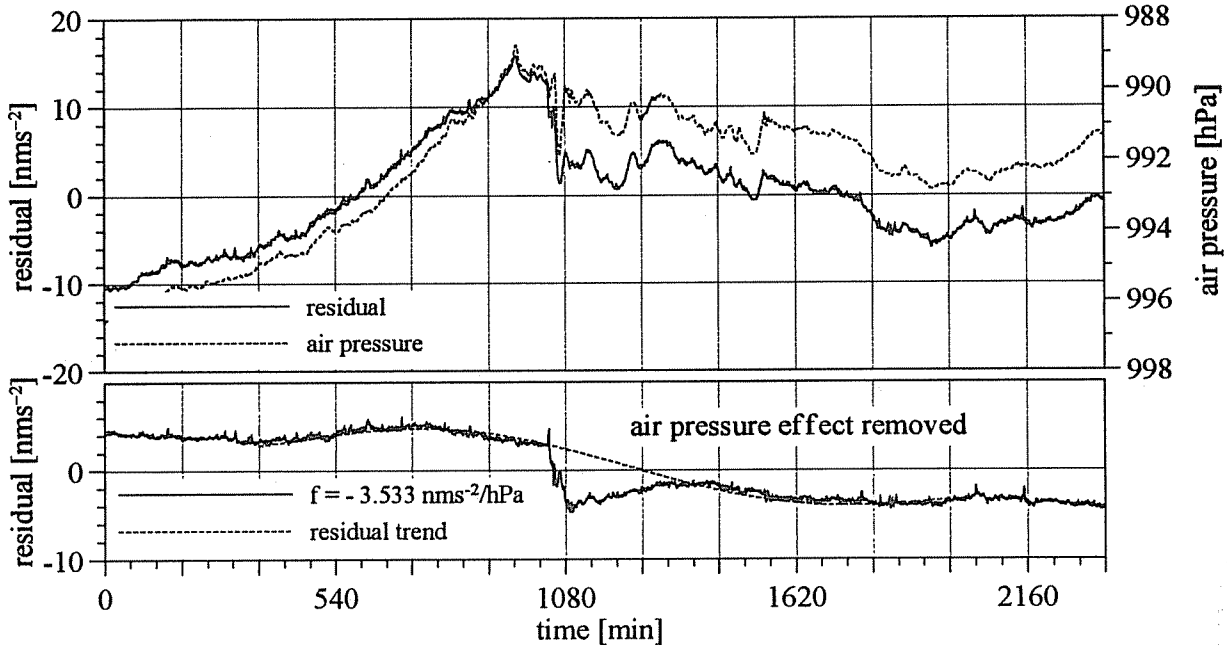

Fig. 2b: Residuals and air pressure effect due to a cold front passage connected with convective activity on 1998 07 27. Time axis starts at 0:00 UTC.

A very oversimplified model of such a process can be used to estimate the gravity effect of vertical air mass redistribution in dependence of the cell size involved. Fig. 3 shows the result for two convective cells of different vertical extent. The model consists of two vertically stacked cylinders with radius r containing air of constant density $\rho = \rho_0 \pm \delta\rho/2$. The vertical air mass exchange thus causes a density variation of $\pm\delta\rho$. The maximum gravity effect occurs at small cylinder radii of a few km only, which is a realistic figure for the horizontal extent of convection cells. The density contrast corresponds to a pressure variation of 1 hPa contributed by each cell with opposite sign. The total air pressure at the bottom remains constant during this convective exchange. The gravity effect due to such a process is in the order of 1 nms^{-2} and thus can explain roughly the offset observed in the gravity residuals. Due to the lack of meteorological data such small scale processes can probably not be modeled in detail.

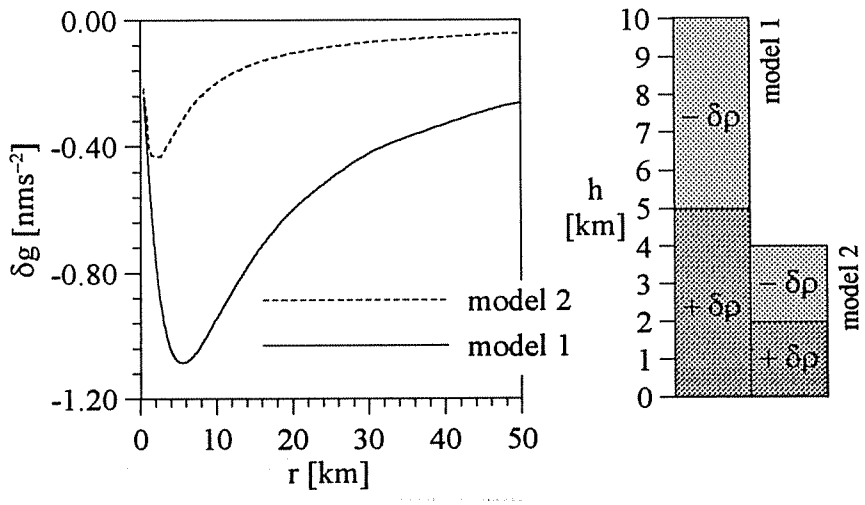

Fig. 3: Gravity effect estimation of air mass exchange in a convective cell of different horizontal and vertical extent. Density contrast $\delta\rho = 1.266\times10^{-3}$ kgm^{-3}. r: cylinder radius, h: cylinder height.

The third case study has been observed on 1998 08 13 (Fig. 4). Again a cold front passage is the cause of the air pressure variations. This example shows clearly, that very short pressure perturbations, even such of less than 20 min duration, are well imaged by the gravity residuals. The offset at the beginning of the event (t = 110 min) is much smaller than that observed on 1998 07 27 (Figs. 2a,b) and cancels out already after about 1 h. The mean admittance factor does not remove the pressure effect completely, as a certain trend still remains in the residuals. When using a locally adjusted admittance factor the trend can be removed. However, the resulting factor is close to the maximum estimate of the gravitational effect. Locally adjusted admittance factors have been calculated also for other air pressure perturbations not discussed in this paper. They range between 2.8 and 4.2 nms^{-2}, in most cases they are close to or a bit higher than 3.5 nms^{-2}. A possible correlation with the type of the meteorological process involved has not been investigated yet.

Conclusions

The case studies discussed in this paper show that short term pressure perturbations, even those of very short (< 20 min) duration, are well reflected by the gravity residuals. In most cases the air pressure admittance factor is close to the figure obtained when investigating the diurnal and semidiurnal tidal frequencies. However, some atmospheric processes (e.g. convective mass redistribution) are not connected with air pressure variations, but nevertheless they can cause a change in gravity. This means that even more refined admittance functions would not be able to remove all atmospheric effects from the gravity residuals.

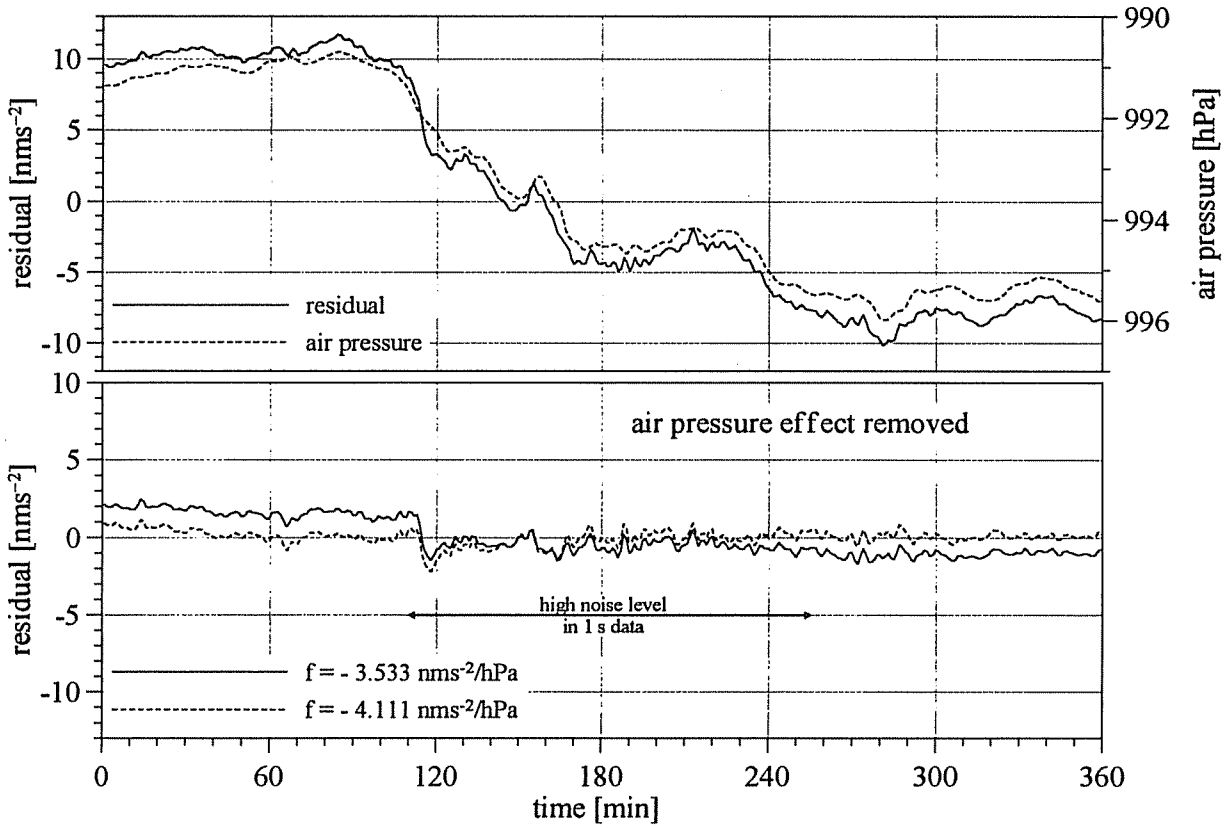

Fig. 4: Residuals and air pressure effect due to a cold front passage connected with convective activity on 1998 08 13. Time axis starts at 16:00 UTC.

References

Meurers, B., 1998: Gravity monitoring with a superconducting gravimeter in Vienna. In: Ducarme, B., Paquet, P. (eds): Proceedings of the 13th International Symposium on Earth Tides, Brussels 1997, 625-634.

Tamura, Y., 1987: A harmonic development of the tide-generating potential. Bulletin d'Informations Mareés Terrestres, 99, 6813-6855.

Vauterin, P., 1997: Graphical interactive software for the analysis of earth tide information. 13th International Symposium on Earth Tides, Brussels.

Wenzel, H.-G., 1996: The nanogal software: Earth tide data processing package ETERNA 3.30. Bulletin d'Informations Mareés Terrestres, vol. 124, 9425-9439.

Acknowledgement

The author wishes to thank P. Melichar (head of Dept.), N. Blaumoser, M. Göschke, S. Haden and R. Steiner from the Geophysical Department of the Central Institute of Meteorology and Geodynamics in Vienna for their cooperation.

Results of Extensometric Tidal Measurements at the Sopron Station

I. P. Eper, Gy. Mentes

Geodetic and Geophysical Research Institute of the Hungarian Academy of Sciences, Sopron

Abstract

Preliminary results of tidal evaluation of strain data obtained by a quartz tube extensometer installed at the Geodynamical Observatory of the Geodetic and Geophysical Research Institute of the Hungarian Academy of Sciences in Sopron (Hungary) are described. The data were preprocessed by a method developed in the institute and the analysis was made by the program ETERNA 3.3.

1. Introduction

In May 1990 a quartz tube extensometer with electrical recording was installed at the Sopron Geodynamical Observatory. The instrument was made in the frame of a cooperation between the Geophysical Institute in Moscow and the Geodetic and Geophysical Research Institute of the Hungarian Academy of Sciences in Sopron (Mentes, 1991). The aim was to monitor and to study the tidal and non tidal variations caused by local tectonic movements.

After the installation the instrument had a large drift during some months, therefore we have had a continuous record usable for tidal and deformation evaluation since 1991. The data recorded from 1991 till 1996 were earlier evaluated for the determination of recent crustal movements (Mentes, 1996). In this paper the tidal evaluation of the record from 1991 till 1993 is described.

In the given time interval the recording was made analogously, the record was read hourly and therefore the preparation of the data was mainly made manually and some special programs were written in language C for preprocessing of the data.

2. The site of the strain mesurements

The Sopron Geodynamical Observatory is about 5 km far from the centre of the town. It is an artificial tunnel driven in gneiss. The coordinates of the observatory are: latitude: 47.7° N; longitude: 16.5° W. Figure 1 shows the scheme of the observatory. The distance of the extensometer from the entrance is about 30 m, the overlay of the gallery is 60 m thick. Due to technical reasons the instrument is not in the tunnel axis. The extensometer is thermally insulated and separated by three doors from the outside. The annual temperature variation in the gallery at the instrument is less then 0.5 °C and the daily one is about 0.05 °C.

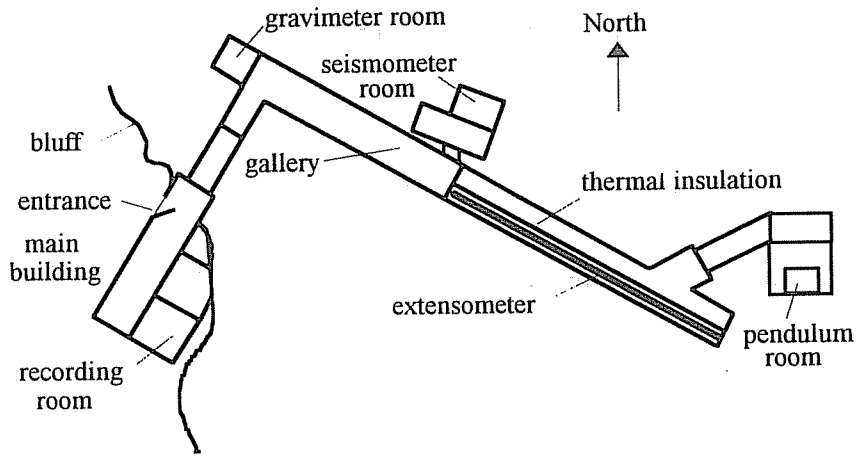

Figure 1. Scheme of the Geodynamical Observatory in Sopron

3. The construction of the extensometer

The extensometers is assembled of 2-2.5 m long quartz tubes which have a diameter of 45 mm and a wall thickness of about 2-3 mm. The linear thermal extension coefficient of the quartz tubes is $0.45 \cdot 10^{-6}$. The individual tube pieces are joined together by means of two-component resin and invar profiles. One end of the extensometer is attached to the rock by means of a stainless steal bolt and concrete and the other end holds the moving plate of the capacitive transducer. The standing plates of the transducer are fixed to the bedrock. The attached quartz tubes are suspended on very fine wires connected to supports making possible the levelling of the quartz tube (Fig. 2). The total length of the instrument is 22 m, its azimuth is 116°. The construction of the extensometers and the principle of the capacitive transducer are described in more detail by Mentes (1991, 1994a, 1994b).

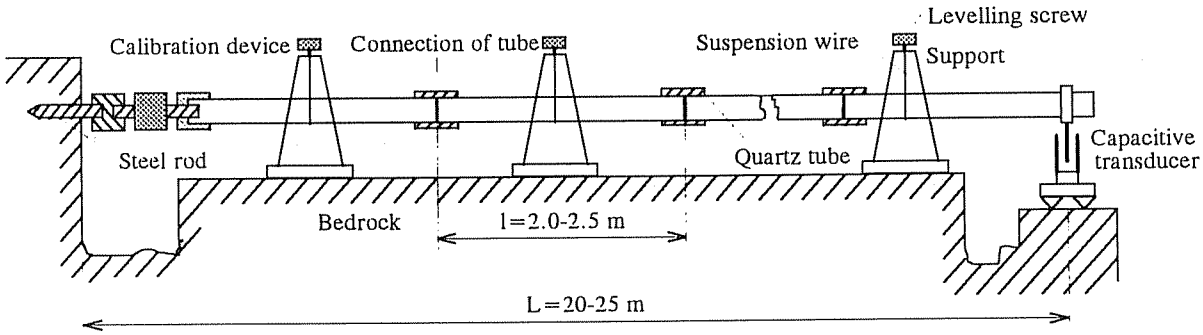

Figure 2. Construction scheme of the long quartz tube extensometer at the Sopron Geodynamical Observatory

The regular, daily calibration of the extensometer is made by a magnetostrictive coil. In addition the instrument was in-situ calibrated in the observatory by the method developed by Mentes (1995, 1998). The calibration factor obtained by these measurements is 0.219 nm/mV.

4. Preprocessing and analysis of the strain data

Figure 3 shows the raw hourly recoded, step-corrected strain data obtained from 01.01.1991 till 31.12.1993. These data were recorded analogously, therefore the step-correction was made partly manually, partly by the program package ETERNA 3.3.

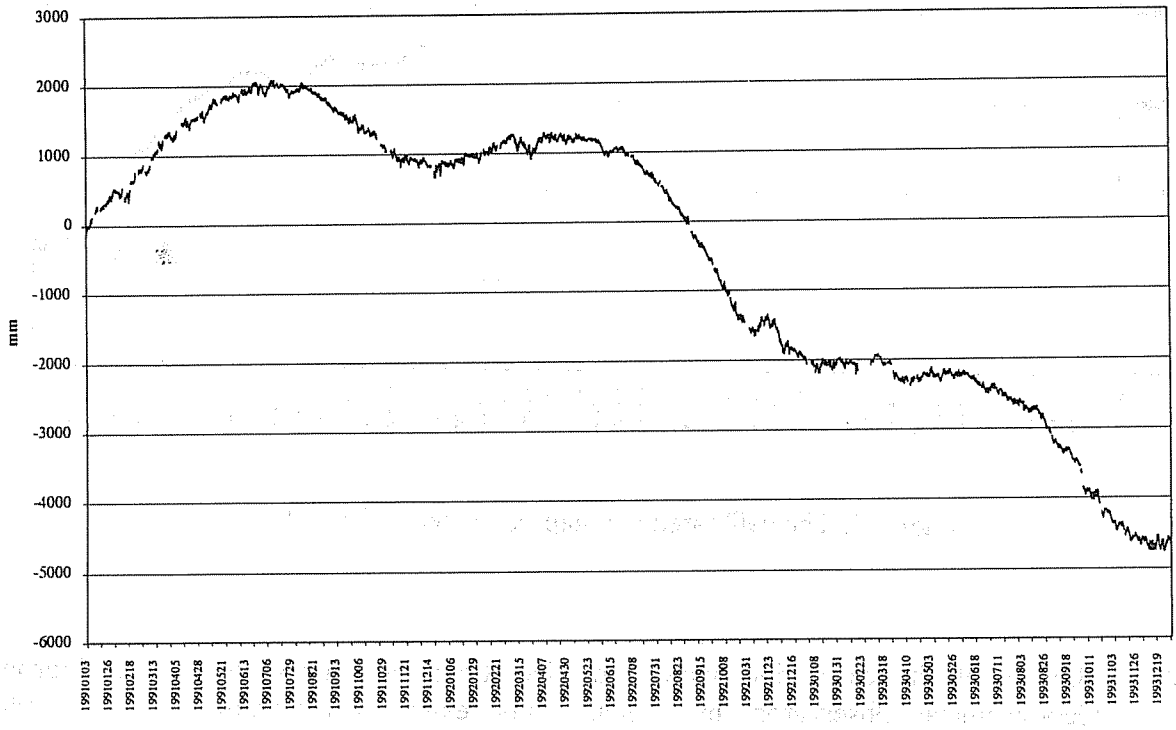

Figure 3. The raw, hourly recorded, step-corrected data from 01.01.1991 - 31.12.1993

A procedure was developed for the interpolation of gaps. First the step-corrected raw data were calibrated, then a curve was fitted at the inflexion points of the data series. This curve was subtracted from the data record. The same procedure was made for the theoretical curve calculated for the same time period by the ETERNA 3.3. These theoretical values were filled into the gaps of the residual curve of the measured data than the subtracted curve was added to this residual curve to obtain the original gap-corrected data. The advantage of this method against gap-corrections using high-pass filter is that the length of the gaps does not increase due to the filtering. The corrected data series was analysed by the program ANALYSE of the package ETERNA 3.3. In Table I. the obtained amplitudes, amplitude factors and phase differences of strain data are given. The amplitude factors refer to the Wahr-Dehant earth model.

For the Fourier-analysis of the strain data a polinomial of the fourth order was fitted to the corrected strain data (Fig. 5). This polinomial was subtracted from the strain data. The residual curve (Fig.6) was Fourier-analysed. The obtained amplitude spectra can be seen in Figure 7.

Figure 4. The calibrated and gap-corrected strain data

Table I. Results of the earth tide analysis of the strain data measured at the Sopron Geodynamical Observatory by a quartz tube extensometer from 01.01.1991 till 31.12.1993

wave	amplitude [nstr]	amplitude factor	phase lead
O1	4.2018 ±0.022	0.637	-3.118 ±1.974
P1	0.8287 ±0.050	0.271	4.293 ±10.634
K1	4.4068 ±0.0164	0.475	0.682 ±1.971
N2	1.1517 ±0.0495	1.189	-11.533 ±2.382
M2	5.8264 ±0.0095	1.152	-14.133 ±0.472
S2	4.269 ±0.020	1.818	-3.566 ±0.632
K2	0.627 ±0.072	0.981	-20.504 ±4.204

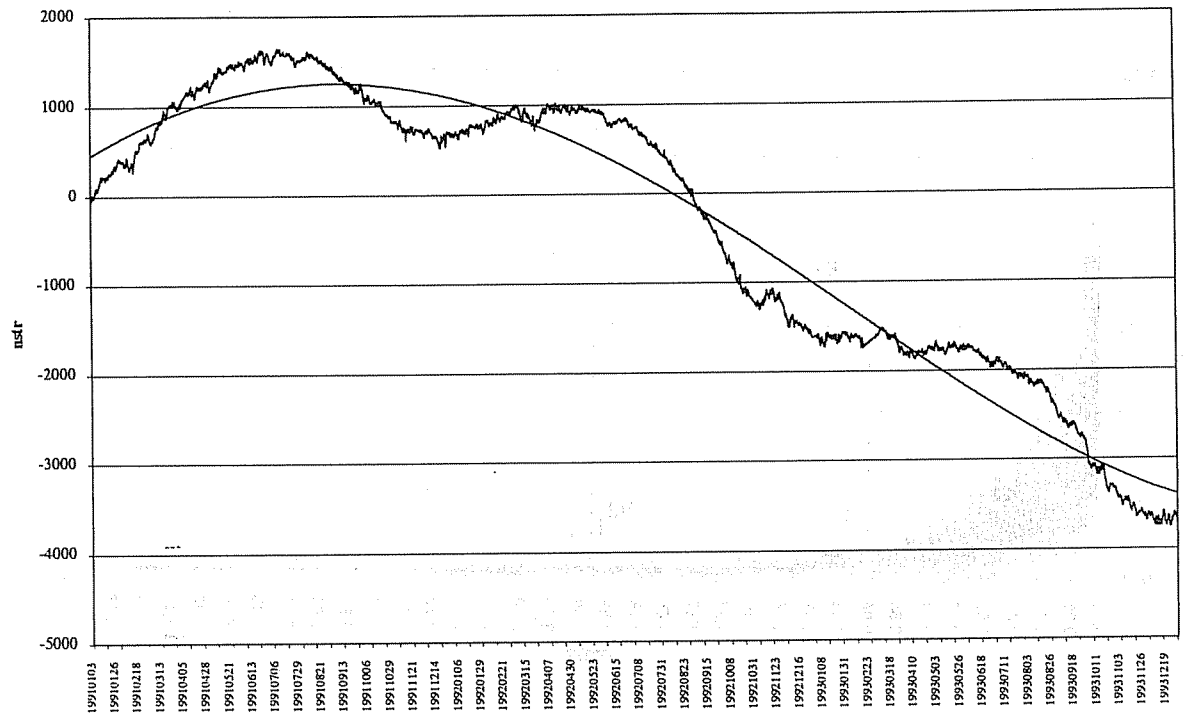

Figure 5. The strain data and the fitted polinomial

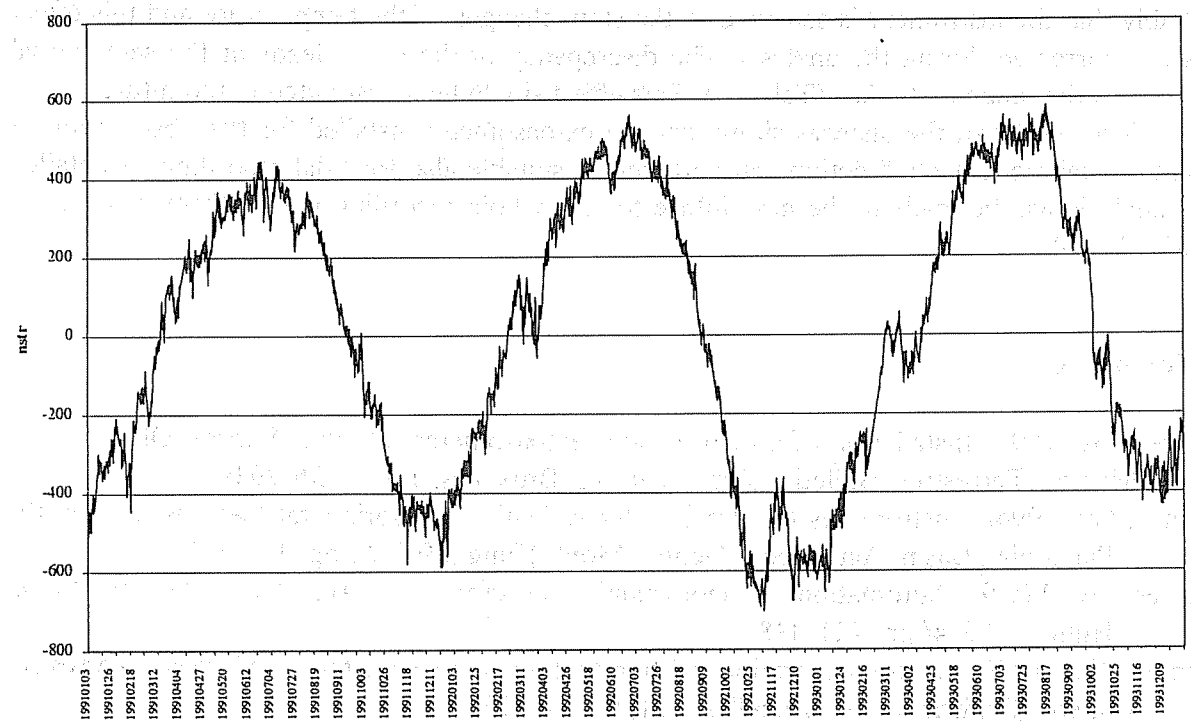

Figure 6. The residual curve after subtracting the trend from the strain data

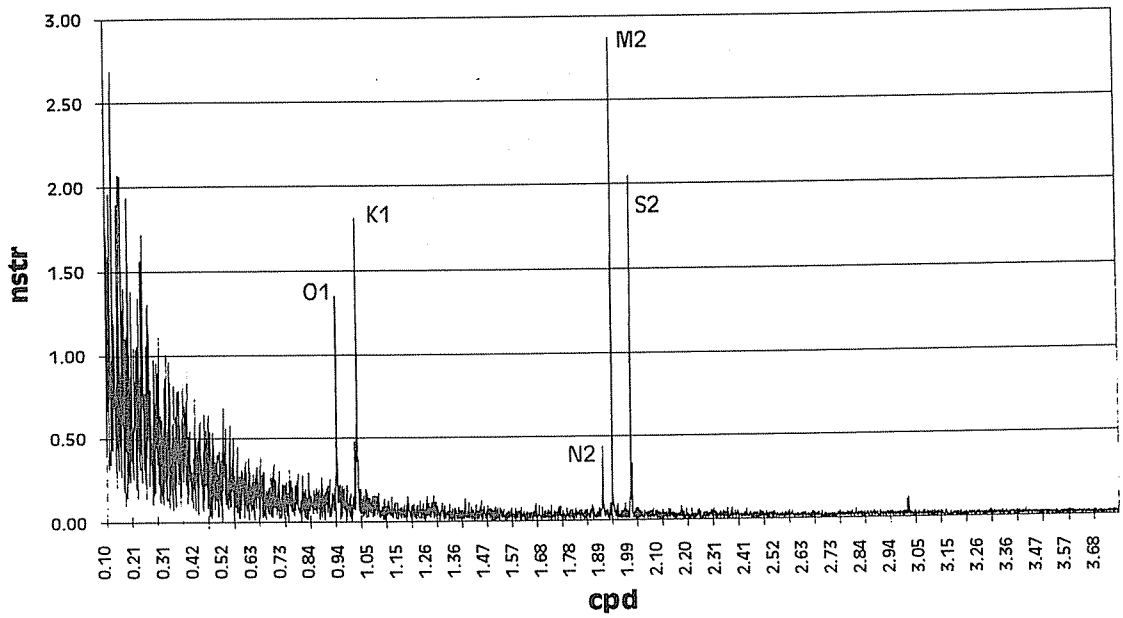

Figure 7. Amplitude spectrum of the strain data measured by the quartz tube extensometer from 01.01.1991 till 31.12.1993

The amplitude spectrum shows disturbances in the long periodic band. The reason is probably that the instrument is sensitive to the slow changes of the temperature and this effect was not corrected during the analysis. The discrepancy of the phase leads at the semidiurnal waves is in the range of 10-20° (Table I.). This effect siould be investigated in the future.

The results of the analysis show that the extensometer installed for the observation of recent crustal movements functions properly and is suitable also for tidal recording. A detailed tidal analysis will be made in the next future for the whole recording period from 01.01.1991 till 31.12.1998.

References

Mentes, Gy. 1991: Installation of a quartz tube extensometer at the Sopron Observatory, Marees Terrestres Bulletin d'Informations, Bruxelles, 110, 7936-7939.

Mentes, Gy. 1994a: Instruments for Precise Determination of Horizontal Deformations in the Pannonian Basin, Acta Geod. Geoph. Mont. Hung.,29/1-2/, pp. 161-177.

Mentes, Gy. 1994b: Automation of Geodynamical Observations, Acta Geod. Geoph. Mont. Hung., 29/3-4/ pp. 421-438.

Mentes, Gy. 1995: In-situ calibration of quartz tube extensometers, Marees Terrestres Bulletin d'Informations, Bruxelles, 121, 9070-9075.

Mentes, Gy. 1996: Continuous Horizontal Crustal Deformation Measurements. Proceedings of the IAG Regional Symposium on Deformations and Crustal Movement Investigations Using Geodetic Techniques, Székesfehérvár, 23-30.

Mentes, Gy. 1998: Calibration of tidal instruments. Proceedings of the 13th International Symposium on Earth Tides, Brussels, 43-50.

Recording of Recent Crustal Movements by Borehole Tiltmeters in the Vicinity of a Tectonic Fault

Gy. Mentes[1], P. Varga[1], H.-J. Kümpel[2]

[1] Geodetic and Geophysical Research Institute of the Hungarian Academy of Sciences, Sopron;

[2] Geological Institute, Section Applied Geophysics, Bonn University.

Abstract

Geodynamical and ground tilt measurements are disturbed by a lot of local effects, e.g. variations of the temperature and ground water level, transpiration of the vegetation, etc., therefore it is very important to investigate the connections between measured tilts and ground motions. In South-Hungary a test area was established at the Mecsek-fault to investigate the movements of the fault. For this reason borehole tiltmeters were installed at both sides of the fault and geodetic (GPS, EDM and leveling) measurements with half-year intervals were also carried out. This complex measuring network gives a good opportunity to study the behaviour of the tiltmeters and develop better interpretation methods for tilt measurements besides the investigation of the motion of the fault.. The paper deals with the first experience of these measurements.

1. INTRODUCTION

Geodynamical deformation measurements play a very important role in the investigation of recent crustal movements and local deformations at the locations of big industrial objects, e. g. dams, nuclear power stations, deposits of dangerous materials, etc. The geodetic measurements (GPS, EDM, leveling) give results with poor time resolution. To study the physics of crust and local deformations and to give an alarm signal if the rate of the deformation suddenly increases continuously recording methods are needed. For these purposes borehole tiltmeters can be used because their installation is relatively of low cost and boreholes ensure a very stable place for them.

The continuously recording borehole tiltmeters and strainmeters are very sensitive to local disturbances e.g. variations of the environmental parameters, ground water levels etc. therefore the elimination of these effects is needed for a correct interpretation of the deformation. At the Mecsek-fault in Hungary a complex measuring network was established to investigate the movements of this fault. The displacements are determined by GPS, electronic dictance measurements (EDM) and levelling twice in a year and continuously by two two-component borehole tiltmeters installed at both sides of the fault. These measurements give a good opportunity to control the tilt measurements in addition to the continuous monitoring of the movements of the fault. The geodetic mesurements contribute to develop an evaluation

method to eliminate the disturbing effects or to separate the output signal into parts produced by the earth and the instrument and therefore to give a better interpretation of tilt measurements. In this paper the first results of the measurements are given.

2. DESCRIPTION OF THE TILTMETERS

The tilt measurements have been carried out by the dual-axis borehole tiltmeters Model 722 made by Applied Geomechanics Inc. (AGI), Santa Cruz, California. This tiltmeter consists of a cylindrical stainless steel body (85 cm long, 5.4 cm in diameter) containing two orthogonal electrolitic precision tilt sensors, amplifiers and signal filters for each of them and a temperature sensor. The tiltmeter is connected to the data logger via a submersible steel-reinforced cable and an external switch box. The resolution of the instrument in a measuring range of ±200 μrad is 0.1 μrad and in a range of ±2000 μrad is 1μrad. The instruments are calibrated by the method developed at the Geodetic and Geophysical Research Institute and at the Geological Institute, Section Applied Geophysics, Bonn University (Mentes et al., 1996).

The tiltmeters are usually installed in shallow boreholes at depths between 2 and 8 m. The borehole has to be drilled with a diameter of about 30 cm, its casing is a PVC pipe that is coupled to the surrounding formation by concrete. Inside the pipe the instrument is fixed by quartz sand in order to obtain a strong coupling to the ground. The signal is transferred via cable to the switch box which is placed in a trunk at the surface together with the power supply and a data logger (Fig. 1.).

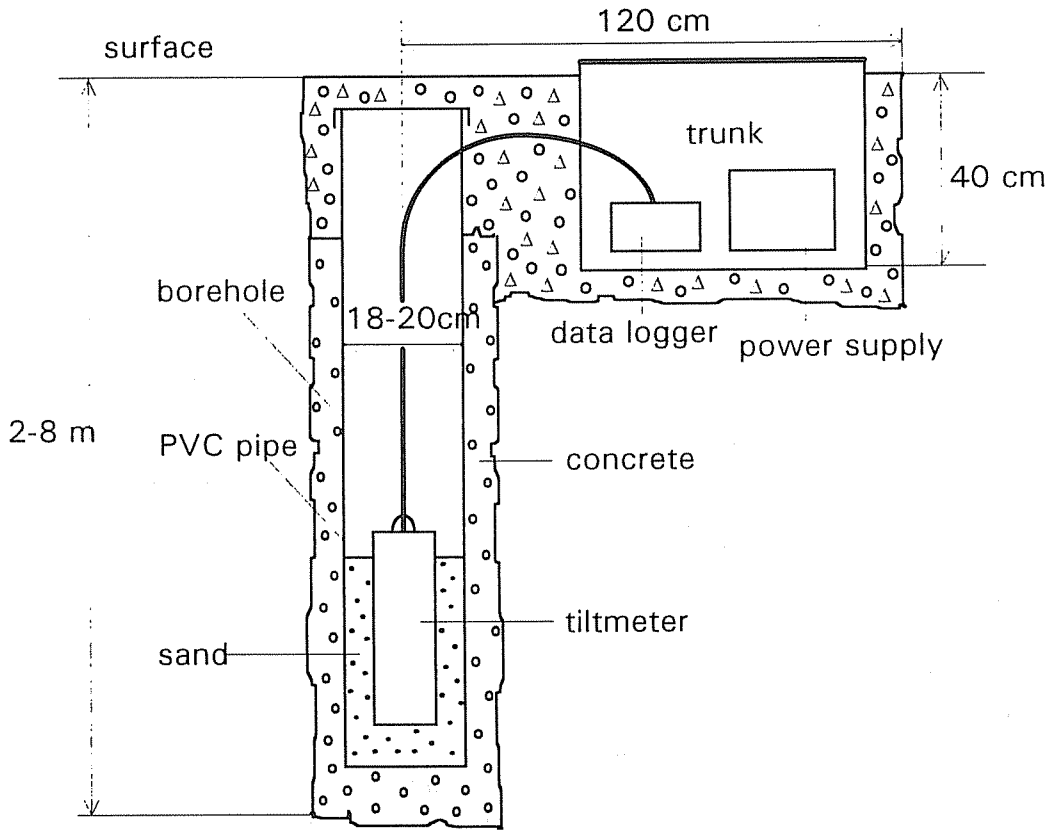

Figure 1. Installation of the Model 722 tiltmeter in the borehole

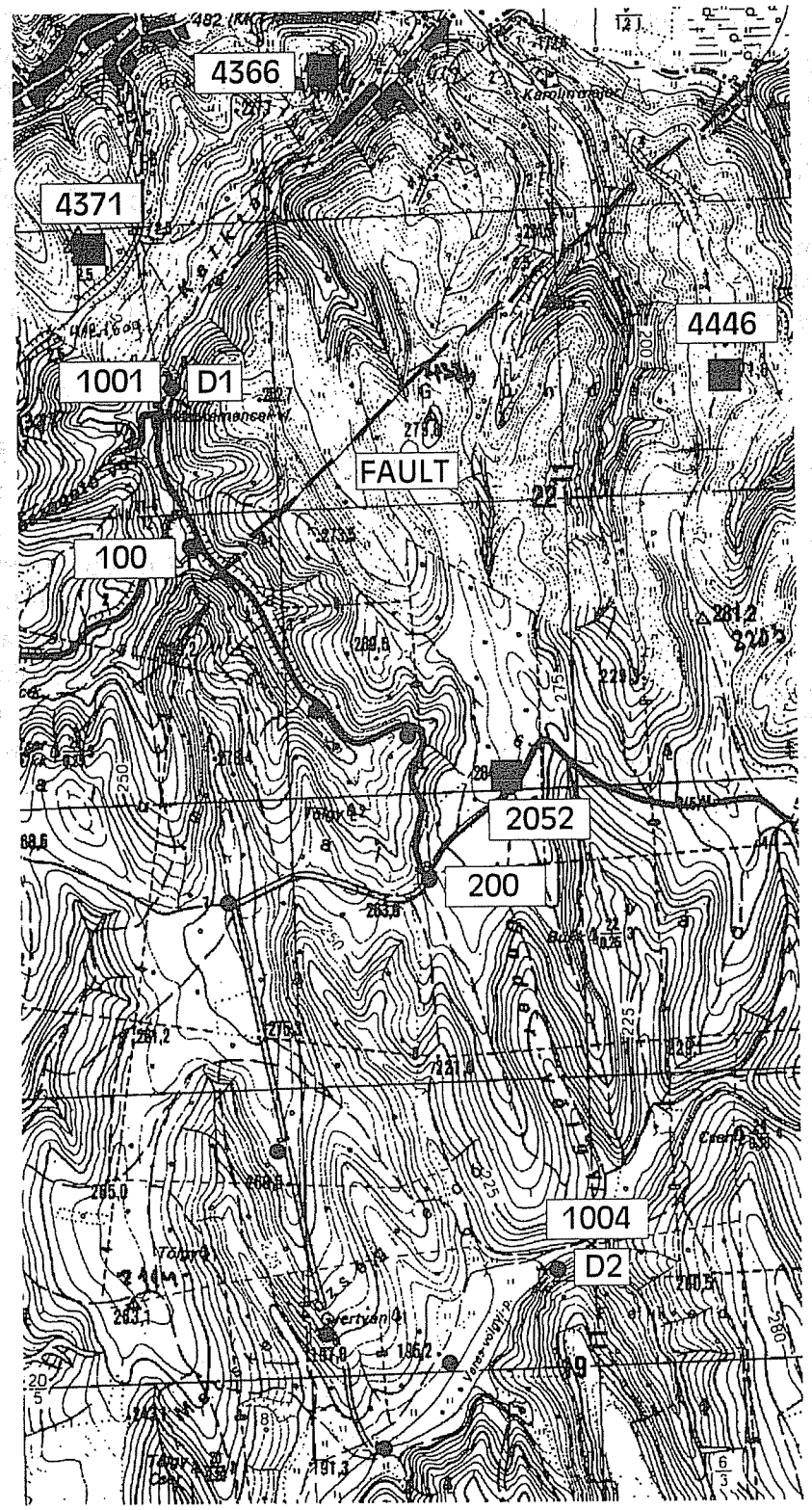

Figure 2. The map of the site of the measurements

3. DESCRIPTION OF THE SITE OF THE MEASUREMENTS

The points for the GPS and EDM measurements are marked by squares and the circles designate the leveling line in the map (Fig. 2.). The concrete pillars of the GPS points and the end points of the leveling line are placed directly on the bedrock. Two other points of the leveling line are deeply founded concrete pillars.The tiltmeters are placed at the ends of the leveling line. At the point D1 the whole borehole is drilled in the bedrock and it has a depth of 3.6 m. At the point D2 the borehole has a depth of 8 m. The deepest part of the borehole is in the bedrock (0.8 m from the bottom) and its upper part (7.2 m from the surface) is in sediment. The Y-direction of both tiltmeters is N-S, so both tiltmeters record tilts of same directions. The sampling period of the tiltmeters is 1 hour. The tiltmeters were installed at the begining of October, 1998.

4. RESULTS OF THE TILT MEASUREMENTS

Figures 3 and 4 show the daily averages of the recorded tilt and the temperature variations of the borehole at the points D1 and D2 from 13.10.1997 till 23.03.1998. It can be seen that the tilts at the North end of the leveling line, at the point D1 are in both directions in the range of about 2 μrad, much less than at the point D2 where the tilt changes more than 100 μrad. The reason is probably the situation of the borehole at the point D2 in sediment and it is on the skirts of a small valley and therefore the movements of the slope of the neighbouring hills (landslides due to precipitation) cause much larger tilts than at the point D1 which is in the bedrock.

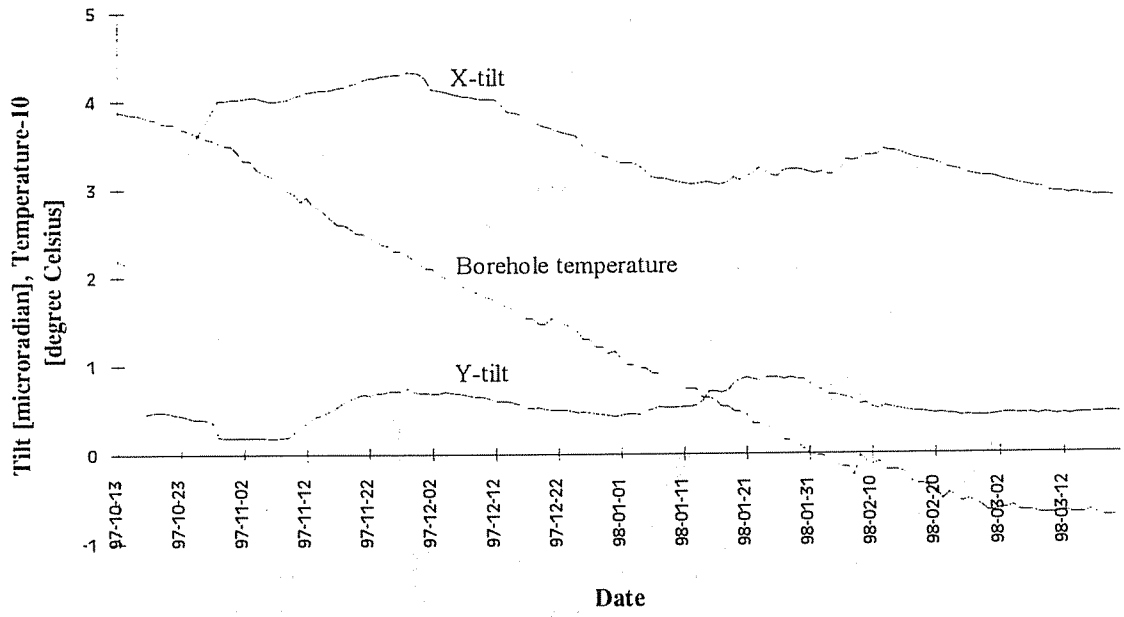

Figure 3. Tilt and temperature variations at the point D1from 13.10.1997 till 23.03.1998

The temperature in the borehole D1 varies from 14 °C to 9 °C because the depth of this borehole (3.6 m) is not sufficient to ensure a stable temperature compared to the point D2 where the depth is 8 m and the temperature is practically constant (13 °C). In this recording

period the change of the outer temperature was about 30 °C. It means that shallow boreholes can damp temperature variations significantly. At both boreholes there was no correlation between the tilts and the temperature variations in the boreholes.

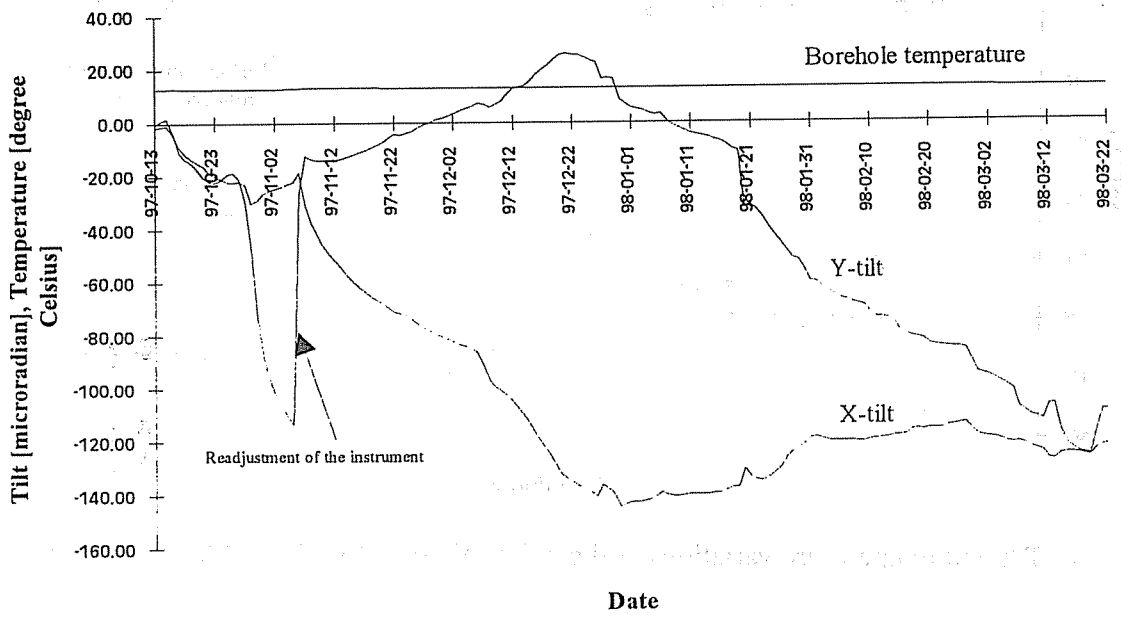

Figure 4. Tilt and temperature variations at the point D2 from 13.10.1997 till 23.03.1998

In March of 1998 a surface temperature sensor was installed at both boreholes to study the connection between the surface and borehole temperature as well as the recorded tilts. Figure 5 and 6 show the raw tilt data and the temperature variations at both points from 24.03.1998 till 10.07.1998.

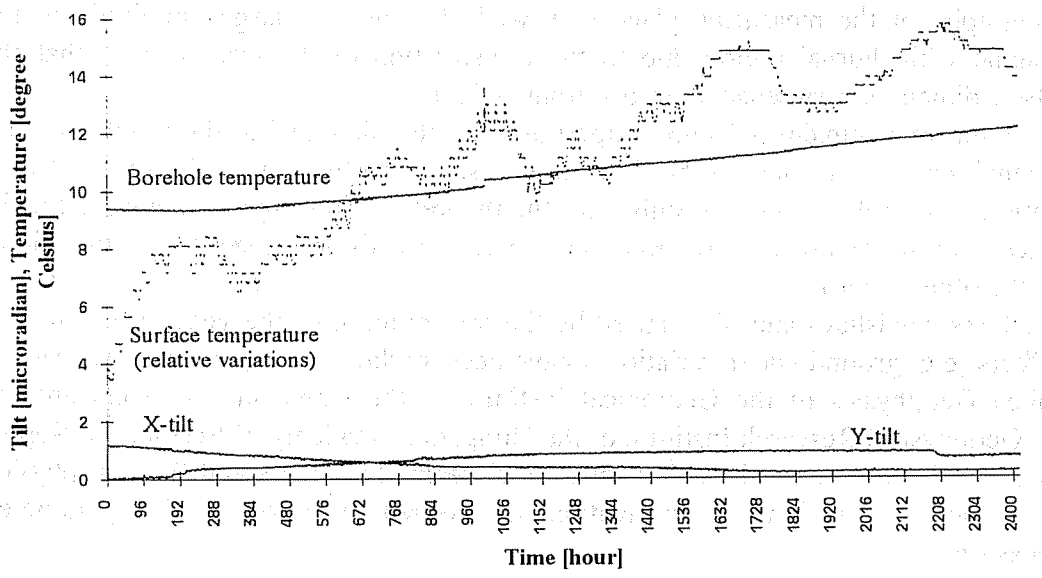

Figure 5. Tilt and temperature variations at the point D1from 24.03.1998 till 10.07.1998

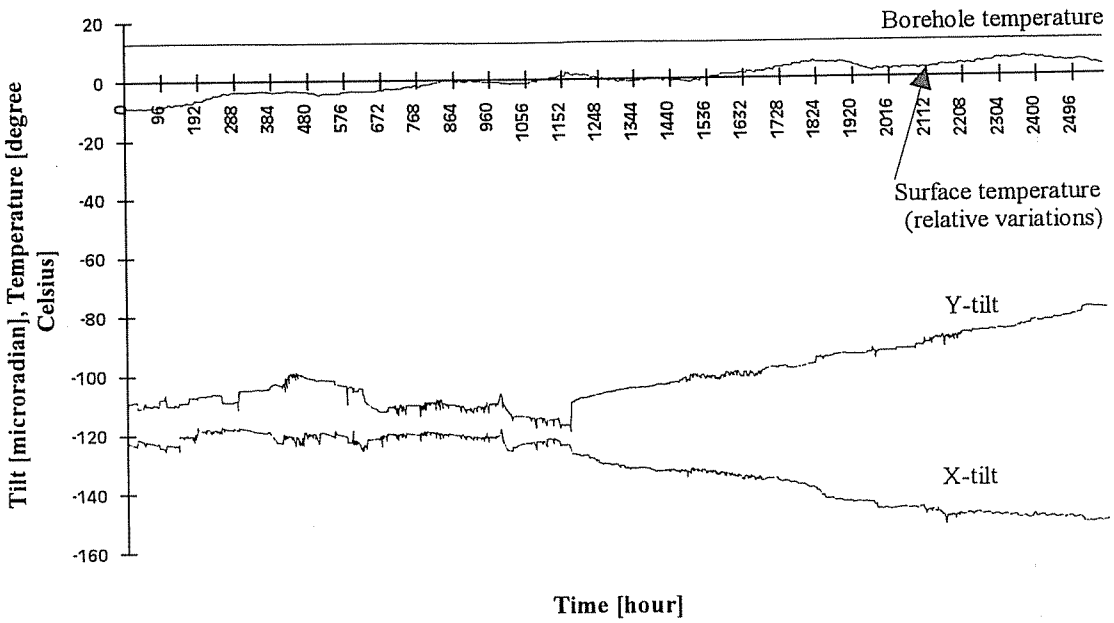

Figure 6. Tilt and temperature variations at the point D2 from 13.10.1997 till 23.03.1998

At the point D1 the range of the tilts is unchanged and the unfiltered data show that the disturbances are very small in the bedrock. At the point D2 the tilt changes are much smaller than in the previous recording period. It means that the borehole in the sediment became stable about half a year after the installation of the instrument. The tilt signals at the point D2 (Fig. 6) are much more disturbed than at the point D1. The reason is the vicinity of the hills (landslides) and the forest. The ground tilt with diurnal period caused probably by the transpiration of the trees can be seen from the middle of May (about from 1200 hours on the time axis) and it is especially "large" in June at the X-tilt. Figure 7 shows both effects much clearly at the point D2. The large tilt caused by rainfall is a landslide. The direction of these tilts can be interpreted from the topography of the measuring place very well. The relative large amplitude of the superposed signal with diurnal period due to the transpiration of the trees proves that the borehole in the sediment is very sensitive to disturbing effects.

Figure 8 shows a semidiurnal signal superposed on the tilt signal at the point D1. This semidiurnal signal was present only in the time interval shown in the Fig. 8. According to the first investigations it correlates very strongly with the theoretical tidal signal calculated for the recording place. For more precise investigations longer records are needed but this signal disapeared in the other records.

Both effects, landslides and tilts caused by the transpiration of the vegetation together with other effects (e.g. ground water variations) have been studied in cooperation between the Section Applied Geophysics of the Geological Institute of the University of Bonn and the Geodetic and Geophysical Research Institute of the Hungarian Academy of Sciences in Sopron (Kümpel et al., 1996; Lehman et al., 1998) for several years. To understand the real physical backgrounds of these effects further investigations are needed and a lot of other parameters have to be measured.

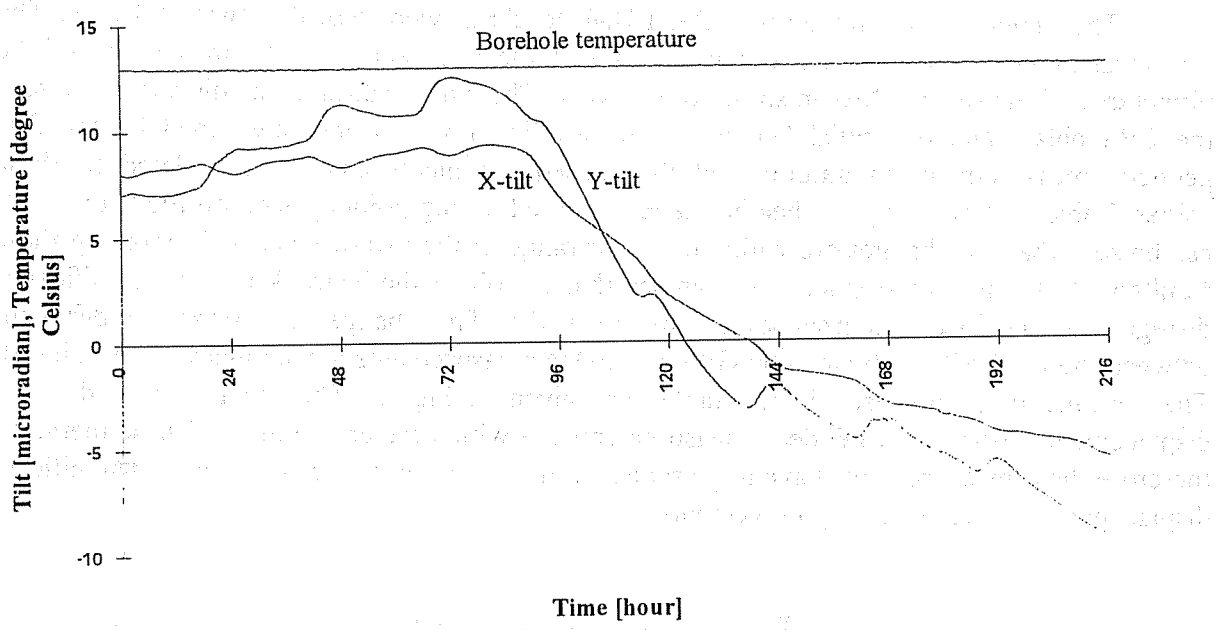

Figure 7. An example for local disturbances (landslide, ground tilt caused by the transpiration of the trees) measured by the borehole tiltmeter at the point D2 from 04.10.1997 till 12.10.1997.

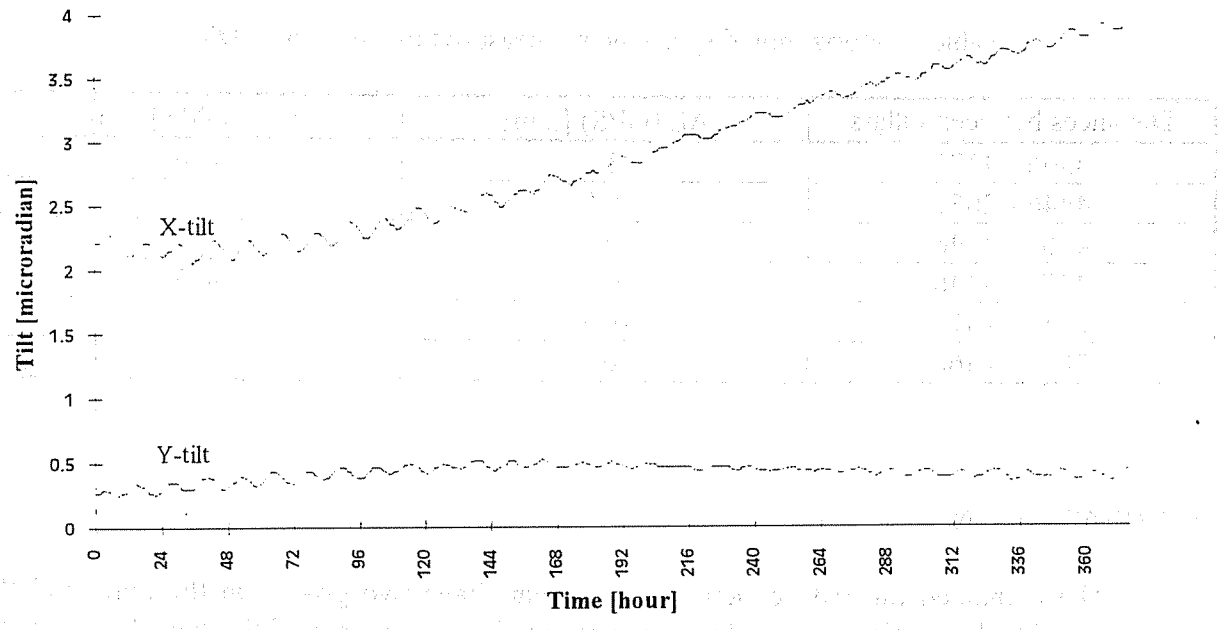

Figure 8. Semidiurnal tilt signal recorded at the point D1 from 12.10.1997 till 28.10.1997.

5. RESULTS OF THE GEODETIC MEASUREMENTS

The geodetic measurements (GPS, EDM, leveling) were repeated twice till now. The first measurements were carried out in autumn of the last year after the installation of the tiltmeters and the second ones in spring of this year. The initial values of the distances between the GPS pillars and the initial heights of the leveling points were determined by the first geodetic measurements in autumn and the subsequent measurements are related to these values. Table I. shows only the height changes of the leveling points placed on the bedrock. It can be seen that the changes are within the error range of the measurements. Comparing these results with the tilt measurements we can say that the tilt of the bedrock is of no significance disregarding the local disturbances of the point D2. The changes of horizontal distances between the GPS pillars obtained by GPS and EDM measurements are summarised in Table II. The marking of points used in the tables are given in Fig. 2. The results show that the displacements obtained by geodetic measurements are within the error range of these methods, therefore these measurements have to be repeated more times in the future to obtain significant displacements if there exist any movements.

Table I. Results of the leveling

Points	ΔH (Height change) [mm]	$\sigma_{\Delta H}$ [mm]
1001	-0.23	±0.59
100	+0.65	±0.56
200	+0.98	±0.56
1004	+0.23	±0.71

Table II. Horizontal displacements measured by GPS and EDM

Distances between pillars	ΔL (GPS) [mm]	ΔL (EDM) [mm]
4366 - 4371	-1.6	-1.4
4446 - 2052	0.9	-
4366 - 4446	0.5	-0.2
4371 - 4446	0.7	-0.3
2052 - 4371	-0.1	-
2052 - 4366	-0.9	-

5. CONCLUSION

The combined tilt and geodetic measurements have two goals. On the one hand the continuous tilt observations give information about the movements of the fault between the geodetic measurements on the other hand the results of geodetic measurements can be used for a better understanding and interpretation of continuous tilt records. Because of the "high" errors of geodetic methods long term simultaneous measurements are needed for the study of connections between tilts and local and tectonic movements.

The obtained data of the tilt observations show that the continuous tilt records in shallow boreholes can be used for monitoring local tectonic movements at faults. To ensure a relatively stable temperature for the instruments the depth of the borehole should be at least 5m. For elimination of local geodynamical effects e.g. landslides, the borehole with whole length should be drilled in the bedrock. To eliminate other local effects a lot of parameters (meteorological, ground water level, etc.) should be also measured. Yearly or two yearly repeated geodetic measurements can be used for controling the continuous tilt observations. These combined measurements can contribute to an unambiguous interpretation of the measured data and to a better understanding of ground dynamics.

Acknowledgements

This research was supported by the grants of the Scientific-Technological collaboration between Germany and Hungary (through DLR/International Bureau and OMFB; project nos.: UNG-047-96 and D-4/96) and by the Hungarian National Scientific Research Foundation (OTKA) in the frame of the research projects T 019030 and T 014896.

References

Mentes, Gy., Lehmann, K., Varga, P., Kümpel, H.-J.: Some Calibration of the Applied Geomechanics Inc. Borhole Tiltmeter Model 722. Acta Geod. Geoph. Hung, Vol. 31(1-2), pp. (1996)79-89.

Kümpel, H.-J., Varga, P., Lehmann, K., Mentes, Gy.: Ground Tilt Induced by Pumping - Preliminary Results from the Nagycenk Test Site, Hungary. Acta Geod. Geoph. Hung, Vol. 31(1-2), pp. (1996)67-79.

Lehmann, K., Mentes, Gy., Kümpel, H.-J., Varga, P.: Approaching Local Ground Dynamics by Measurements of Ground Tilt. In Kahmen/Brückl/Wunderlich (Eds.): Geodesy for Geotechnical and Structural Engineering. Institut für Landesvermessung und Ingenieurgeodäsie, Abteilung Ingenieurgeodäsie, TU Wien, 1998, pp. 99-104.

EARTH TIDE GENERATED VARIATIONS OF SECOND DEGREE GEOPOTENTIAL

P Varga,[1] E W Grafarend,[2] J Engels[2]

The time–dependent part of the gravity potential, the "deformation potential" $\delta w(\underline{x},t)$ (Grafarend, 1990) fulfils the Poisson equation

$$\text{div grad } \delta w(\underline{x},t) = -4\Pi G \delta\varrho(\underline{x},t)\,.$$

Because no loss of mass during this deformation the variation of denisty $\delta\varrho(\underline{x},t)$ can be given with the continuity equation

$$\delta\varrho(\underline{x},t) = -\,\text{div}\,[\varrho(\underline{x})\underline{d}(\underline{x},t)]$$

In above expressions δw is the deformation potential, $\varrho(x)$ the initial density, $\underline{d}(\underline{x},t)$ the time (t) dependent displacement vector, $\underline{x}$ is the source point within the Earth, G denotes the gravitational constant. With the use fo above expression for time–depend mass density the Newtonian potential is

$$\delta w(\underline{x}^*,t) = -G\int\limits_{(v)} \frac{\text{div}\,[\varrho(\underline{x})\underline{d}(\underline{x},t)]}{||\underline{x}^* - \underline{x}||}\,d^3\underline{x}\,, \tag{1}$$

In (1) $\underline{x}^*$ is a field point of the Earth's surface. The equation for source term in (1) is composed by a dilatational ($\underline{D}(\underline{x},t)$ and by a transport displacement ($\underline{T}(\underline{x},t)$ term:

$$\text{div}\,[\varrho(\underline{x})\underline{d}(\underline{x},t)] = D(\underline{x},t) + T(\underline{x},t) = \varrho(\underline{x})\,\text{div}\,(\underline{x},t) + \langle \text{grad}\,\varrho(\underline{x})|\underline{d}(\underline{x},t)\rangle \tag{2}$$

The denominator in (1) expressed in spherical coordinates (λ,ϕ,r) could be expanded into orthonormal scalar spherical surface fundtions with associated Legendre functions

$$\frac{1}{||\underline{x}^* - \underline{x}||} = \frac{1}{\underline{r}^*}\sum_{n=0}^{\infty}\sum_{m=-n}^{n}\frac{1}{2n+1}\left(\frac{r}{r^*}\right)^n Y_{nm}(\lambda^*,\phi^*)Y_{nm}(\lambda,\phi)\,. \tag{3}$$

[1]Geodetic and Geophysical Research Institute of the Hungarian Academy of Sciences, H-9401 Sopron, POB 5, Hungary

[2]Department of Geodetic Science, Stuttgart University, Keplerstr. 11, D–7000 Stuttgart 1, Germany,

which convergs uniformly on and outside the Earth' s surface ($r \leq r^*$).

The displacement vector at the surface in general case can be decomposed into sheroidal $R^{nm}(\underline{r},t), S^{nm}(\underline{r},t)$ and torodial $T^{nm}(\underline{r},t)$ components and can be expressed as a vector spherical harmonics (Merriam, 1986; Wilhelm, 1986)

$$\begin{aligned}\underline{d}(\underline{x},t) &= \sum_{n=0}^{\infty}\sum_{m=-n}^{+n}[r^{nm}(r,t)\underline{R}_{nm}(\lambda,\phi)+s^{nm}(r,t)\underline{S}_{nm}(\lambda,\phi)+\\ &+t^{nm}(r,t)\underline{T}_{nm}(\lambda,\phi)]\,. \end{aligned} \tag{4}$$

Because the earth tides and related phenomena (such as surface and internal normal load) generated only spheroidal, no torodial components the last term of (4) can be neglected and substituting (2),(4) and (4) into (1)

$$\begin{aligned}\delta w(\underline{x}^*,t) = -\frac{G}{r^*}\int_{(v)}\sum_{n_1=0}^{\infty}\sum_{m_1=-n_1}^{+n_1}\frac{1}{2n_1+1}\left(\frac{r}{r^*}\right)^{n_1}Y_{n_1m_1}(\lambda^*,\phi^*)Y_{n_1m_1}(\lambda,\phi)\cdot\\ \cdot\sum_{n_2=0}^{\infty}\sum_{m_2=-n_2}^{+n_2}\left\{\left[\frac{2}{r}r^{n_2m_2}+\frac{d}{dr}r^{n_2m_2}-\frac{[n_2(n_2+1)]^{1/2}}{r}s^{n_2m_2}\right]\cdot\right.\\ \cdot\varrho(\underline{x})Y_{n_2m_2}(\lambda,\phi)+\\ \left.+\frac{d\varrho}{dr}[r^{n_2m_2}Y_{n_2m_2}(\lambda,\phi)]\right\}d^3\underline{x}\,. \end{aligned} \tag{5}$$

In the r.h.s. of (5) the first term represents the dilatational part while the second one the transportational part of the potential variation.

The displacement, field assuming spheroidal displacement field alone, could be represented according to Love–Shida hypothesis as

$$\begin{aligned} d_\lambda &= l(r)(\gamma r\cos\phi)^{-1}\partial V_{\mathrm{TID}}/\partial\lambda\\ d_\phi &= l(r)(\gamma r)^{-1}\partial V_{\mathrm{TID}}/\partial\phi\\ d_r &= h(r)\gamma^{-1}V_{\mathrm{TID}}\,, \end{aligned} \tag{6}$$

where l and h are the Shida and the Love numbers, respectively, γ is the mean gravity acceleration and V_{TID} denotes the tidal potential.

$$V_{\mathrm{TID}} = \sum_{n=0}^{\infty}\sum_{m=-l}^{+l}V_{nm}\,Y_{nm}(\lambda^*,\phi^*)\,. \tag{7}$$

With the use of (6) and (7) displacement field can be given as follows (*Grafarend, 1986*)

$$\begin{aligned} d_{\lambda_{nm}} &= l(r)(\gamma r\cos\phi)^{-1}V_{nm}\partial Y_{nm}(\lambda,\phi)/\partial\lambda \\ d_{\phi_{nm}} &= l(r)(\gamma r)^{-1}V_{nm}\partial Y_{nm}(\lambda,\phi)/\partial\phi \\ d_{r_{nm}} &= h(r)\gamma V_{nm}Y_{nm}(\lambda,\phi)\,. \end{aligned} \tag{8}$$

Consequently

$$\begin{aligned} r^{nm}(r) &= h_n(r)\gamma^{-1}V_{nm} \\ s^{nm}(r) &= l_n(r)[n(n+1)]^{1/2}\gamma^{-1}V_{nm} \end{aligned} \tag{9}$$

If the displacement field assumint a radial mass density distribution of a symmetric non–rotating elastic isotropic (SNREI) Earth model $\varrho = \varrho(r)$, $l = l(r)$, $h = h(r)$, while $\partial\varrho/\partial\lambda = \partial\varrho/\partial\phi = 0$, and (5) gives

$$\begin{aligned} &\delta w_{nm}(\underline{x}^*t) = \\ &-G\int_{(v)}\Bigg\{\{\rho(r)(1/r^*)[1/(2n_1+1)](r/r^*)^{n_1}Y_{n_1m_1}(\lambda^*,\phi^*)Y_{n_1m_1}(\lambda,\phi)\}\cdot \\ &\cdot\Bigg\{\left[2/(\gamma r)h_n(r)+(1/\gamma)\frac{\partial h_n(r)}{\partial r}-n_2(n_2+1)/(\gamma r)l_n(r)\right]\cdot \\ &\cdot V_{n_2m_2}Y_{n_2m_2}(\lambda,\phi)+[(1/\gamma)\partial\varrho(r)/\partial r h_n(r))^{n_2}V_{n_2m_2}Y_{n_2m_2}(\lambda,\phi)]\Bigg\}\Bigg\}dx^3\,. \end{aligned}$$

The above expression with (9) and with use of the ortonormality relation

$$\int_{(S)}V_{n_1m_1}(\lambda,\phi)\cdot V_{n_2m_2}(\lambda,\phi)dx^2 = \begin{cases} 4\pi \text{ if } n_1=n_2, m_1=m_2 \\ 0 \text{ if } n_1\neq n_2, m_1\neq m_2 \end{cases}$$

Can be written as

$$\begin{aligned} \delta w_{nm}(\underline{x}^*,t) &= -4\Pi G\cdot\int_0^{r^*}\Bigg\{\frac{\varrho(r)}{r^*}\left[\frac{1}{2n+1}Y_{nm}(\lambda^*\phi^*)\right]\cdot \\ &\cdot\Bigg\{\left[\frac{2}{\gamma r}h_n(r)+\frac{1}{\gamma}\frac{dh_n(r)}{dr}-\frac{n(n+1)}{\gamma r}l_n(r)\right]V_{nm}+ \\ &+\left[\frac{d\varrho(r)}{dr}\cdot\frac{1}{\gamma}h_nV_{nm}\right]\Bigg\}\Bigg\}\cdot\left(\frac{r}{r^*}\right)^n r^2dr = \\ &= \frac{-4\pi GY_{nm}(\lambda^*,\phi^*)V_{nm}}{\gamma r^*(2n+1)}\int_0^{r^*}\Bigg\{\varrho(r)\left[2\frac{h_n(r)}{r}+\frac{dh_n(r)}{dr}-\right. \end{aligned}$$

$$-\frac{n(n+1)l_n(r)}{r}\Big] + h_n(r)\frac{d\varrho(r)}{dr}\Big\}\left(\frac{r}{r^*}\right)^n r^2 dr\,. \qquad (10)$$

(10) leads with some modifications to the following expression

$$\begin{aligned}\delta w_{nm}(\underline{x}^*,t) &= -4\Pi G/[\gamma(2n+1)(r^*)^{n+1}]V_{nm}Y_{nm}(\lambda^*,\phi^*)\cdot \\ &\cdot\int_0^{r^*}\Big\{\varrho(r)\Big[\frac{dh_n(r)}{dr}r^{n+2}+2h_n(r)r^{n+1}- \\ &-n(n+1)l_n(r)r^{n+1}\Big]+\frac{d\varrho(r)}{dr}h_n(r)r^{n+2}\Big\}dr\,. \qquad (11)\end{aligned}$$

From the last term of the r.h.s. of (11) shuld be removed the derivative of the density function $\varrho(r)$ because this function is not known within the Earth with neded accuracy. The partial integration of this expression gives

$$\int_0^{r^*}\frac{d\varrho(r)}{dr}h_n(r)r^{n+2}dr = -\int_0^{r^*}\varrho(r)\left[\frac{dh_n(r)}{dr}r^{n+2}+h_n(r)(n+2)r^{n+1}\right]dr$$

because

$$\int_0^{r+\varepsilon}\frac{d(\varrho(r)r^{n+2}h(r))}{dr}dr = 0$$

for every $\varepsilon > 0$. This problem treated in detail in Grafarend et al., 1997.

If this consideration is used in (11) the "deformation potential" finally can be given in simpler form:

$$\begin{aligned}\delta w_{nm}(\underline{x}^*,t) &= 4\pi G/\left[\gamma(2n+1)(r^*)^{n+1}\right]V_{nm}Y_{nm}(\lambda^*,\phi^*)\cdot \\ &\cdot\int_0^{r^*}\varrho(r)\left[n(n+1)l_n(r)r^{n+1}+nh_n(r)r^{n+1}\right]dr \qquad (12)\end{aligned}$$

(12) gives the relation between the potential variation due to deformation (r.h.s.) and the change in gravity potential (l.h.s.) (7):

$$\delta w_{nm}(\underline{x}^*,t) = k_n(r^*)V_{\mathrm{tid}_{nm}} = k_n(r^*)V_{nm}Y_{nm}(\lambda^*,\phi^*)\,, \qquad (13)$$

Therefore (12) and (13) give the following relation of the Love-Shida numbers

$$\begin{aligned}k_n(r^*) &= 4\Pi Gn/\left[\gamma(2n+1)(r^*)^{n+1}\right]\cdot \\ &\cdot\int_0^{r^*}-\varrho(r)r^{n+1}[(n+1)l_n(r)+h_n(r)]dr\,. \qquad (14)\end{aligned}$$

For example if n=2

$$k_n(r^*) = \frac{8\Pi G}{5\gamma r^{*3}} \int_0^{r^*} \varrho(r) \cdot r^3[(h_2(r) + 3l_2(r)]dr\,. \tag{15}$$

In relative units $G = 3/4\Pi, r^* = 1, \gamma = 1, \varrho_{\text{mean}} = 1$

$$k_2(r^*) = \frac{6}{5} \int_0^{r^*} \varrho(r) \cdot r^3(3l_2(r) + h_2(r)]dr\,. \tag{16}$$

Equation (2) with the use of (13) and the dilatational ($D(x,t)$) and transport displacement ($T(x,t)$) terms of the density variation caused by the potential variation δw_{nm} give

$$\begin{aligned} D(\underline{x},\underline{t}) &= \varrho(x)\text{div}(x,t) = \tfrac{1}{\gamma \underline{r}^*}\left(2h_n + r\tfrac{dh_n}{dr} - n(n+1)l_n\right) V_{TID_{nm}} Y_{nm}(\lambda^*,\phi^*) \\ T(\underline{x},t) &= <\text{grad}\varrho(x)|d(x,t)> = \tfrac{d\varrho(r)}{dr}\tfrac{h_n}{\gamma} V_{TID_{nm}} Y_{nm}(\lambda^*,\phi^*) \end{aligned}$$

Therefore

$$\begin{aligned} \delta\varrho(\underline{x},t) &= D(\underline{x},t) + T(\underline{x},t) = \\ &= -\left\{\tfrac{\varrho}{\gamma \underline{r}^*}\left[nh_n + r\tfrac{dh_n}{dr} - n(n+1)l_n\right] + \tfrac{d\varrho}{dr}\tfrac{hn}{\gamma}\right\} + V_{TID_{nm}} Y(\lambda,\phi) \end{aligned} \tag{17}$$

In case of tides $n = 2$ the variation of the polar moment of inertia δC caused by zonal (long–periodic) tides ($m = 0$) is

$$\begin{aligned} \delta C &= \int_{(v)} \delta\varrho r^2 \cos^2\phi d^3x = -\frac{2}{3}\int_{(v)} \delta\varrho r^2 \left(1 - \frac{Y_{2,0}(\lambda\phi)}{\sqrt{5}}\right) d^3x = \\ &-\frac{2}{3}\int_0^{r^*}\int_{(s)} \left\{\frac{\varrho}{\gamma r}\left[2h_2 + r\frac{dh_2}{dr} - 6l_2\right] + \frac{d\varrho}{dr}\frac{h_2}{\gamma}\right\} V_{TID_{2,0}} Y_{2,0}(\lambda\phi) \cdot \\ &\cdot \left(1 - \frac{Y_{2,0}(\lambda\phi)}{\sqrt{5}}\right) r^4 dx^2 dr = \\ &= \frac{8\pi}{3\sqrt{5}} V_{TID_{2,0}} \int_0^{r^*} \left\{\frac{\varrho}{\gamma r}\left[2h_2 + r\frac{dh_2}{dr} - 6l_2\right] + \frac{d\varrho}{dr}\frac{h_2}{\gamma}\right\} r^4 dr \end{aligned}$$

After partial integration the last equation can be written as

$$\delta C = -\frac{16\pi}{3\sqrt{5}}\frac{V_{TID_{2,0}}}{\gamma}\int_0^{r^*} \delta r^3(h_2 - 3l_2)dr = \frac{2r^{*3}\sqrt{5}}{3\gamma} k_2 V_{TID_{2,0}} \tag{18}$$

The zonal tidal potential is

$$V_{TID_{2,0}} = 3G^* \left(\sin^2 \delta - \frac{1}{3} \right)$$

With the use of suitable numerical values for the Doodson constant (G^*) and declination (δ)

$$\delta C = 7.6 \cdot 10^{29} \mathrm{kgm}^2$$

The typical value for the half period of the zonal waves is around 10^6s, therefore for the time derivative of the polar moment of inertia in case of tidal disturbances is

$$\frac{dC}{dt} = 7.6 \cdot 10^{23} \mathrm{kgm}^2 s^{-1}$$

The time derivative of the second zonal geopotential coefficient J_2 with the use of MacCullagh's formula gives

$$\frac{dJ_2}{dt} = \frac{d(C-A)}{dt} \frac{1}{Mr^{*2}}$$

where M is the mass of the Earth and A is the equatorial moment of inertia. In case of the incompressible Earth

$$\frac{dC}{dt} + \frac{2dA}{dt} = 0$$

and consequently

$$\frac{dJ_2}{dt} = \frac{3}{2} \frac{dC}{dt} \left(Mr^{*^2} \right)^{-1} = \frac{\sqrt{5} k_2 r^*}{M\gamma} \frac{dV_{TID_2,0}}{dt} = 3.2 \cdot 10^{-22}$$

This value is, in the time–interval of the zonal tides, apparently smaller than the value obtained from laser ranging to geodetic satellites (Varga, 1999) $\frac{dJ_2}{dt} = -8.5 \cdot 10^{-18} s^{-1}$ or the time derivative derived from geological data: $\frac{dJ_2}{dt} = -1.6 \cdot 10^{-19} s^{-1}$

Acnowledgements. This work was completed during the stay of P.Varga at the Geodetic Institute of Stuttgart University in 1997 and 1998 supported by the Alexander von Humboldt fundation and was financed also by the Hungarian Science Fundation (Grant TO 14896).

References

Grafarend E 1986: Three–dimensional deformation analysis: global vector spherical harmonic and local finite element representetion. *Tectonophysics* 130, 337–359.

Grafarend E 1990: The spacetime height system. Proceedings of the Workshop on Precise Positioning, Hannover

Grafarend E, Engels J, Varga P 1996: The spacetime gravitational field of a deformable body. *Journal of Geodesy*, 72, 11–30.

Merriam J B 1986: Transverse stress Green's functions. *Journal Geophys. Res.* 91, 13903–13913.

Varga P 1999: Temporal variation of second degree geopotential. *Jornal of Geodesy* (in print) .

Wilhelm H 1986: Sheroidal and torsional global response functions. *J.Geophys.*, 59, 16–22.

Some Remarks on the Recent Tidal Potentials

Xi Qinwen

(Center for Analysis and Prediction, China Seismological Bureau, Beijing, China, 100036)

1. About the pseudo-waves

Some pseudo-waves may be included in the tidal potential obtained by using analytical method (Roosbeek, etc 1994). Xi (1998) has expressed the tidal potential as follows

$$V = \frac{fM}{R}\sum_{n=2}^{\infty}\left(\frac{\rho}{R}\right)^n \sum_{m=0}^{n}\frac{1}{2n+1}\overline{P}_n^m(\cos\theta_p)\overline{C}_n^m(\theta_s, H) \tag{1}$$

Where $\overline{P}_n^m(\cos\theta_p)$ is a fully normalized associated Legendre function, and $\overline{C}_n^m(\theta_s, H)$ is surface spherical harmonics, which have been defined by Xi (1997) and has a recurrent formula in which

$$\overline{C}_n^n = \sqrt{\frac{2(2n+1)}{3n}}\overline{C}_1^1\overline{C}_{n-1}^{n-1} - \sqrt{\frac{(2n+1)(2n-1)}{4n(n-1)}}\kappa\sin^2\theta\overline{C}_{n-2}^{n-2} \tag{2}$$

It can be used to obtain the tidal waves of degree n and order n. The $\overline{C}_1^1\overline{C}_{n-1}^{n-1}$ will produce the tidal waves of order n and $n-2$, the processes of producing waves like the modulation which produce the side-high frequency (order n) and side-low frequency (order $n-2$). The waves of order $n-2$ produced by the first part of the expression (2) will be canceled by that produced by the second part of the expression (2). If they could not be fully canceled by each other due to the truncation errors, the remainder errors would generate so called "**pseudo-waves**". Although we may prove that

$$\begin{aligned}
&\sqrt{\frac{2(2n+1)}{3n}}\overline{C}_1^1\overline{C}_{n-1}^{n-1} = \sqrt{\frac{2(2n+1)}{3n}}\overline{P}_1^1(\cos\theta)\cos H\,\overline{P}_{n-1}^{n-1}(\cos\theta)\cos[(n-1)H] \\
&= \sqrt{\frac{(2n+1)(2n-1)}{4n(n-1)}}\kappa\sin^2\theta\,\overline{P}_{n-2}^{n-2}(\cos\theta)\cos(nH) + \sqrt{\frac{(2n+1)(2n-1)}{4n(n-1)}}\kappa\sin^2\theta\overline{C}_{n-2}^{n-2} \\
&= \overline{P}_n^n(\cos\theta)\cos(nH) + \sqrt{\frac{(2n+1)(2n-1)}{4n(n-1)}}\kappa\sin^2\theta\overline{C}_{n-2}^{n-2}
\end{aligned} \tag{3}$$

It indicates that the first part in (2) has included the second part in (2), but one can not use (3) for developing a tidal potential, only (2) can be used.

Not only Xi's potentials (Xi, 1989) but Roosbeek's potential (Roosbeek, 1996) really include some so called **"pseudo-waves"** . Of course, one may filter them out, but they may not be exactly canceled by adding one order of magnitude in computation because they are always at a level of the truncation errors.

2. About the time-dependent amplitudes

In 1883, Darwin developed a tidal potential, in which the lunar ascending node was not be consider as an argument and the amplitudes are time dependent. This potential is not a fully harmonic development.

In some recent tidal potentials (Hartmann etc., 1995, Roosbeek, 1996, Tamura, 1987) the amplitudes of tidal waves are also time dependent, so they could not be counted as fully harmonic developments also. The form of a wave in the recent tidal potentials can be written as follows

$$y(t) = (a + bt)\cos(\omega t + \varphi) \tag{4}$$

It means the amplitudes are modulated by time. The variation of $y(t)$ is as Figure 1.

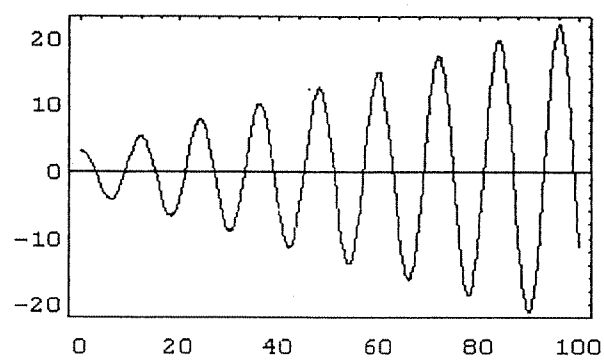

Fig. 1. The variations of y (t)

Our concern is on the magnitude of the time dependent amplitudes of the recent tidal potentials (Cartwright, Tamura, Roosbeek, Hartman and Wenzel). If one computes the tidal amplitudes for an epoch which is far away form the epoch J2000, then the recent tidal potentials will give very unusual tidal amplitudes (Wenzel, personal communication, 1997).

In addition, on basis of the theory of the ordinates combination, the combination of addition for (4) is

$$\begin{aligned} Y_m(t) &= y(t+m) + y(t-m) \\ &= 2\cos(m\omega)(a+bt)\cos(\omega t+\varphi) - 2bm\sin(m\omega)\sin(\omega t+\varphi) \end{aligned} \tag{5}$$

In which, an additional term $-2bm\sin(m\omega)\sin(\omega t+\varphi)$ appears. Therefore, the expression $2\cos(m\omega)$ may not be used to define the frequency transfer function as usual in that case. The problem is the same for the combination of subtraction $Z_m(t)$.

As a same reason, the filtered values (M_i or N_i) in Venedikov's analysis method, for

example, is

$$M_i^\tau = \sum_{t=-23.5}^{+23.5} C_t^\tau y(t)$$

$$= \sum_{t=-23.5}^{+23.5} C_t^\tau \sum_{n=1}^{p} H_n \cos\Phi_n(T_i)\cos(\omega_n\ t) - \sum_{t=-23.5}^{+23.5} C_t^\tau \sum_{n=1}^{p} H_n \sin\Phi_n(T_i)\sin(\omega_n\ t)$$

$$= \sum_{n=1}^{p} \sum_{t=-23.5}^{+23.5} H_n \cos\Phi_n(T_i) C_t^\tau \cos(\omega_n\ t) - \sum_{n=1}^{p} \sum_{t=-23.5}^{+23.5} H_n \sin\Phi_n(T_i) C_t^\tau \sin(\omega_n\ t) \qquad (6)$$

It is no longer right to be written as

$$M_i^\tau = \sum_{n=1}^{p} H_n \cos\Phi_n(T_i) \sum_{t=-23.5}^{+23.5} C_t^\tau \cos(\omega_n\ t) - \sum_{n=1}^{p} H_n \sin\Phi_n(T_i) \sum_{t=-23.5}^{+23.5} C_t^\tau \sin(\omega_n\ t) \qquad (7)$$

Because the H_n, which is time dependent in the expression $\sum_{t=-23.5}^{+23.5} H_n \cos\Phi_n(T_i) C_t^\tau \cos(\omega_n\ t)$, is not a constant it can not be taken out from the expression.

All of the problems above mentioned are caused by the time dependent amplitudes in the recent tidal potentials.

3. Making a wave with time dependent amplitude fully harmonic

Regarding to the variation t in the brackets of the expression (4), the unit is generally in Julian Century. It can be strictly written as follows

$$y(t) = (a + bT)\cos(\omega\ t + \varphi). \qquad (8)$$

Where T is in Julian century. For fully harmonizing, the expression (8) can be transformed to

$$y(t) = a * \cos(\omega\ t + \varphi) + b * c * \frac{T}{c}\cos(\omega\ t + \varphi). \qquad (9)$$

When c is big enough, we have

$$\frac{T}{c} = \sin\left(\frac{T}{c}\right),$$

so that

$$y(t) = a * \cos(\omega t + \varphi) + b * c * \sin\left(\frac{T}{c}\right)\cos(\omega t + \varphi)$$

$$= a * \cos(\omega t + \varphi) + b * \frac{c}{2}\sin[(\omega t + \frac{T}{c}) + \varphi] - b * \frac{c}{2}\sin[(\omega t - \frac{T}{c}) + \varphi]. \qquad (10)$$

It means that the wave with time dependent amplitude in (8) can be resolved into three fully harmonic waves in (10).

Besides the main wave $a * \cos(\omega t + \varphi)$ with the basic frequency in (10), the part $b * c * \sin(\frac{T}{c})\cos(\omega t + \varphi)$ in (10) had been modulated to two waves, a side-high frequency $b * \frac{c}{2}\sin[(\omega t + \frac{T}{c}) + \varphi]$ and a side-low frequency $-b * \frac{c}{2}\sin[(\omega t - \frac{T}{c}) + \varphi]$.

In other words, the two fully harmonic waves with side frequency are equivalent to the wave with time dependent amplitude. That is

$$b * c * \sin(\frac{T}{c})\cos(\omega t + \varphi) = b * \frac{c}{2}\sin[(\omega t + \frac{T}{c}) + \varphi] - b * \frac{c}{2}\sin[(\omega t - \frac{T}{c}) + \varphi] \qquad (11)$$

For example, if we take $b = 20$, $c = 10000$, $\omega = 60°$, $\varphi = 0$ and $T = 10.5 + t/876600$, Then the variations and the spectra of the left side (before modulation) and the right side (after

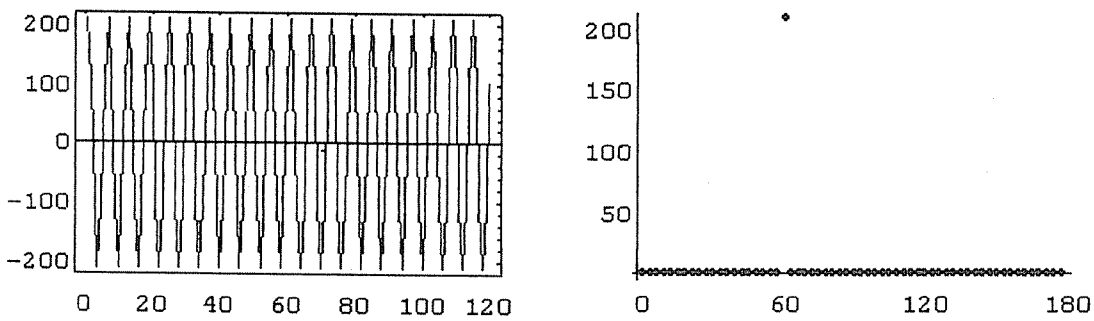

Fig. 2. The variations and the spectra of the modulating wave

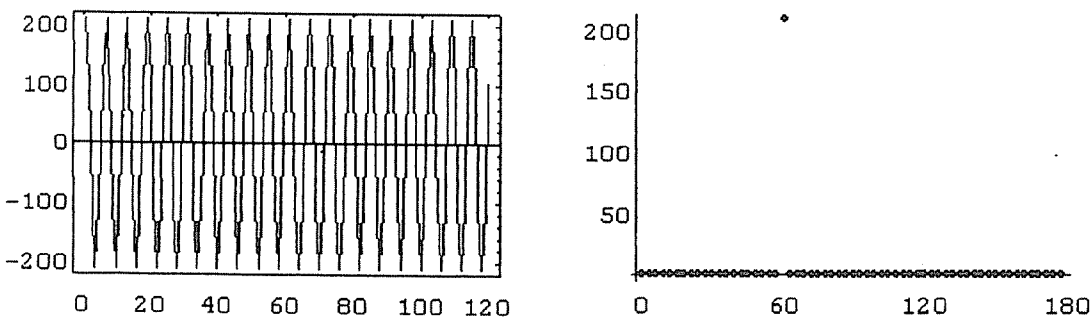

Fig. 3. The variations and the spectra of the modulated waves

modulation) in (11) can be shown as Figure 2 and Figure 3 respectively. When the value of c is big enough, the choice of which has only influence on the amplitudes of both of the side frequency, but no influence on the results of the difference of both of the side frequency in (11).

References

Hartmann, T., Wenzel, H.-G., (1995). Catalogue HW95 of the Tidal Generating Potential. BIM, 123, 9278-9301.

Roosbeek, F., (1993). Development du potentiel generateur des marees par Mathematica. Louvain-La-Neuve.

Roosbeek, F., V. Dehant., (1994). About the Pseudo-new periodic waves in the tide generating potential based on an analytical method. BIM. 120, 9002-9004. Brussels.

Roosbeek, F., (1996). RATGP95: A harmonic development of the tide generating potential using an analytical method. Geophys. J. Int., 126, 197-204.

Tamura, Y., (1987). A harmonic development of the tide-generating potential. BIM, 99, 6813-6855. Brussels.

Wenzel, H.-G., (1997). Personal communication by Email.

Xi Qinwen, (1989). The precision of the development of the tidal generating potential and some explanatory notes. BIM 105, 7396-7404, Bruxelles.

Xi Qinwen, (1998). The Surface Spherical Harmonics and the Development of Tidal Generating Potential. Proceedings of the Thirteenth International Symposium on Earth Tides, 325-329. Brussels.

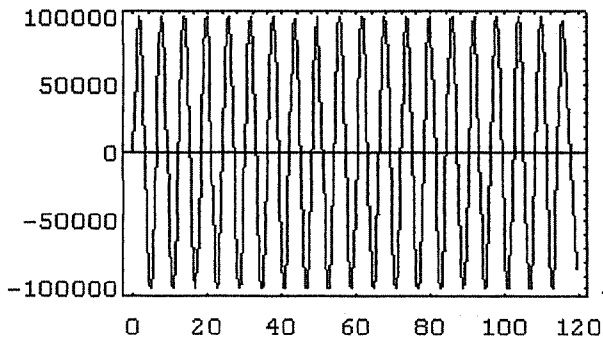

Fig.4. The wave of $b * \frac{c}{2} \sin[(\omega t + \frac{T}{c}) + \varphi]$

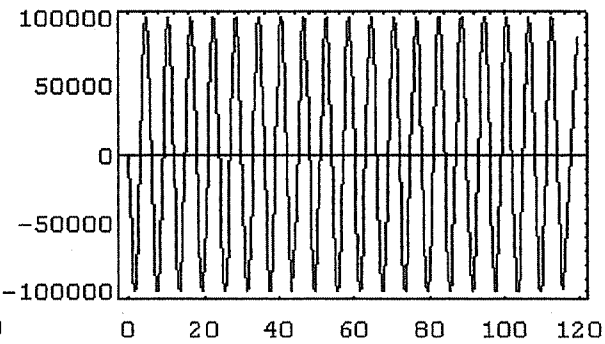

Fig. 5. The wave of $-b * \frac{c}{2} \sin[(\omega t - \frac{T}{c}) + \varphi]$

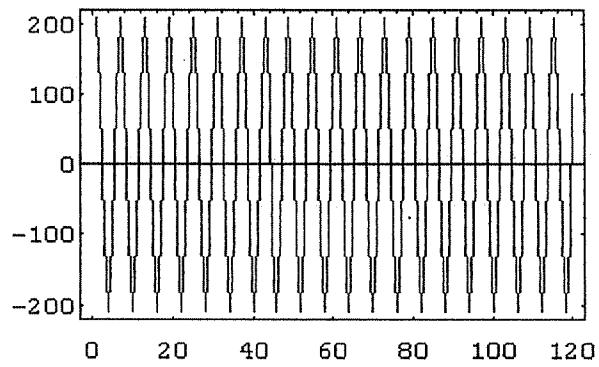

Fig. 6. The wave of $b * c * \sin(\frac{T}{c}) \cos(\omega t + \varphi)$

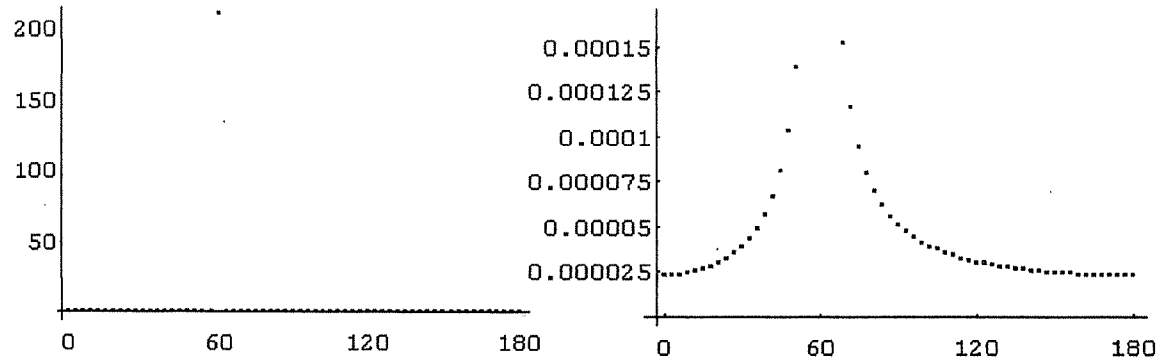

Report of the activities of the Working Group IV « Calibration of the Gravimeters »

M.van Ruymbeke and B.Ducarme
Royal Observatory of Belgium,
Av. Circulaire, 3, 1180 Brussels, Belgium

Introduction:

During the meeting organized in Jena for the Working Group VII [this issue of the BIM], G. Jentzsch has accepted to welcome our proposition to discuss about the problems concerning the calibration of gravimeters.

It was an opportunity to analyse the present situation and we can formulate some general remarks.

We are looking for methods which could achieve an accuracy better than 0.1% [Baker T.,1998].

Description of the problem:

We are concerned by the scale factor of gravimeters recording gravity variations, mainly tidal ones.

For the metrologist, any measurement aims to obtain the ratio between a quantity to scale and an another one selected like « standardized unit ».

For the tidal gravimeters, the situation is the same. A well known variation of gravity is induced and recorded by the instrument. The admittance between the signal and the modulation of gravity gives the scale factor as well as the phase characteristics of the instrument. It is sometimes interesting to determine the transfer function independently of the scale factor. When it is possible to modulate externally the restoring force of a gravimeter one can determine directly its transfer function by injecting a step function or sinusoidal signals[Richter & Wenzel, 1991; Wenzel H.-G., 1994; Van Camp & al., 1999].

What kind of processes could modify the acceleration felt by the gravimeter mass?

<1> The attraction of a moving mass is an obvious way to modify the gravitational field of the Earth and calibrate gravimeters. However it is a very weak action and a sufficient signal to noise ratio exists only for superconducting gravimeters.

<2> A second method consists to move the gravimeter in selected locations with different gravity values. This is the principle of the « Calibration

lines ». Modulations of the gravity values can be very large and the signal to noise ratio does not limit of the accuracy.

<3> A third method consists to tilt the gravimeters to change the moment of force applied to the instrument. Systematic errors occur due to the changes of the gravimeter mechanical equilibrium and the 0.1% accuracy does not seem to be accessible through this technique[Kopaev A.,1998].

<4> A fourth method is based on the physical equivalence between the gravitational mass and the inertial mass. It is thus possible to calibrate a gravimeter by inertial forces e.g. those induced by sinusoidal motions.

The calibration processes <2>,<3> and <4> require to move the gravimeters. Additional mechanical systems are required for processes <1> and <4>.

The calibration process <2> is generally used to calibrate an intermediate standard of the field gravimeters the so called « micrometric screw ». The instruments using a feedback system can use calibration lines to calibrate directly the feedback force if the range of the first ones does not exceed the range of the second one.

It should be pointed out that the intercomparisons in one station of several gravimeters is not a « calibration » "senso strictu".

The tidal gravimeters:

Nowadays the principal types of instruments able to record tidal gravity signals are :

-the superconducting gravimeters (SCG)
-the LaCoste-Romberg spring gravimeters (LCR)
-the Scintrex gravimeters (SCI)
-the Askania gravimeters (ASK)

Recently some authors used also

-the absolute gravimeters (ABS)

No calibration is required for absolute instruments(ABS) which are directly referenced to the wavelength of a laser beam and the time scale of an atomic clock.
This type of gravimeter is the best one to measure the gravity values along a calibration line. Its use to record tides during a long time [Francis O., 1997] will remain marginal. It is generally used for intercomparisons with tidal instruments during a few days to calibrate them.

For spring gravimeters (LCR) & (ASK), a mechanical system modulates the elastic restoring force proportionnally to the rotation of a micrometer. After determination of its scale factor by intercomparisons on « calibration lines », the micrometer is used to determine the sensitivity of the gravimeters during tidal registration.
To record tides with (LCR) or other astaticized gravimeters it is necessary to use a restoring force working in the feedback mode in order to minimize the elastic after-effects inherent to the astatisation.
Some (ASK) are also equipped with a system allowing to put additional masses (balls) on the beam. The equivalent force was scaled against gravity by the maker. The precision of the method is poor as it is necessary to tilt the instrument in order to put and remove the ball.

For the (SCI), it is not possible to modulate the feedback force directly. However the scale factor seems to be very stable[Ducarme & al., 1997]. So the « maker calibration » checked on « calibration lines » can be used for tidal records.

For (SCG), it is not possible to move the instruments on « calibration lines » and no internal modulation of the restoring force is possible with the required accuracy. The so-called « electrostatic calibration » gives only apparent changes of sensitivity. Direct calibration is possible only through methods <1> and <2>.

Sources of errors:

The scale factor of an instrument has to be related to absolute units.

During the transfer process, two kinds of errors could exist which are systematic or random.

The first kind defined as systematic, is directly affecting the scale factor. This error is constant independantly of the number of calibrations.

The second kind which is defined like a random noise, is limiting the precision of the calibration. This kind of error decreases with the increase of the number of determinations.

We can have a very high repeatability of the results of calibration, meaning a low level of random noise, associated with very large systematic errors.
This risk is especially important for frequency dependent processes when the excitation periods are short like in process <4>. The slope of adjustment could be modified by an attenuation of amplitude due to low pass filtering of the mechanical or the parts of the system. As this effect is frequency dependent like the acceleration itself, the systematic errors have to be corrected by

determinining the transfer function of the filters. It becomes thus possible to compensate the damping of the filters at different frequencies.
Systematic errors could exist in the process of transfer from the micrometer to the gravimeter itself of the scale factor (dead zone in the mechanichal transmission, long term drift, ...).
For process <1>, the gravimeters need sufficiently heavy mass to obtain significant signals. The risk exist of systematic errors induced by the mechanical effects due to the displacement of large masses.

Finally it is very important to know how the calibration process itself can modify the gravimeter records, altering its sensitivity and/or drift.

Selection of the methods:

It is clear that some methods are obsolete or will never reach the required accuracy. We shall try to summarize here some of the most promizing approaches.

Cryogenics instruments(SCG)

-Interesting results have been already obtained with mass calibration <1>,[Achilli & al., 1995; Casula & al.,1998]. However this experiment requires a special geometry for the instrument and is thus not applicable everywhere. It does not provide the transfer function as it is working at zero frequency.

-The most popular method has been so far the intercomparison with another relative instrument during a few months [Francis & al.,1997], or with an absolute gravimeter during a few days [Hinderer & al.,1998]. The precision is close to the required 0.1% one. The accuracy is equivalent to the precision when the primary standard is an absolute gravimeter. When using a relative instrument you should take into account the additional uncertainty on its calibration. Attention should be paid to the difference between the transfer functions of the instruments involved in the intercomparison.

-A special inertial device has been realised and tested [Richter B., 1991; Richter & al.,1995].Very high accuracy is claimed but no convincing results have been published so far.

Spring gravimeters

Much more calibration effort has been devoted recently to (LCR) than to (ASK) or (SCIN). We shall thus focus our attention on the first type of instrument.

-The signal to noise ratio is generally not sufficient to apply the mass calibration method <1> at the 0.1% accuracy level [Czapo, Szatmari,1995].

-The most popular method for (LCR) is the use of the micrometric screw which in turn has been calibrated using calibration lines. The calibration of the micrometer is better than 0.01%. The problem is to extrapolate results obtained in the several hundred milligal range to the tidal range. It is why special base lines of a few milligal range have been established in Germany and China[Wenzel H.G.,1995]. The second problem is to calibrate accurately the tidal records using the micrometric screw. Recent tests show that the apparent changes of sensitivity are accurately followed by the calibrations[van Ruymbeke M.,1998].

-Inertial platforms have been successfully tested[van Ruymbeke M.,1989], but much effort has still to be devoted to reach the required accuracy.

Conclusions:

The 0.1% of accuracy on a phenomenon which has a so small amplitude as the tides is at the limit of instrumentation and any method to improve calibration is useful to improve the gravimeters themselves.

We suggest to organize a meeting of people concerned by the determination of the scale factor of the gravimeters to overview the different approaches, including realistic evaluation of the accuracies. An intercomparison of results obtained by various ways is essential to eliminate the risk of systematic errors which are different in the various methods.

Bibliography:

Achilli V., Baldi P., Casula G., Errani M., Focardi S., Guerzoni M., Palmonari F., Raguni G., *A calibration system for superconducting gravimeters*. Bulletin Géodésique, **69**, 73-80.

Baker T.,*Tidal gravity observations and Earth tide model.* Proc.13th Int. Symp.on Earth Tides, Brussels july 22-25,1997, Observatoire Royal de Belgique, Série Géophysique, 287-294, 1998

Casula G., Baldi P., Salemi G., *Tidal Analysis of daea recorded by a superconducting gravimeter in Italy.* Proc.13th Int. Symp.on Earth Tides, Brussels july 22-25,1997, Observatoire Royal de Belgique, Série Géophysique, 611-616, 1998

Csapo G., Szatmari K.G., *Apparatus for moving mass calibration of LaCoste-Romberg feedback gravimeters.* Metrologia, **32**, 225-230.

Ducarme B., Somerhausen A., *Tidal gravity recording at Brussels with a SCINTREX CG3-M gravity meter.*
Bull. Inf. Marées terrestres, **126**, 9611- 9634, 1997.

Francis O., *Calibration of the C021 superconducting gravimeter in Membach (Belgium) using 47 days of absolute gravity measurements.*
IAG Symposia: Gravity, Geoïd and Marine Geodesy, Springer Verlag, **117**, 212-219, 1997

Francis O., Ducarme B., van Ruymbeke M., *One year of registration with the C021 cryogenic gravimeter at station Membach.*
IAG Symposia: Gravity, Geoïd and Marine Geodesy, Springer Verlag, **117**, 336-342,1997

Hinderer J., Amalvict M., Florsch N., Francis O., Mäkinen J., *On the calibration of superconducting gravimeters with the help of absolute gravity measurements.*
Proc.13th Int. Symp.on Earth Tides, Brussels july 22-25,1997, Observatoire Royal de Belgique, Série Géophysique, 557-564, 1998

Kopaev A., Yushkin V., Ducarme B., *Tide gravity recording with a quartz gravimeter Sodin-209 at ORB, Brussels.*
Proc.13th Int. Symp.on Earth Tides, Brussels july 22-25,1997, Observatoire Royal de Belgique, Série Géophysique, 51-57, 1998

Richter B., *Calibration of superconducting gravimeters.*
Cahiers Centre Europ. Géodyn. et Séismologie, **3**, 99-107

Richter B., Wenzel H.-G., *Precise instrumental phase lag determination by the step response method.*
Bull. Inf. Marées Terrestres, **111**, 8032-8052.

Richter B., Wilmes H., Nowak I., *The Frankfurt calibration system for relative gravimeters.*
Metrologia, **32**, 217-223, 1995

Van Camp M., Wenzel H.-G., Schott P., Vauterin P., Francis O., *Accurate transfer function determination for superconducting gravimeter.*
Submitted to Geoph. Research Letters, 1999

van Ruymbeke M., *A Calibration system for gravimeters using a sinusoidal acceleration resulting from a vertical periodic movement.*
Bull. Geod., **63**, 223-235, 1989

van Ruymbeke M., *Internal precision of calibration for la Coste&Romberg gravimeters equipped with a feedback system.*
Proc.13th Int. Symp.on Earth Tides, Brussels july 22-25,1997, Observatoire Royal de Belgique, Série Géophysique, 59-68, 1998

Wenzel H.-G., *Accurate instrumental phase lag determination for feedback gravimeters.*
Bull. Inf. Marées Terrestres, **118**, 8722-8734, 1994

Wenzel H.-G., *Die Vertikale Gravimetereichlinie Karlsruhe.*
H.Dräheim 80Geburstag, E.Kuntz 70Geburstag und H.Malzer 70Geburstag; Geod. Inst. Univ. Karlsruhe, 273-282, 1995.